

The Theory of Long and Short Range Interactions
for Solvated Electrons.

Naira Farquharson Kennedy

Ph.D.

Chemistry Department, University of Glasgow.

July, 1978.

ProQuest Number: 13804145

All rights reserved

INFORMATION TO ALL USERS

The quality of this reproduction is dependent upon the quality of the copy submitted.

In the unlikely event that the author did not send a complete manuscript and there are missing pages, these will be noted. Also, if material had to be removed, a note will indicate the deletion.



ProQuest 13804145

Published by ProQuest LLC (2018). Copyright of the Dissertation is held by the Author.

All rights reserved.

This work is protected against unauthorized copying under Title 17, United States Code
Microform Edition © ProQuest LLC.

ProQuest LLC.
789 East Eisenhower Parkway
P.O. Box 1346
Ann Arbor, MI 48106 – 1346

Acknowledgments

I should like to thank my supervisor, Dr. Brian G. Webster, for his guidance, support and encouragement, and many invaluable discussions.

Thanks must also go to my parents for their backup support, and latterly to my wife.

I am grateful to the Science Research Council for a Research Studentship.

<u>Chapter</u>	<u>Contents</u>	<u>Page</u>
	Summary	1
I	<u>Experimental Clues: The Aims and Scope of This Work</u>	
	A. Some Data on the Solvated Electron: The Nature of the Trapping Site in Water.	3
	B. Aim and Scope of this Investigation.	6
	References I.	8
II	<u>Long-Range Interactions - The Continuum Model</u>	
	A. The Main Types of Treatment.	10
	B. Theory of Wavefunctions in Dielectrics.	12
	C. The Quasi-Adiabatic and Hartree-Fock Approximations.	18
	D. History of Continuous Dielectric Type Models and Critique of Methods.	22
	E. A Flexible Analytical Hartree Type Model: Long-Range Polarisation Effects.	28
	F. Footnote: Similar Models.	34
	References II.	38
	Tables II.	40
	Figures II.	45
III	<u>Self-Consistent Field Molecular Orbital Theory</u>	
	A. Introduction.	53
	B. Basic SCF Theory: The Hartree-Fock Method for Closed Shells.	53
	C. The Roothaan-Hall Equations for Closed Shells.	58
	D. Treatment of Open Shells: The UHF Wavefunction.	59
	E. Choice of Basis Sets.	60
	F. Approximate Methods - CNDO and INDO.	62
	References III.	68

<u>Chapter</u>	<u>Contents</u>	<u>Page</u>
IV	<u>Water Clusters: Short-Range Interactions</u>	
	A. Introduction and Comments on Criteria for Solvation.	71
	B. Theoretical Models of Other Workers: Water Dimers and Larger Clusters.	72
	C. Investigation of the Hydrated Electron in Water and Ice: Methods and Results.	80
	D. Water Multimers.	87
	References IV.	90
	Tables IV.	92
	Figures IV.	100
V	<u>Methanol and Ammonia: Short-Range Interactions</u>	
	A. The Methanol Tetramer: An INDO Study.	114
	B. An Ab Initio Study of Possible Electron Trapping on an (NH ₃) ₂ Cluster: The Effect of Basis Diffuseness.	117
	C. Non-Regular Geometries: The Umbrella Vibration of NH ₃ ⁻ .	123
	D. Conclusions : The Nature and Scope of Short-Range Effects on Electron Solvation.	126
	References V.	128
	Tables V.	131
	Figures V.	152
VI	<u>Short and Long-Range Effects: A Resolution</u>	
	A. General Method of Approach.	160
	B. Derivation of a Suitable Potential.	160
	C. Incorporation of the Potential in the Cluster Model: Approximate Methods.	163
	D. The Optimum Model ?	168
	E. Addendum: Experiment Versus Theory.	170
	References VI.	172
	Tables VI.	173

Summary

On the basis of a review of experimental data on electron trapping in crystalline ice and liquid water, it may be conjectured that these media trap electrons at defect sites, which may be present in some quantity naturally, and can be augmented by additives or radiative disruption. This work reports the results of theoretical investigations into structures and situations possibly favourable to electron capture.

Calculations are performed, using a flexible analytical wavefunction, on an electron trapped in a cavity in a linear, isotropic and homogenous dielectric in order to assess the contributions of long-range effects to electron trapping.

Attention is then focussed on the short-range effects due to the detailed nature of the trapping site. After a discussion on possible criteria for trapping, two possible structures of a water dimer are examined, using a minimal basis set in ab initio UHF SCF MO calculations. The behaviour of energies, spin densities and excitation energies as intermolecular distance varies is discussed and the relevance of each structure to electron solvation is considered.

This is succeeded by UHF INDO calculations on a water tetramer trapping site, using additional diffuse orbitals, and similar investigations on an $(\text{H}_2\text{O})_{12}$ cluster.

Other solvents are not neglected: the breathing modes of a methanol tetramer with up to eight molecules in two solvation shells are examined, and the behaviour of such structures with an excess electron considered. A larger basis set ab initio UHF calculation on an ammonia dimer illustrates the importance of hyperdiffuse orbitals in such treatments, and concludes that such a dimer in isolation will not stabilise a trapped electron.

Since non-regular geometries may be relevant, especially in the

initial capture of an electron, the umbrella vibration of NH_3 is studied by ab initio UHF methods, with and without hyperdiffuse orbitals; in the excess electron state, the effect of these latter is marked, but no evidence of stabilisation with respect to the neutral state is apparent.

Examination and discussion of all these results leads to several conclusions: (i) because of the essentially arbitrary nature of its parameterisation, the INDO method cannot yield definitive results on electron solvation.

(ii) some structures can be labelled as possible electron traps, and others can be considered unlikely. This is detailed in the text.

(iii) in all the structures studied, absolute energetic stabilisation with respect to the neutral state was not achieved; it is concluded that the long-range effects of the medium are an essential factor in stabilisation, and must be included in the SCF calculations.

The work concludes with an examination of the theoretical basis for molecular calculations which involve a surrounding dielectric medium, and identifies three main levels of approximation. The most sweeping of these is put forward as a useful guide to the magnitude of stabilisation energies, and suggestions for future work are made.

I

Experimental Clues: the Aims and Scope of this WorkA. Some Data on the Solvated Electron: the Nature of the Trapping Site in Water

Electron solvation in liquids has a long history.

Ever since the observation of the dissolution of sodium in liquid ammonia (1), observations on, and theorising about the phenomenon have mushroomed. Extensive reviews of all types of experimental observation of the species are plentiful (1-8). By restricting consideration to a few solvents, and examining information relating to the nature of the trapping site, one may gain insight on which to base theoretical studies. Such an approach is adopted in this work.

The e.s.r. spectrum of the excess electron in ice has been examined both in 2-5 M alkaline glasses (9), which cannot be very representative of ice structure, and in ice lightly doped with NH_4F (11, 12) and with alkali metal ions (10). The latter case shows an independence of the spectrum on the doping cation, especially at low concentrations, with an increase in resolution as the doping concentrations are lowered. The same effect obtains on gradual warming, and has been attributed to the removal of direct dipolar interactions as the trapped electron population diminishes. A quintet (9) or septet of lines, showing a uniform spacing of $\sim 5-6$ G and indicating interactions with four or six equivalent protons, is observed, and the role of the protons in the splitting is confirmed when deuteration causes collapse of the ^{HYPER-}fine structure, with narrowing of the electron resonance line. Such data suggest (a) a localisation of the trapped electron in ice on a small number of equivalently arranged water molecules, and (b) that the traps are not part of the regular ice structure, since the ion

concentration is found to regulate the spectral intensity.

Further confirmation of this latter point is provided by the work of Kawabata et al. (11-13). It was found during pulse radiolysis experiments that doping crystalline ice with 10^{-2} M NH_4F produced spectra with absorbances and optical decay properties identical to those of pure ice, but with up to a six-fold increase in optical density. Thus the solute appears to increase the number of trapping sites, without itself influencing the spectrum of the trapped species. Production of a defect centre is inferred, and comparison of NH_4Cl and NH_4OH dopings shows F^- to be the active agent.

Yet more evidence of the defect nature of traps in ice is provided by the repeated irradiation of 10^{-2} M NH_4F doped and pure D_2O crystalline ice (12). Successive irradiations at 106 K caused the optical density of absorption to increase by a final factor of about seven, while subsequent annealing at 143 K and recooling restored the original absorption characteristics. The inference here is that traps produced by radiation are "frozen" into the ice, with an energy barrier of ≤ 143 K (≤ 0.01232 eV). Whether many of these pre-exist in non-irradiated ice is still a moot point, with arguments for (14) and against (15). Probably, in low temperature ice, the number of thermally generated traps is small in any case.

The absence of a sudden discontinuity in the optical spectrum when the ice-water phase boundary is traversed (14) is interesting, and suggestive of the same defect-type trap in water, and of localisation of the electron, while a steady increase in e^- yields with temperature indicates easier trap formation. G for ice at 77 K is $\sim 10^{-4}$ - 10^{-3} , (4) comparing markedly with 2-3 for ordinary water (4) and suggesting increased trap production as the icelike structures fragment.

Solvation of the species in water is extremely rapid. Absorption

appears in the infra-red at ~ 2 p sec ⁽¹⁶⁾, and the complete spectrum, identical to that originally measured by Boag and Hart ⁽¹⁷⁾ is established at 4 p sec, although this time may be even smaller ⁽²⁵⁾. Such a result precludes gross rearrangement of a cluster by rotation or even vibration, but admits O-H group rotation ($\tau \sim 10^{-12}$ sec) ⁽¹⁸⁾ and electronic long-range relaxations.

It is of interest to note that the longer-term orientational polarisation of the medium has no effect on the optical spectrum.

Uniformity of traps in ice and water is also hinted at. The half-width of the optical absorption is rather small (~ 0.5 eV) ^(19, 20) and shows none of the anomalous "photo-shuttle" effects peculiar to alkaline glasses ^(14, 27), but photobleaches almost totally uniformly at all wavelengths ⁽¹¹⁾.

The evidence would seem to point to trapping in water and ice by a defect structure containing few molecules, which pre-exists before electron capture but may make some minor readjustments within ~ 4 p sec of the event. There is probably only one main type of trapping centre.

More data on the contributions of long and short-range interactions in water are provided by experimental studies of Jortner et al. ^(21, 22), where the optical spectrum of e_s^- was observed in D_2O vapour down to a density of 0.2 g cm⁻³. At ~ 663 K the optical peak shows only a slight blue shift on increasing density up to ~ 0.8 g cm⁻³, when it rises more sharply. Such data show localised trapping on a small cluster to be possible. The change in $h\nu$ at higher densities may indicate that the excited state wavefunction is raised more in energy on clustering than the ground state one. Since the ground state has been inferred to be localised, it may be that the electron becomes more diffuse, losing some of its long-range medium stabilisation energy, on excitation. However, since interactions in H-bonded water differ from those in the vapour phase, conclusions cannot be definite. Recently, some workers have

performed theoretical calculations on the electron affinity of an isolated water monomer, using a LCAO-MO-SCF formalism with the inclusion of diffuse orbitals (26, 28, 29).

Chipman (29) suggests that the monomer might have a positive electron affinity, at its regular geometry, but indicates that his present results are by no means conclusive.

A noteworthy point may be added. A shoulder in the ice spectrum, first noted by Shubin et al. (23) appears at about 2.3 eV. Independent observations of Kevan (24) show that photobleaching efficiency in γ -irradiated single crystal ice sets in sharply at 2.3 eV upwards. A transition to a bound state at the spectral peak of ~ 1.9 eV is implied, with transitions to the continua commencing at 2.3 eV, which would give the spectrum in ice (and water) the observed asymmetry characteristic of the species in most solvents. This shoulder is confirmed at 2.2-2.5 eV by Kawabata et al. (11b).

B. Aims and Scope of this Investigation

The above experimental data indicate the nature of possible trapping sites in water and ice, and the behaviour of electrons in these situations.

It was decided (a) to limit investigations of trapping and solvation to (i) water and ice (ii) ammonia (iii) methanol

(b) to examine theoretically the feasibility of trapping being due to short-range molecular forces alone, with due consideration being given to various types of structure, levels of approximation in calculation, and criteria for solvation

(c) to examine the effects of long-range interactions, such as polarisation, on solvation

(d) to combine the purely structural models and long-range formalism in an exact or approximate scheme, depending on the

complexity of the result.

In this thesis, we first examine the various methods used to describe long-range polarisation effects, and develop an analytical yet flexibly optimised expression for the energy of an electron in a dielectric. Short-range effects are then examined by a series of ab initio and modified INDO calculations on various small molecular clusters with and without an extra electron. It is concluded that even with the most flexible basis set, such calculations alone cannot model a trapped electron, despite the claims of some workers in the field.

Finally, the theoretical basis of a model combining long and short-range interactions is examined, exact and approximate analytical expressions being derived. Suggestions for future theoretical work are made.

10. J. J. Burdett, R. S. Stein and J. D. Dunitz, *J. Chem. Phys.*, **55**, 1111 (1971).

(a) L. Savolainen, *J. Chem. Phys.*, **51** (1971) 2672.

(b) H. Kawabata, S. Okabe and S. Taniguchi, *J. Chem. Phys.*, **52**, 2855.

Kawabata, S. Okabe and H. Morita, *Chem. Phys. Lett.*, **10**, 111 (1971).

Kawabata, S. Okabe and H. Morita, *Chem. Phys. Lett.*, **10**, 111 (1971).

11. J. J. Burdett and S. Hixon, *J. Chem. Phys.*, **55**, 2032 (1971).

(a) J. J. Burdett and G. J. Hochmader, *J. Chem. Phys.*, **55**, 2032 (1971).

References I

1. W. Weyl, Pogg. Ann., 121 (1864) 601.
2. F.S. Dainton, Endeavour, 26 (1967) 115.
3. U. Schindewolf, Angew. Chem., Int. Ed. 7 (1968) 7.
4. E.J. Hart and M. Anbar, The Hydrated Electron, Wiley, N.Y. 1970.
5. R. Catterall and N.F. Mott, Advan. Physics, 18 (1969) 665.
6. B.C. Webster and G. Howat, Radiat. Res. Rev., 4 (1972) 259.
7. (a) Metal-Ammonia Solutions, Colloque Weyl I, eds. G. Lepoutre and M.J. Sienko, W.A. Benjamin, N.Y. 1964.
- (b) Metal-Ammonia Solutions, Colloque Weyl II, eds. J.J. Lagowski and M.J. Sienko, Butterworths, London, 1970.
- (c) Electrons in Fluids, (Colloque Weyl III) eds. J. Jortner and N.R. Kestner, Springer-Verlag, Berlin, 1973.
- (d) Colloque Weyl IV, J. Chem. Phys., 79 (1975) No.26.
8. Electron-Solvent and Anion-Solvent Interactions, eds. L. Kevan and B.C. Webster, Elsevier, Amsterdam, 1976.
9. L. Kevan, J. Am. Chem. Soc., 87 (1965) 1481.
10. J.E. Bennett, B. Mile and A. Thomas, J. Chem. Soc., A (1969) 1502.
11. (a) K. Kawabata, J. Chem. Phys., 55 (1971) 3672.
- (b) K. Kawabata, S. Okabe and S. Taniguchi, J. Chem. Phys., 57 (1972) 2855.
12. K. Kawabata, S. Okabe and H. Horii, Chem. Phys. Lett., 20 (1973) 586.
13. K. Kawabata, H. Horii and S. Okabe, Chem. Phys. Lett., 14 (1972) 223.
14. I.A. Taub and K. Eiben, J. Chem. Phys., 49 (1968) 2499.
15. J.A. Ghormley and C.J. Hochanadel, J. Phys. Chem., 75 (1971) i.
16. P.M. Rentzepis, R.P. Jones and J. Jortner, J. Chem. Phys., 59 (1973) 766.

17. J.W. Boag and E.J. Hart, J. Am. Chem. Soc., 84 (1962) 4090.
18. S.K. Garg and C.P. Smyth, J. Phys. Chem., 69 (1965) 1294.
19. K. Eiben and I.A. Taub, Nature, 212 (1966) 1002.
20. O.F. Kodzhaev, B.G. Ershov and A.K. Pikaev, Izv. Akad. Nauk. SSSR Otd Khim. Nauk 1968, 246.
21. A. Gaathon, G. Czapski and J. Jortner, J. Chem. Phys., 58 (1973) 2648.
22. A. Gaathon and J. Jortner in Electrons in Fluids, ref.7(c).
23. V.N. Shubin, V.A. Zhigunov, V.I. Zolotarevsky and P.I. Dolin, Nature, 212 (1966) 1002.
24. L. Kevan, J. Phys. Chem., 76 (1972) 3830.
25. p.207, Ref.8.
26. B.C. Webster, J. Phys. Chem., 79 (1975) 2809.
27. G.V. Buxton, F.S. Dainton, T.E. Lantry and F.P. Sargent, Trans. Faraday Soc., 66 (1970)2962.
28. K. D. Jordan and J.J. Wendoloski, Chem. Phys., 21 (1977) 145.
29. D.M. Chipman, J. Phys. Chem., to be published.
30. J.C. Thomson, Electrons in Liquid Ammonia, O.U.P., 1976.

II

Long-Range Interactions - The Continuum ModelA. The Main Types of Treatment

Various methods have been evolved for the description of the excess electron in liquids and solids.

(i) The polaron model

One of the earliest schemes was the polaron model of Pekar ⁽⁵⁾, which (See Fig. II. A.1) treats the excess electron as a wavefunction localised in a continuous, linear, isotropic homogenous dielectric. Once localised, the electron orients the dielectric polarisation vector so as to deepen the trapping potential - this has been referred to as "digging its own hole." Such a model allows for the long-range effects of dielectric polarisation, but ignores any local structure in the vicinity of the trapped species. Although it is reasonable to treat a distant piece of the trapping medium as a continuous dielectric, the discrete nature of the solvent near the trapping centre must somehow be acknowledged. However, this approach has the advantage of mathematical simplicity.

(ii) The cavity continuum model

An improvement on this, due to Jortner ⁽¹⁶⁾, introduced the idea of an electron centred on a spherical cavity in a linear, homogenous and isotropic dielectric (See Fig. II. A.2). This treats the surrounding medium as continuous at a distance from the trapping centre, but allows for empty space near the centre of the charge distribution, as would be the case for an electron centred on a cluster of molecules. The idea of a cavity is also in accord with experimental data on volume expansion (1, 21, 22).

Refinement of the electronic wavefunction for this model (a) by

the author, using analytical methods (See Section II. E) and (b) by Carmichael and Webster ⁽²⁶⁾ has shown it to be surprisingly good at mimicking the gross energetic properties of the solvated electron.

(iii) The semicontinuum models

This refinement of the cavity continuum model generally consists of a dielectric containing a cavity as before, but with the inclusion of a number of dipoles within the cavity, in an attempt to simulate more detailed local interactions in the solvent (See Fig. II. A.3). Such models have been developed by Jortner et al. ^(8, 34) and Kevan et al. ^(29, 33), the included dipoles being treated as point multipoles, and the number within the cavity being varied from 4 to 12. Allowances can be made for temperature dependence by relating T to the average dipole direction via the Langevin equation, and more than one shell of dipoles can be included in the calculation. This model can be tailored to fit some experimental data with reasonable accuracy.

(iv) Other approaches

Methods involving inclusion of short-range effects by detailed SCF calculations on molecular clusters are dealt with in Chapters III - VI, and the methods of Iguchi ⁽²⁾ and Tachiya et al. ⁽³⁾ are discussed in Section II.F.

The present chapter examines in detail the methods and validity of the cavity continuum model, considering both the quasi-adiabatic and Hartree approaches. In Section II.E the author's own analytical wavefunction for the ground state of this model is described, and comments are made on the significance and applicability of the ensuing results.

B. Theory of Wavefunctions in Dielectrics

This section is devoted to a more rigorous derivation of the relevant energy terms in the cavity continuum models of solvated electrons. The full derivations are presented here, because papers in the field not only skim over the origins of the expressions, but also contain errors and ambiguities which still excite controversy (6, 7, 8, 11).

The analysis which follows will be in S.I. units, with modification to c.g.s. or a.u. as necessary.

It can be shown ⁽⁹⁾ that if an arbitrary charge distribution is assembled in the presence of dielectrics, then the total energy required to achieve this is

$$W = \frac{1}{2} \int \rho(\underline{r})V(\underline{r})d\tau \text{ ————— (II. B.1),}$$
 where $\rho(\underline{r})$ is the final free charge density at \underline{r} , and $V(\underline{r})$ the final potential at \underline{r} . In the case of point charges, to avoid singularities, we must employ the potential due to all the other charges, exclusive of the one whose position we consider, i.e.,

$$W = \frac{1}{2} \int \rho(\underline{r})V'(\underline{r})d\tau \text{ ————— (II. B.2),}$$
 where $\rho(\underline{r}) = \sum_i Q_i \delta(\underline{R}_i - \underline{r})$, \underline{R}_i being the position of the i th charge and $V'(\underline{R}_i)$ the potential at \underline{R}_i , due to all charges save Q_i .

The W term is evaluated with reference to the state where the dielectric is unmoved, but the charge distribution removed to infinity, and dissipated; it involves (a) the energy required to assemble the distribution in vacuo, (b) the energy required to polarise the dielectric and (c) the energy of interaction between the charge distribution and the induced dielectric polarisation.

$$W = E + \Pi + \epsilon \text{ ————— (II. B.3)}$$

Now the free charge distribution feels two potentials: one due to the other parts of itself, V_f , and one due to the induced charges in the dielectric, V_p .

$$\text{Thus } V = V_f + V_p$$

The self-energy of the free charge distribution is

$E = \frac{1}{2} \int \rho(\underline{r}) V_f(\underline{r}) d\tau$ ————— (II. B.4), and the energy due to the charge-medium interaction alone is

$$\begin{aligned} \epsilon = \Pi + \epsilon &= W - E = \frac{1}{2} \int \rho(\underline{r}) V(\underline{r}) d\tau - \frac{1}{2} \int \rho(\underline{r}) V_f(\underline{r}) d\tau \\ &= \frac{1}{2} \int \rho(\underline{r}) V_p(\underline{r}) d\tau \text{ ————— (II. B.5)} \end{aligned}$$

Similarly, the energy required to assemble the charge distribution in an already polarised dielectric, neglecting the self-energy term, is

$$\epsilon = \int \rho(\underline{r}) V_p(\underline{r}) d\tau \text{ ————— (II. B.6)}$$

so that Π , the energy to polarise the dielectric, is

$$\Pi = \epsilon - \epsilon = - \frac{1}{2} \int \rho(\underline{r}) V_p(\underline{r}) d\tau \text{ ————— (II. B.7)}$$

This polarisation energy, or medium rearrangement energy, represents the energy required to polarise and orient the molecules of the dielectric.

The successful evaluation of these terms depends on the calculation of V_p , and the difficulty reflects the complexity of the model chosen.

With a continuous dielectric extending over all space, one may write

$$\underline{F} = \underline{E} - \frac{\underline{D}}{\epsilon_0} \text{ ————— (II. B.8),}$$

where \underline{E} is the field due to all charges, $\frac{\underline{D}}{\epsilon_0}$ is the field due to the charges only (\underline{D} being the electric displacement vector), and \underline{F} is the net field due to the induced polarisation charges.

Thus $\underline{E} = \frac{D}{d\epsilon_0} - \frac{D}{\epsilon_0}$ (since in a linear, homogenous, isotropic

dielectric, $\underline{E} = d \epsilon_0 \underline{D}$, d being the dielectric constant).

$$\Rightarrow \underline{E} = -\frac{1}{\epsilon_0} \left(1 - \frac{1}{d}\right) D$$

$$\Rightarrow \nabla V_p = -\left(1 - \frac{1}{d}\right) \nabla V_f \quad \text{--- (II. B.9)}$$

$$\text{since } -\nabla V_p = \underline{E} \text{ and } -\nabla V_f = \frac{D}{\epsilon_0}$$

Boundary conditions thus ensure that

$$V_p = -\left(1 - \frac{1}{d}\right) V_f \quad \text{--- (II. B.10)}$$

Thus the total energy of the charge-dielectric system, excluding the self-energy of the free charge distribution, is

$$\underline{E} = \int \rho \psi = \frac{1}{2} \int V_p(\underline{r}) \rho(\underline{r}) d\tau = -\frac{1}{2} \left(1 - \frac{1}{d}\right) \int V_f(\underline{r}) \rho(\underline{r}) d\tau,$$

$$\text{i.e. } \underline{E} = \frac{1}{2} \left(1 - \frac{1}{d}\right) \langle \psi | V_f | \psi \rangle \quad \text{--- (II. B.11),}$$

if ψ is a wavefunction describing a negative free charge distribution.

The introduction of a cavity into the dielectric causes complication, since d is now a non-continuously differentiable function, and equation (II. B.10) will not, in general, apply. As is well known, ⁽¹⁰⁾ the potential $V_p(\underline{r})$ due to a dielectric medium with polarisation \underline{P} is

$$\begin{aligned} V_p(\underline{r}) &= \frac{1}{4\pi\epsilon_0} \int_{\underline{r}'} \frac{\underline{P}(\underline{r}') \cdot (\underline{r} - \underline{r}')}{|\underline{r} - \underline{r}'|^3} d\tau' \\ &= \frac{1}{4\pi\epsilon_0} \int_{\underline{r}'} \underline{P}(\underline{r}') \cdot \nabla_{\underline{r}'} \left(\frac{1}{|\underline{r} - \underline{r}'|} \right) d\tau' \quad \text{--- (II. B.12),} \end{aligned}$$

where the integration is over the volume of the dielectric.

Application of the vector identity

$$\nabla \cdot (f \underline{A}) = f \nabla \cdot \underline{A} + \underline{A} \cdot \nabla f, \text{ followed by the Divergence Theorem,}$$

yields

$$V_p(\underline{r}) = \frac{1}{4\pi\epsilon_0} \oint_{\mathcal{S}} \frac{\underline{P}(\underline{r}') \cdot d\mathcal{S}(\underline{r}')}{|\underline{r} - \underline{r}'|} - \frac{1}{4\pi\epsilon_0} \int_{\underline{r}'} \frac{\nabla_{\underline{r}'} \cdot \underline{P}(\underline{r}')}{|\underline{r} - \underline{r}'|} d\tau' \quad \text{--- (II. B.13)}$$

where τ is the volume of the dielectric, and \mathcal{S} is its bounding surface.

(We see that if the dielectric has no cavity, then the first integral becomes zero, and the second is merely $-(1 - \frac{1}{d})V_f$, providing we have a linear, isotropic, homogenous dielectric: see below). (Also, $d\mathcal{S}'$ points out of the dielectric by convention).

Thus we may replace the dielectric by a series of bound volume charges $\rho' = -\nabla \cdot \underline{P}$, and surface charges $\sigma' = \underline{P} \cdot \underline{\tilde{n}}$, where $\underline{\tilde{n}}$ is the unit normal vector pointing out of the dielectric ⁽¹⁰⁾. In the case of a cavity in such a medium, it is more convenient to use the unit normal vector pointing out of the cavity into the dielectric, $\underline{\tilde{n}}'$, and hence $\sigma' = -\underline{P} \cdot \underline{\tilde{n}}'$.

When the charge distribution is spherically symmetric and confined to the cavity,

$$\rho' = \nabla \cdot \underline{P} = (1 - \frac{1}{d})\nabla \cdot \underline{D} = (1 - \frac{1}{d})\rho_f = 0, \text{ the second integral}$$

vanishes and thus

$$\begin{aligned} * \quad V_p(\underline{r}) &= \frac{1}{4\pi\epsilon_0} \int_{\mathcal{S}'} \frac{\underline{P}(\underline{r}') \cdot d\mathcal{S}'(\underline{r}')}{|\underline{r} - \underline{r}'|} = -\frac{1}{4\pi\epsilon_0} \oint \frac{\underline{P}(\underline{r}') \cdot d\mathcal{S}'(\underline{r}')}{|\underline{r} - \underline{r}'|} \\ &= -\frac{1}{4\pi\epsilon_0} \oint_{\mathcal{S}'} \frac{P(r') d\mathcal{S}'(r')}{r_{>}} \end{aligned}$$

where $r_{>} = \max(r, r')$, (Spherical symmetry simplifies the $\frac{1}{|\underline{r} - \underline{r}'|}$ term)

and thus

$$\begin{aligned} V_p(r) &= -\frac{(1 - \frac{1}{d})}{4\pi\epsilon_0} \int_0^{2\pi} \int_0^\pi \frac{D(R_0)R_0^2}{r_{>}} \sin \theta' d\theta' d\psi' \\ &= -\frac{(1 - \frac{1}{d})}{\epsilon_0} \frac{D(R_0)R_0^2}{r_{>}}, \quad r_{>} = \max(r, R_0) \end{aligned}$$

Since $D(R_0) = \frac{Q}{4\pi R_0^2}$, where Q is the total charge contained

within the cavity,

$$V_p(r) = -(1 - \frac{1}{d}) \frac{Q}{4\pi\epsilon_0 r_{>}}$$

* the negative sign appears if we change our convention so that $d\mathcal{S}'$ points into the dielectric, that is, out of the cavity.

That is,

$$V_p(r) = -\left(1 - \frac{1}{d}\right) \frac{Q}{4\pi\epsilon_0 R_0} \quad \text{if } r \leq R_0, \quad \text{and } V_p(r) = -\left(1 - \frac{1}{d}\right) \frac{Q}{4\pi\epsilon_0 r} \quad \text{if } r > R_0$$

———— (II. B.13.a)

Thus, since the charge Q is contained in the cavity,

$$\epsilon = \frac{1}{2} \int \rho(r) V_p(r) d\tau = -\frac{1}{2} \left(1 - \frac{1}{d}\right) \cdot \frac{Q^2}{4\pi\epsilon_0}, \quad \text{or, in au,}$$

$$\epsilon = -\frac{Q^2}{2R_0} \left(1 - \frac{1}{d}\right) \quad \text{———— (II. B.14).}$$

If the charge is not confined to the cavity, but is permitted to be diffuse but still spherically symmetric, then Q above is replaced

by $\int_0^{R_0} \rho(r') r'^2 dr'$, and the second term of equation II. B.13 is non-zero, being

$$-\frac{\left(1 - \frac{1}{d}\right)}{4\pi\epsilon_0} \int_{\tau} \frac{\rho(r')}{r_{>}} d\tau', \quad \text{where } r_{>} = \max(r, r'), \quad \text{i.e.,}$$

$$-\frac{\left(1 - \frac{1}{d}\right)}{4\pi\epsilon_0} \left\{ 4\pi \int_{R_0}^r \frac{\rho(r') r'^2}{r} dr' + 4\pi \int_r^{\infty} \frac{\rho(r') r'^2}{r'} dr' \right\}$$

Thus

$$V_p(r) = -\frac{\left(1 - \frac{1}{d}\right)}{\epsilon_0} \left\{ \int_0^{R_0} \frac{\rho(r')}{r} r'^2 dr' + \int_{R_0}^r \frac{\rho(r')}{r} r'^2 dr' + \int_r^{\infty} \frac{\rho(r') r'^2}{r'} dr' \right\}$$

when $r > R_0$ ——— (II. B.15)

and $V_p(r) = V_p(R_0)$ when $r \leq R_0$. Thus, for the spherically symmetric case of the cavity model,

$$\left. \begin{aligned} V_p(r) &= -\left(1 - \frac{1}{d}\right) V_f(r) \quad \text{when } r > R_0 \\ &= -\left(1 - \frac{1}{d}\right) V_f(R_0) \quad \text{when } r \leq R_0 \end{aligned} \right\} \text{———— (II. B.16)}$$

which is of the same form as equation (II. B.10), and identical to it in the absence of a cavity. This resemblance exists because of the assumption of spherical symmetry, however, and is not a general one, since in non-spherical cases the surface integral loses the simple form of equation II. B.13.a.

We have, from the above potential

$$\xi = -\frac{1}{2}\langle\psi|V_p|\psi\rangle = \frac{1}{2}\left(1 - \frac{1}{d}\right)\langle\psi|V_f|\psi\rangle, \quad \text{--- (II. B.17)}$$

$$\xi = -\langle\psi|V_p|\psi\rangle \text{ and } \Pi = \frac{1}{2}\langle\psi|V_p|\psi\rangle,$$

where V_p is defined as in II. B.16.

Generally, for an arbitrary cavity in the medium,

$$V_p(\underline{r}) = \frac{1}{4\pi\epsilon_0} \left\{ \oint_S \frac{\sigma'(\underline{r}')d\mathcal{S}(\underline{r}')}{|\underline{r}-\underline{r}'|} + \int_{\tau'} \frac{\rho'(\underline{r}')d\tau'}{|\underline{r}-\underline{r}'|} \right\} \quad \text{--- (II. B.18a)}$$

where $\sigma' = -\underline{P}\cdot\hat{n}'$ and $\rho' = -\nabla\cdot\underline{P}$: $\underline{P} = \left(1 - \frac{1}{d}\right)\underline{D}$.

$$\therefore V_p(\underline{r}) = -\frac{\left(1 - \frac{1}{d}\right)}{4\pi\epsilon_0} \left\{ \oint_S \frac{\underline{D}(\underline{r}')\cdot d\mathcal{S}(\underline{r}')}{|\underline{r}-\underline{r}'|} + \int_{\tau'} \frac{\nabla\cdot\underline{D}(\underline{r}')d\tau'}{|\underline{r}-\underline{r}'|} \right\}.$$

Now, we may write the first integral as

$$I = \oint_S \frac{\underline{D}(\underline{r}')\cdot d\mathcal{S}(\underline{r}')}{|\underline{r}-\underline{r}'|} = \int_{\text{int}} \left\{ \nabla_{\underline{r}'}\cdot\left\{ \frac{\underline{D}(\underline{r}')}{|\underline{r}-\underline{r}'|} \right\} \right\} d\tau', \text{ where the integration}$$

is over the interior volume of the cavity.

$$\therefore I = \int_{\text{int}} \underline{D}(\underline{r}')\cdot\nabla_{\underline{r}'}\left\{ \frac{1}{|\underline{r}-\underline{r}'|} \right\} d\tau' + \int_{\text{int}} \nabla\cdot\underline{D}(\underline{r}') \frac{1}{|\underline{r}-\underline{r}'|} d\tau',$$

$$\text{i.e., } I = \int_{\text{int}} \underline{D}(\underline{r}')\cdot\nabla_{\underline{r}'}\left\{ \frac{1}{|\underline{r}-\underline{r}'|} \right\} d\tau' + \int_{\text{int}} \frac{\rho_f(\underline{r}')}{|\underline{r}-\underline{r}'|} d\tau'$$

$$\therefore V_p(\underline{r}) = -\frac{\left(1 - \frac{1}{d}\right)}{4\pi\epsilon_0} \left\{ \int_{\text{int}} \underline{D}(\underline{r}')\cdot\nabla_{\underline{r}'}\left\{ \frac{1}{|\underline{r}-\underline{r}'|} \right\} d\tau' + \int_{\text{all space}} \frac{\rho_f(\underline{r}')}{|\underline{r}-\underline{r}'|} d\tau' \right\} \quad \text{--- (II. B.18)}$$

$$\text{i.e., } V_p(\underline{r}) = -\left(1 - \frac{1}{d}\right)V_f(\underline{r}) - \frac{\left(1 - \frac{1}{d}\right)}{4\pi\epsilon_0} \int_{\text{int}} \underline{D}(\underline{r}')\cdot\nabla_{\underline{r}'}\left\{ \frac{1}{|\underline{r}-\underline{r}'|} \right\} d\tau', \quad \text{--- (II. B.19)}$$

which is the general expression for the potential due to medium polarisation. As before,

$$\xi = -\frac{1}{2}\langle\psi|V_p|\psi\rangle, \text{ where } V_p \text{ is represented by equation II. B.19.}$$

The second term is the one which causes difficulty, and it is convenient to assume either a spherical distribution of charge, or the absence of a cavity in most calculations, since the term then vanishes.

More subtle problems arise when the potential expressions are considered in the light of dielectric relaxation times and electron-medium correlation, and these are considered in the next section.

C. The Quasi-Adiabatic and Hartree-Fock Approximations

(i) Since the potential ~~field~~ acting on a trapped electron is dependent on the polarisation of the medium, the speed with which the medium polarisation can respond to instantaneous changes in the position of the trapped species is of great importance.

The total medium polarisation is comprised of three contributions (9)

(a) the polarisation due to electron-nuclear displacement; normally termed the optical, or electronic polarisation, this readjusts rapidly to electric field changes,

(b) that due to nuclear movements such as stretching and bending

(c) that due to rotation of molecules.

The disparity in relaxation times between (a) and (b) and (c) is such that we usually write

$\underline{P} = \underline{P}_e + \underline{P}_i$ (5, 6), where \underline{P}_e is the electronic polarisation, and \underline{P}_i the inertial, as represented by (b) and (c).

Now the trapped electrons will, in general, tend to be less strongly bound than the electrons of the medium molecules, and will therefore, by the Virial Theorem, have lower kinetic energies and velocities. If their binding energies are comparable with those of the medium electrons, then a Hartree-type wavefunction is in order (6, 13), but if the energies of the excess species are lower, they may not be able to follow the motions of the medium electrons (and hence the

fluctuations in \underline{P}_e), and the adiabatic approximation may be more apposite (5, 6, 13).

(ii) The (Quasi) Adiabatic Approximation

If the velocity of a trapped electron is so low that it cannot follow the motions of the medium electrons, then we may write (5) for the total wavefunction

$$\Psi(\underline{r}_m, \underline{r}_t) = \psi(\underline{r}_t) \chi(\underline{r}_m; \underline{r}_t), \quad \text{--- (II. C.1)}$$

where m refers to the coordinates of all the medium electrons, and t to those of the trapped electron. Thus ψ , the trapped electron wavefunction, has no specific correlation with the medium electrons, but the faster-moving medium electrons have a wavefunction depending on the position of the trapped electron.

Gourarary and Adrian (13) have shown that the usual adiabatic approximation, (14) involving particles of greatly disparate mass, is valid but that it cannot be rigorously proven for the case of two sets of electrons.

The approximation, when applied to the trapped electron case, they term the quasi-adiabatic approximation, and conclude that it is probably valid as long as the trapped electron does not spend much time within the atomic cores of the medium.

Thus, within the quasi-adiabatic approximation as adopted by Pekar (5) and the early papers of Jortner (15, 16), the inertial polarisation, \underline{P}_i , sees only the time-averaged distribution of the excess electron, whereas the electronic polarisation, \underline{P}_e , adjusts instantly to the species' motion. Since the potential well created by \underline{P}_e follows the trapped electron instantaneously, and is everywhere the same in a homogenous dielectric, it is a position-independent constant potential so long as the electron remains in the medium, and the energy of the electron/ \underline{P}_e interaction is independent of \underline{r} .

Now, if D_s is the static dielectric constant, and D_o the optical,

$$\underline{P} = \left(1 - \frac{1}{D_s}\right) \underline{E} \quad \text{--- (II. C.2)}$$

and $\underline{P}_e = \left(1 - \frac{1}{D_o}\right) \underline{E} \quad \text{--- (II. C.3)}$

and $\therefore \underline{P}_i = \left(\frac{1}{D_o} - \frac{1}{D_s}\right) \underline{E}$, and equation II. B.10 becomes

$$V_p = -\left(\frac{1}{D_o} - \frac{1}{D_s}\right) V_f, \text{ usually written } V_p = -\beta V_f$$

Thus equation II. B.11 would give

$$\epsilon = \frac{1}{2} \beta \langle \psi | V_f | \psi \rangle + K, \quad \text{--- (II. C.4)}$$

where the first term represents the electron/ \underline{P}_i interaction, and the second the electron/ \underline{P}_e one. This approach is still used by some authors (2a, 2b), but it has been pointed out (17) that whereas in F-centre theory, the binding energy of the excess electron is low and the quasi-adiabatic theory may be justified, solvated electrons in polar media have a greater binding energy of the order of 1-2 eV, precluding the use of this method.

(iii) The Hartree-(Fock) Approximation

A more suitable method for the situation where the medium and trapped electrons have comparable velocities is the Hartree-Fock method, well described elsewhere (13, 18). When the velocities of the two sets of electrons are comparable, the medium electrons will respond instantly to spatial shifts of the trapped electrons, and vice versa. Since a rigorous treatment of this correlation would involve configuration interaction methods, it is usually ignored, and the assumption made that the medium electrons see an averaged field due to the trapped electron, and vice versa, the wavefunction being written as

$$\underline{\Psi}(\underline{r}_m, \underline{r}_t) = \underline{\psi}(\underline{r}_t) \underline{\psi}(\underline{r}_m) \quad \text{--- (II. C.5)}$$

Since all exchange between the two sets of electrons is neglected, even that of a medium electron and a trapped one of opposite spin, this is more properly termed a Hartree approximation. The neglect of this "correlation polarisation" term is not serious if the trapped electron is not too diffuse (13, 17), i.e., if its binding energy is reasonably high.

It follows that in the Hartree Approximation both \underline{P}_i and \underline{P}_e see a time-averaged distribution of the trapped electron, and thus the self-consistent trapping potential contains a \underline{P}_i and a \underline{P}_e contribution; that is, \underline{P}_e no longer follows the detailed motion of the trapped electron, but provides a position-dependent trapping potential.

Equation II. B.11 becomes

$V_p = - (1 - \frac{1}{D_s}) V_f$ in this approximation, and the corresponding electron/medium energy

$$\epsilon = \frac{1}{2} (1 - \frac{1}{D_s}) \langle \psi | V_f | \psi \rangle,$$

or $\epsilon = \frac{1}{2} (\beta + \gamma) \langle \psi | V_f | \psi \rangle$, ——— (II. C.6)

if $\gamma = (1 - \frac{1}{D_0})$

Thus the essential difference between the two approximations is that the $\langle \psi | V_f | \psi \rangle$ term is preceded by β in the quasi-adiabatic case, and by $(\beta + \gamma)$ in the Hartree case (17).

D. History of Continuous Dielectric Type Models and Critique of Methods

Early theories of the solvated electron evolved from work on so-called F centres, that is, electrons trapped in defects in ionic crystals such as alkali halides (5, 13, 19, 20).

In a crucial paper on electron trapping in crystals, Landau (19) showed that local crystal disturbances can cause localisation of the normally diffuse and periodic electronic wavefunction; such a temporary trapping then intensifies the local polarisation field, which in turn reacts to deepen the potential trapping the electron. Such a self-sustaining process has been referred to as the electron "digging its own hole." This idea seemed naturally applicable to excess electron states in liquids, and when some of the volume expansion data on metal/ammonia solutions (1, 21, 22) was considered, a model involving electronic trapping in cavities in dielectrics was indicated. This approach was adopted by Ogg (4), who considered an electronic charge totally confined within a cavity of radius R_0 .

By equation II. B.14,

$\epsilon = -\frac{Q^2}{2R_0} \left(1 - \frac{1}{D_s}\right)$, and if the de Broglie wavelength of the particle is set equal to the cavity diameter,

$$\lambda = \frac{h}{p} = 2R_0 \Rightarrow p = \frac{h}{2R_0},$$

i.e., $E_{\text{tot}} = KE + \epsilon = \frac{h^2}{4R_0^2 \cdot 2m} - \frac{Q^2}{2R_0} \left(1 - \frac{1}{D_s}\right)$, or, in au,

$$E_{\text{tot}} = \frac{\pi^2}{2R_0^2} - \frac{1}{2R_0} \left(1 - \frac{1}{D_s}\right) \quad \text{--- (II. D.1)}$$

Neglecting $\frac{1}{D_s}$ and setting $\frac{dE_{\text{tot}}}{dR_0} = 0$ gives

$$R_0 = 2\pi^2 \text{ au} = 19.74 \text{ au}$$

and $E_{\text{tot}} = -\frac{1}{8\pi^2} \text{ au} = -0.013 \text{ au} = -0.34 \text{ eV}$.

Although this model predicts an overlarge cavity radius, it does highlight the rôle of long-range medium polarisation effects in electron trapping.

Other models were developed by the Russian school (5, 23, 24) in which F-centre ideas were taken over and generalised, that of Pekar being particularly advanced, in that he uses a fairly flexible analytical wavefunction for the electron and a self-consistent potential. No cavity is employed.

In his first paper (5a), he uses what we now recognise as the quasi-adiabatic approximation (See Section II.C) in treating an electron localised in a crystal, and derives a functional for the total energy of the electron and inertially polarised medium in the form of equation II. B.17, using

$$J(\psi) = E_{\text{tot}} = \langle \psi | -\frac{\nabla^2}{2} | \psi \rangle + \frac{1}{2} \left(\frac{1}{D_0} - \frac{1}{D_s} \right) \langle \psi | V_f(r) | \psi \rangle,$$

where $V_f(r) = - \int \frac{\psi'^2(r')}{|r-r'|} dr'$. Taking a function of the form

$$\psi = N (1 + ar + br^2) e^{-ar}, \quad \text{--- (II. D.2)}$$

Pekar's equations give*

$$a = 0.6585 \left(\frac{1}{D_0} - \frac{1}{D_s} \right); \quad b = 0.4516a^2; \quad E = -0.164 \left(\frac{1}{D_0} - \frac{1}{D_s} \right) \quad \text{--- (II.D.3)}$$

In a second paper (5b), in which he purports to give details of calculations for an inertially polarising medium, he involves the total medium polarisation, not merely the inertial part, in the SCF calculation, which is equivalent to using a Hartree-type approximation (See Section II.C) for the medium/excess electron interaction.

* Letting μ , the reduced mass of the electron equal the usual electron mass.

Thus

$$E_{\text{tot}} = \langle \psi | -\frac{\nabla^2}{2} | \psi \rangle + \frac{1}{2} \left(1 - \frac{1}{D_s}\right) \langle \psi | V_f(r) | \psi \rangle, \text{ and}$$

$$a = 0.6585 \left(1 - \frac{1}{D_s}\right); \quad b = 0.4516a^2; \quad E = -\left(2 - \frac{1}{D_s}\right)^2 0.164 \text{ au} \quad \text{---(II.D.4)}$$

is the result.

Although Pekar neglects the additive term due to the interactions with the electronic polarisation of the medium. In the first paper, and confuses his polarisation terms in the second, the method in the second paper is the best for the model chosen, and the wavefunction, as will be seen later (Section II.E) almost as flexible as necessary.

The synthesis of dielectric and cavity models was first performed by Jortner ⁽¹⁶⁾, in a quasi-adiabatic non-SCF cavity model of electrons solvated in liquid ammonia.

This uses energy expressions of the type

$$E' = \langle \psi | -\frac{\nabla^2}{2} | \psi \rangle + \epsilon$$

$$= \langle \psi | -\frac{\nabla^2}{2} | \psi \rangle + \left(\frac{1}{D_0} - \frac{1}{D_s}\right) \langle \psi | V_f | \psi \rangle$$

(See equations III. B.17), where, however, the SCF expression for V_f is not used, the simple one

$$V(r) = \left. \begin{array}{l} -\frac{\beta}{r} \quad r > R_0 \\ -\frac{\beta}{R_0} \quad r \leq R_0 \end{array} \right\} \text{being used instead (See equations II. B.13)}$$

(This potential assumes all the charge to be in the cavity).

Substitution of a single-parameter 1s type Slater function, $\sqrt{\frac{\mu^3}{\pi}} e^{-\mu r}$ for ψ , and minimisation of E' with respect to μ , gives a variational solution for the electronic energy in the field of the inertial polarisation. To this is added the inertial part of the medium rearrangement energy, Γ , and finally an electronic polarisation term which involves the total energy of interaction of the electron and

electronic medium polarisation.

Several flaws appear in this early model. The use of the quasi-adiabatic model for electrons in polar liquids has since been rejected by Jortner (17) in favour of a Hartree-type model, because of the greater velocity of such bound electrons. Tachiya (7) has recently criticised Jortner's use of the expression

$\pi = \frac{1}{2} \int_{R_0}^{\infty} \psi_{1s}^2 \left[\frac{\beta}{r} \right] 4\pi r^2 dr$, on the grounds that with the fixed potential $-\frac{\beta}{r}$,

the correct energy expression is

$$= \frac{\beta}{2R_0} \quad (\text{See equation II. B.14}).$$

This is true, but Jortner has improved on this by inserting a diffuse wavefunction in the fixed potential, and it would be far more inconsistent to compute ϵ as $\langle \psi | -\frac{\nabla^2}{2} | \psi \rangle + \beta \langle \psi | \frac{1}{r} | \psi \rangle$, but keep π as $\frac{\beta}{2R_0}$. However, Jortner himself points out (11) that his expression

$$\pi = \frac{1}{2} \int_{R_0}^{\infty} \psi_{1s}^2 \left[\frac{\beta}{r} \right] 4\pi r^2 dr \text{ is wrong, and that}$$

$$\pi = \frac{1}{2} \int_{R_0}^{\infty} \psi_{1s}^2 \left[\frac{\beta}{r} \right] 4\pi r^2 dr = \frac{\beta}{2} \langle \psi | \frac{1}{r} | \psi \rangle \quad (\text{See Equation II.B.17})$$

is the correct one.

Other objections may be noted:

(i) π , being dependent on ψ , should be included in the variational procedure

(ii) $E' + S^e$, where S^e (Jortner's notation) is the "contribution of the electronic polarisation to the energy" is quoted as the total single-particle electronic binding energy; S^e , however, given as $-\frac{\chi}{2\bar{r}}$, \bar{r} being the mean electronic radius, contains an implicit medium electronic polarisation term;

$E' - \frac{\chi}{\bar{r}}$ should be used, and the one electron E_{1s} and E_{2p} values quoted by Jortner are thus incorrect. However, the total energy,

$E = E' + S^e + \Pi^i$, (where the i is added to emphasise that this is the inertial part of the polarisation energy) $_e$, is not affected, since the extra Π^e term implicit in S^e combines with the Π^i to give Π , leaving a true electronic contribution to the electron/medium energy in S^e .

(iii) Under the adiabatic approximation, the electron should be treated as a point charge interacting with the electronic polarisation. Thus, when no cavity is present, $S^e = -\frac{\gamma}{2r}$ is a good approximation, or, when the electron is restricted to a cavity, $S^e = -\frac{\gamma}{2R_0}$, but the present situation is more complex. Fortunately, the abandonment of the adiabatic model removes this problem.

Later, a Hartree-type model was adopted by Jortner, in which these problems were overcome and the expressions III. C.6 were used, i.e.,

$$E_{\text{tot}} = \langle \psi | -\frac{\nabla^2}{2} | \psi \rangle + \frac{(A+\gamma)}{2} \langle \psi | V_f | \psi \rangle,$$

where

$$V_f(r) = \int_0^r \frac{\rho(r') dr'}{|\mathbf{r} - \mathbf{r}'|} \quad \text{if } r > R_0, \text{ and}$$

$$V_f(r) = V_f(R_0) \quad \text{if } r \leq R_0$$

Application of this to the ground state of water with

$$\psi_{1s} = \sqrt{\frac{\lambda^3}{\pi}} e^{-\lambda r} \quad \text{gives}$$

$$E_{\text{tot}} = -1.30^* \text{ eV at } R_0 = 0\text{\AA}, \text{ and } -0.91 \text{ at } R_0 = 3.3 \text{\AA}$$

A freshly excited 2p state is defined in which the wavefunction,

$$\psi_{2p} = \sqrt{\frac{\mu^5}{\pi}} r e^{-\mu r} \cos \theta \quad \text{is assumed to be affected by the original}$$

inertial 1s medium polarisation (which has not yet relaxed).

Spherically symmetric potentials are assumed in order to avoid the

difficulties of the second term of II. B.19. Estimation of $h\nu =$

$E_{2p} - E_{1s}$ gives 1.35 eV at $R_0 = 0\text{\AA}$ and 0.93 eV at $R_0 = 3.3 \text{\AA}$, with an

* Not 1.32 eV, as quoted in the original paper.

oscillator strength of ~ 1 at $R_0 = 0.0$, indicating that most of the spectrum is due to this transition. As the cavity radius decreases to zero, this model predicts an increase in the $1s \rightarrow 2p$ transition energy, up to 1.35 eV, which falls short of the experimental value of 1.72 eV, and indicates, unrealistically, a zero cavity radius.

It was realised by Kevan et al. (25) that a more flexible ground-state wavefunction might affect the results, and they used a linear combination of $1s$ and $2s$ type functions of the form

$$\Psi = N(\psi_{1s} + \alpha \psi_{2s}), \text{ obtaining a "heat of solvation"}$$

$H_s = 1.81$ eV (i.e., $E_{\text{tot}} = -1.81$ eV) and $h\nu = 2.18$ eV at $R_0 = 0$. It was also noted that $h\nu$ decreased as R_0 increased, but mathematical complexity debarred further calculation. Thus their results imply that the use of a more flexible wavefunction causes $h\nu$ to agree with the experimental value at a finite cavity radius.

It is clearly of interest to explore the limits of wavefunction flexibility, and this has been achieved by Carmichael and Webster (26), who used numerical wavefunctions of high accuracy, obtaining $H_s = 1.440$ eV and $h\nu_{1s \rightarrow 2p} = 1.529$ eV for water, at $R_0 = 0 \text{ \AA}$, a result more like that of Jortner (17) and Pekar (5) rather than that of Kevan et al. They have also pointed out that in evaluating the oscillator strengths of transitions, one should use the difference in single-particle energies of the states, not the difference in total energies, since the wavefunctions in the transition moment integral have the former, not the latter, as their eigenvalues.

$$f^l(1s \rightarrow 2p) \text{ is derived as } 0.714 \text{ and } f^v(1s \rightarrow 2p) \text{ as } 0.917.$$

While this work represents the limit to which such a model can be developed, it is nevertheless useful to have a simple analytical function which can be used in place of the numerical one at various cavity radii and in various media; such a model was developed by the

present author, and is described in section E, where long-range polarisation effects are investigated.

Obviously, the microscopic structure of a solvent near the zone of electron localisation will have a detailed effect which is not allowed for in the continuous dielectric type models, and this has led to the development of structural and semicontinuum models.

E. A Flexible Analytical Hartree Type Model: Long-Range Polarisation Effects

(i) Introduction

In this model, the Jortner Hartree-type approximation was used in conjunction with the flexible analytical wavefunction to obtain ground-state energies for the hydrated electron. While not as accurate as the numerical Carmichael and Webster function ⁽²⁶⁾, it was nevertheless found to be sufficiently close in the 1s state, and the analytical form allows for a more compact statement of the function.

(ii) Method

In the Hartree-type SCF model, the total energy is given by expressions II. C.6; i.e.,

$$E_{\text{tot}} = KE + \epsilon = \langle \psi | -\frac{\nabla^2}{2} | \psi \rangle + \frac{(\beta + \alpha)}{2} \langle \psi | V_f | \psi \rangle,$$

$$\text{where } V_f(r) = \int_0^r \frac{\rho(r')}{|r-r'|} dr' \text{ if } r > R_0$$

$$\text{and } V_f(r) = V(R_0) \text{ if } r \leq R_0$$

For the 1s state, a three-parameter wavefunction of the form

$$\psi = N_1(1 + ar + br^2)e^{-kr}$$

was used, where N_1 is a normalising factor, and a , b and k are adjustable parameters. Such a function is more flexible than that of Pekar ⁽⁵⁾, who used a two-parameter expression where $k = a$.

E_{tot} was evaluated using these equations, giving rise to an analytical expression; this was one of considerable complexity, containing some 10,000 terms. The expression for E_{tot} using a 3-parameter wavefunction is in fact so involved as to preclude analytical evaluation of this sort using 4 or more parameters.

Using an IBM 370/155 machine and a steepest descent minimisation programme specially written by the author, the values of a , b and k were optimised to yield the lowest value of E_{tot} for a given cavity radius, additional computations on medium polarisation energies, % change in cavity, etc., being performed at the same time.

The optical spectrum was studied by means of a similar calculation on a 2p state affected by the old inertial polarisation due to the 1s state, but the new optical polarisation due to the 2p state. (A Franck-Condon type transition).

The single parameter wavefunction

$$\psi_{2p_z} = N_2 r e^{-gr} \cos \theta$$

was employed.

(iii) Results

Optimised parameters, total energies and single particle energies for the ground state at various cavity radii are displayed in Table II. E.1.

The formulation of Pekar places E_{tot} at -1.45 eV when $R_0 = 0.0$, whereas this more flexible function gives an energy of -1.439 eV, a value upheld by the numerical Carmichael and Webster calculations (26). Slight error in Pekar's figures must be assumed. The present method is accurate for the 1s state, as is illustrated by its agreement with the numerical wavefunction, but allows simple definition of $\psi(r)$ because of its analytical form.

Decreasing the cavity radius seems to stabilise the system, as remarked by Jortner, with the greatest stability at $R_0 = 0.0$, which suggests at first sight a polaron model for the hydrated electron. Figure II. E.1 shows this energetic trend. Such a view is however naïve. Cross-cavity repulsion forces, such as those introduced in some of the semicontinuum models (8), will counteract a total collapse, stabilising the cavity at some interim radius. Naïve also is the assumption that the medium will behave like an isotropic, homogeneous or even linear dielectric at short range. However, it has sufficed to show that, under the assumptions made, an electron may remain trapped and will tend to localise further, with a concomitant lowering of E_{tot} until stopped by short-range repulsive forces.

Expansion of the cavity leads to a drop in the value of k , as shown by Table II. E.1 and Fig. II. E.2, indicating increasing diffuseness of the electron. Taken with Fig. II. E.3, the interrelation of cavity size and electron localisation can be seen; the trend is towards shrinkage of both the cavity and the electron distribution. More useful are the concepts of the mean charge radius,

$$\bar{r} = \langle \psi | r | \psi \rangle \quad \text{--- (II. E.1)}$$

and the percentage of charge within the cavity, given by

$$100 \int_0^{R_0} \psi^2 dr, \quad \text{--- (II. E.2)}$$

where R_0 is the cavity radius.

Table II. E.2 shows both these criteria. While trapped, the electron is fairly diffuse, this diffuseness, as gauged by \bar{r} , increasing with R_0 , as shown in Fig. II. E.3. Similarly, Fig. II. E.4 graphs $P^2(r) = r^2 R^2(r)$ normalised against R_0 for some cavity radii underlining the outward shift with increasing R_0 .

However, the percentage of charge retained in the cavity is seen

to increase with R_0 , reaching 50% at 4\AA° and 75% at 10\AA° (Table II. E.2). The cavity expansion overtakes the outward spread of the wavefunction.

Other data such as medium polarisation energies show a similar trend, lessening as R_0 expands, since the increasingly diffuse charge polarises the dielectric to a lesser extent; these trends are exhibited in Table III. E.3.

Similar SCF calculations on the 2p state (using a one-parameter wavefunction) assumed it to be freshly excited; that is, the medium electronic polarisation was allowed to relax, but not the slower inertial polarisation. This was assumed to be the situation obtaining immediately after a $1s \rightarrow 2p$ transition.

Thus the potential for the 2p state in au is

$$V_p(r) = -\left(1 - \frac{1}{D_0}\right)V_{f_{2p}} - \left(\frac{1}{D_0} - \frac{1}{D_s}\right)V_{f_{1s}}, \quad \text{--- (II. E.3)}$$

and the energy of the unrelaxed excited state is,

$$\begin{aligned} E_{2p} = & \langle \psi_{2p} | -\frac{\nabla^2}{2} | \psi_{2p} \rangle + \left(1 - \frac{1}{D_0}\right) \langle \psi_{2p} | V_{f_{2p}} | \psi_{2p} \rangle \\ & - \frac{1}{2} \left(1 - \frac{1}{D_0}\right) \langle \psi_{2p} | V_{f_{2p}} | \psi'_{2p} \rangle + \left(\frac{1}{D_0} - \frac{1}{D_s}\right) \langle \psi_{2p} | V_{f_{1s}} | \psi_{2p} \rangle \\ & - \frac{1}{2} \left(\frac{1}{D_0} - \frac{1}{D_s}\right) \langle \psi_{1s} | V_{f_{1s}} | \psi_{1s} \rangle, \end{aligned}$$

where the terms are, respectively, the kinetic energy, the electron/electronic polarisation interaction energy, the electronic polarisation energy of the medium, the electron/inertial polarisation interaction energy and the inertial polarisation energy of the medium.

Thus

$$\begin{aligned} E_{2p} = & \langle \psi_{2p} | -\frac{\nabla^2}{2} | \psi_{2p} \rangle + \gamma \langle \psi_{2p} | V_{f_{2p}} | \psi_{2p} \rangle + \beta \langle \psi_{2p} | V_{f_{1s}} | \psi_{2p} \rangle \\ E_{2p} = & \langle \psi_{2p} | -\frac{\nabla^2}{2} | \psi_{2p} \rangle + \underset{1s}{\gamma} \langle \psi_{2p} | V_{f_{2p}} | \psi_{2p} \rangle + \beta \langle \psi_{2p} | V_{f_{1s}} | \psi_{2p} \rangle \end{aligned}$$

where $\gamma = \left(1 - \frac{1}{D_0}\right)$ and $\beta = \left(\frac{1}{D_0} - \frac{1}{D_s}\right)$

As before, the energy E_{2p} was minimised with respect to the parameter g , and energies for various cavity radii obtained, as shown in Table II. E.4.

This time, as illustrated in Fig. II. E.5, an optimal cavity radius is in evidence at $\sim 6\text{\AA}$, corresponding to an energy of -0.379 eV. However, since the optical transition to the 2p state is assumed to be of Franck-Condon type, where the cavity radius and inertial polarisation do not have time to relax, this gives no clue as to the optimal R_0 for the ground state. One might expect (17, 25) to obtain such information by fitting the calculated optical absorption energy to the observed value of 1.72 eV for water at 300 K (27), but as Fig. II. E.6 shows, only at $R_0 = 0.0 \text{\AA}$ does $h\nu$ (1.56 eV) begin to approach this. That this is a feature of the model and not of the wavefunctions has already been illustrated by numerical calculations (26); the claim of Fueki, Feng and Kevan to have surpassed this limit with an analytic function (25) must be regarded with circumspection. The blue shift on compression illustrated in Fig. II. E.6 is in qualitative agreement with experiment (28).

Examination of g indicates increasing difuseness as R_0 increases, and examination of \bar{r} confirms this. Table II. E.5 indicates an expansion of the mean charge radius with R_0 , but shows it to be greater than the corresponding ground state 1s values. For instance, at $R_0 = 1.0 \text{\AA}$, $\bar{r}_{1s} = 2.25 \text{\AA}$, but $\bar{r}_{2p} = 4.30 \text{\AA}$, and at $R_0 = 10 \text{\AA}$, $\bar{r}_{1s} = 8.08 \text{\AA}$ while $\bar{r}_{2p} = 10.60 \text{\AA}$. Excitation, as would be expected, tends to expand the charge. The charge contained in the cavity (See Table II.E.5) is again correspondingly less, being 75.3% at $R_0 = 10 \text{\AA}$ for the ground state as against 51.0% for the excited state at the same radius. Such expansion is depicted in Fig. II. E.7, which illustrates the radial parts of the $2p_z$ function for different cavity radii.

(iv) Conclusion

Within its limitations, the model functions well. Trends in the energetics have been studied as the cavity size is varied, and the extent and degree of containment of the charge assessed. Values of the optical transition energies approach the experimental ones to a surprising degree for such a crude model, and the behaviour of $h\nu$ on compression is qualitatively reproduced. It should be noted that this is all obtained by the input of two experimentally observed parameters; the more complex semicontinuum models of some workers reproduce the data more accurately (8, 29, 30), but at the expense of a large number of both experimentally observed and arbitrarily adjustable variables; such models may mimic observation better, but their predictive value would be questionable.

However, while this model may duplicate some long-range effects quite well, it is inadequate for describing the detailed short-range effects due to the structure of the fluid and the properties of its constituent molecules. The continuum cavity SCF model has shown us that electron localisation in a dielectric is possible and has given us the approximate energies involved; it is for the structural models to provide details about short-range effects.

F. Footnote; Similar Models

Other methods of treatment, in a similar vein to those in this chapter, may be mentioned, namely the oriented dipole technique of Iguchi (2a, 2b) and the configuration coordinate model of Tachiya et al. (3a, 3b).

In the former model, Iguchi treats the medium as a large collection of discrete identical point dipoles, instead of as a continuous dielectric, and splits the polarisation contributions into a temperature-dependent orientation effect, which cannot follow the trapped electron, and a molecular polarisation part, which can. This is similar to the quasi-adiabatic approach, save that here the effects of molecular bonding are included in the quickly-relaxing part of the polarisation, rather than in the inertial part.

The field due to dipole orientation alone, $U(r)$, is obtained via

$$U(\underline{r}) = -e \int \frac{\underline{P}(\underline{r}') \cdot (\underline{r} - \underline{r}')}{|\underline{r} - \underline{r}'|^3} d\tau \quad \text{--- (II. F.1)}$$

(in c.g.s. units)

$$= -4\pi e \int_r^\infty P(r) dr \quad \text{--- (II. F.2)}$$

If P , due to the permanent dipole moment μ_0 alone, is radially symmetric.

Iguchi then obtains $P(r)$ via the Langevin equation (9), namely

$$P(r) = n_m \mu_0 \left(\coth \frac{\mu_0 E}{kT} - \frac{kT}{\mu_0 E} \right),$$

where n_m is the number of molecules per unit volume at the temperature T .

$n_m = n_0 (1 + a(T - T_0))$ is also assumed, where T_0 is 273 K.

Solution of $\left[-\frac{\hbar^2}{2m} \nabla^2 + U(r) - W \right] \Psi = 0$ gives the single-particle energy of the solvated electron trapped by the orientational

polarisation of the medium. Iguchi then adds the orientational medium polarisation energy,

$$\Gamma_{\text{dd}} = \iint \frac{P(\underline{r})P(\underline{r}')}{|\underline{r} - \underline{r}'|^3} d\tau d\tau' - 3 \iint \frac{P(\underline{r}) \cdot (\underline{r} - \underline{r}') P(\underline{r}') \cdot (\underline{r} - \underline{r}')}{|\underline{r} - \underline{r}'|^5} d\tau d\tau' \quad \text{--- (II F.3)}$$

which is the energy required to orient the dipoles against their mutual repulsion.

Finally, the total electron-medium energy due to molecular polarisation is added, this being

$$S_i^e = 4\pi e \int_{\bar{r}_i}^{\infty} P_{\text{mol}}(r') dr' = -2\pi e^2 n_m \frac{\alpha}{\bar{r}_i} \quad \text{--- (II. F.4)}$$

where \bar{r}_i is the mean radius of the orbital for the state i .

Quite good agreement with respect to heats of solvation, excitation energies, and temperature dependent spectral shifts is obtained by this method, but a further and more realistic attempt by Iguchi to introduce a cavity worsens agreement (2b).

Iguchi's method has the advantage of accounting for temperature dependence, but uses not merely an adiabatic type of approach, which is in some doubt (17), but one in which the whole of the molecular polarisability, instead of just the electronic part, is assumed to have an extremely small relaxation time.

Tachiya et al.'s configuration coordinate model is based on a different philosophy. They point out that the orientational polarisation determines the final energy, and that, since it relaxes more slowly than the electronic polarisation, one may construct a configuration coordinate diagram of energy versus polarisation just as one may construct diagrams of energy versus nuclear separation for a diatomic molecule. They point out two ways of obtaining the orientational polarisation energy: the expression of Jortner et al. gives

$$\Pi = 2\pi \left(\frac{1}{\epsilon_0} - \frac{1}{\epsilon_s} \right) \int P^2 d\tau \quad \text{--- (II. F.5)}$$

on a continuum model; the expression of Iguchi (2a) corrected by Tachiya (3c) gives

$$\Pi = \pi \int_{r>L} P^2 \left(1 - \frac{L^2}{4r^2} \right) d\tau, \quad \text{--- (II. F.6)}$$

where L is the distance between adjacent point dipoles, the energy being totally due to dipole-dipole repulsions. Tachiya et al. then observed that both of these have the form

$\Pi = \gamma \int P^2 d\tau$, and that γ is greater by a factor of three or four in the first expression.

They therefore proceed to perform the calculation so that the calculated heat of hydration of the electron is equal to the observed value of 1.7 eV, by adjustment of γ , obtaining an intermediate value of $\gamma = 5.5$.

They naturally suggest that the first expression overestimates and the second underestimates γ , but no explanation of the dichotomy is afforded. The present author suggests that equation II. F.5, derived in section II.B, is substantially correct, and that equation II. F.6, involving only the permanent polarisation of point dipoles and their repulsion energies, and neglecting the induced part of the inertial polarisation due to bending and stretching, gives only part of the total inertial polarisation Π . Thus, although a smaller value of Π , corresponding to $\gamma = 5.5$, will give a larger heat of hydration, it has been shown by Carmichael and Webster (26) that the continuum model in the Jortner formalism will not give a greater E_{tot} than 1.45 eV.

Furthermore, in the Tachiya model, the polarisation is varied until the lowest energy is obtained, whereas a Jortner-type model does this automatically. The Tachiya model may therefore be useful in

describing some unrelaxed states, but this author sees no reason for using it to calculate ground-state 1s or even inertially relaxed 2p states.

Of all the models surveyed in this chapter, it appears that the Jortner-type Hartree cavity model, as represented by Carmichael and Webster, and the author's own calculations, is the most defensible, if it is recognised that cross-cavity H-H repulsions and interactions at short range are ignored. However, the values of $H_g = 1.45$ eV as against the experimental 1.7 eV for H_2O are worrying. Any corrections such as the neglected repulsions would lower H_g , as would allowance for dielectric saturation effects. Further improvements seem to lie in the introduction of short range effects, which will slightly modify the powerful long-range trapping potential, and will also account for initial trapping, which occurs in $\lesssim 4 \times 10^{-12}$ sec for H_2O (31), a time much less than the relaxation time of the inertial polarisation.

References II

1. R.R. Hentz and D.W. Brazier, *J. Chem. Phys.*, 54 (1971) 2777.
2. (a) K. Iguchi, *J. Chem. Phys.*, 48 (1968) 1735.
(b) K. Iguchi, *J. Chem. Phys.*, 51 (1969) 3137.
3. (a) M. Tachiya, Y. Tabata and K. Oshima, *J. Phys. Chem.*, 77 (1973) 263.
(b) M. Tachiya, Y. Tabata and K. Oshima, *J. Phys. Chem.*, 77 (1973) 2286.
(c) M. Tachiya, *J. Chem. Phys.*, 60 (1974) 2275.
4. (a) R.A. Ogg, *J. Amer. Chem. Soc.*, 68 (1946) 155.
(b) R.A. Ogg, *Phys. Rev.*, 69 (1946) 669.
5. (a) S. Pekar, *Sov. J. Phys.*, 10 (1946) 341.
(b) S. Pekar, *Sov. J. Phys.*, 10 (1946) 347.
6. J. Jortner, *Mol. Phys.*, 5 (1962) 257.
7. M. Tachiya, *J. Chem. Phys.*, 56 (1972) 6269.
8. D.A. Copeland, N.R. Kestner and J. Jortner, *J. Chem Phys.*, 53 (1970) 1189.
9. C.J.F. Bottcher, *Theory of Electric Polarisation*, Elsevier, Amsterdam, 1973.
10. D. Corson and P. Lorrain, *Introduction to Electromagnetic Fields and Waves*, W.H. Freeman and Company, San Francisco, 1962.
11. J. Jortner, *J. Chem. Phys.*, 57 (1972) 587.
13. B.S. Gouraray and F.J. Adrian, *Solid State Physics*, 10 (1960) 127.
14. M. Born and K. Huang, *Dynamical Theory of Crystal Lattices*, p.402, O.U.P., New York, 1956.
15. J. Jortner, *J. Chem. Phys.*, 27 (1957) 823.
16. J. Jortner, *J. Chem. Phys.*, 30 (1959) 839.
17. J. Jortner, *Radiat. Res. Suppl.*, 4 (1964) 24.

18. J.C. Slater, Quantum Theory of Atomic Structure, Vols.I and II, McGraw-Hill, N.Y., 1960.
19. L. Landau, Phys. Z. Sowjet, 3 (1933) 664.
20. N.F. Mott and R.W. Gurney, Electronic Processes in Ionic Crystals: O.U.P., 1953.
21. W.N. Lipscomb, J. Chem. Phys., 21 (1953) 52.
22. U. Schindewolf, R. Vogelsong and K.W. Boddeker, Angew. Chem. Int. Ed. Engl., 6 (1967) 1076.
23. A.S. Davydov, Zh. Eksp. Teor. Fiz., 18 (1948) 913.
24. M.F. Deigen, Zhur. Eksp. Teor. Fiz., 26 (1954) 300.
25. K. Fueki, D-F. Feng and L. Kevan, Chem. Phys. Lett., 4 (1969) 313.
26. I.C. Carmichael and B.C. Webster, J. Chem. Soc., Faraday Trans. II, 70 (1974) 1570.
27. E.J. Hart and W.C. Gottschall, J. Am. Chem. Soc., 71 (1967) 2102.
28. U. Schindewolf in: Metal Ammonia Solutions, Proc. Colloque Weyl II, eds. M. Sienko and J.J. Lagowski, Butterworth, London, 1970.
29. K. Fueki, D-F. Feng, I. Kevan and R.E. Christoffersen, J. Phys. Chem., 75 (1971) 2297.
30. N.R. Kestner, Theory of Electrons in Polar Fluids in Electrons in Fluids, eds. J. Jortner and N.R. Kestner, Springer-Verlag, Berlin, 1973.
31. P.M. Rentzepis, R.P. Jones and J. Jortner, J. Chem. Phys., 59 (1973) 766.
33. K. Fueki, D-F. Feng and L. Kevan, J. Phys. Chem., 74 (1970) 1976.
34. A. Gaathon and J. Jortner in ref.30, p.429.
35. R.R. Hentz, Farhataziz and E.M. Hansen, J. Chem. Phys., 55 (1971) 4933.

TABLE II. E.1

1s ground state of cavity continuum model. Parameters and total energies

a	L	k	$R_0(\text{\AA}^c)$	$E_{\text{tot}}(\text{eV})$
0.6063810	0.1969609	0.6531700	0	-1.438575
0.6763780	0.1986580	0.6404009	1	-1.423945
0.5978920	0.2182389	0.5626110	2	-1.300962
0.5793020	0.2136630	0.4752800	3	-1.130322
0.5558500	0.1904120	0.4021659	4	-0.9814352
0.4913670	0.1792630	0.3520949	5	-0.8621777
0.5976689	0.1723440	0.3104540	6	-0.7657071
0.6175390	0.1685200	0.2798200	7	-0.6883588
0.5839710	0.3319310	0.2602119	8	-0.6201384
0.6611470	0.1281559	0.2276130	9	-0.5736178
0.5829020	0.3431480	0.2196810	10	-0.5241349

TABLE II. E.2

1s ground state of cavity continuum model.
Cavity radii, \bar{r} and % charge within cavity

$R_0 (A^0)$	$\bar{r}(A^0)$	% charge in cavity
0	2.248857	0
1	2.296614	9.040057
2	2.734307	30.56958
3	3.336785	45.76544
4	4.010876	54.79335
5	4.672568	61.23030
6	5.312502	66.24449
7	5.944705	70.06462
8	6.744312	71.36682
9	7.278027	74.27205
10	8.07716	75.33464

TABLE II. E.2

1s ground state of cavity continuum model. Potential, kinetic and medium polarisation energies

R_0 (Ao)	PE(eV)	KE(eV)	Inertial Medium Polarisation Energy(eV)	Optical Medium Polarisation Energy(eV)	Total Polarisation Energy(eV)
0	-5.8175375	1.4340181	1.6008177	1.2717752	2.8725929
1	-5.6675186	1.3745537	1.5595264	1.2389708	2.7984972
2	-4.5992622	0.9700944	1.2655754	1.0054407	2.2710161
3	-3.6219425	0.6581147	0.9966480	0.7917906	1.7884378
4	-2.9208508	0.4608194	0.8037294	0.6385254	1.4422541
5	-2.4428692	0.3440599	0.6722034	0.5340342	1.2062368
6	-2.0972443	0.2698672	0.5770976	0.4584771	1.0355740
7	-1.8359480	0.2181932	0.5051969	0.4013554	0.9065523
8	-1.6234102	0.1814671	0.4467130	0.3548926	0.8016056
9	-1.4584074	0.1465131	0.4013093	0.3188215	0.7201309
10	-1.3237906	0.1295247	0.3642666	0.2893929	0.6536595

TABLE II. E.4

2p excited state of cavity continuum model.Energies and exponent of wavefunction*

<u>g</u>	<u>R₀(A°)</u>	<u>ε_{2p}(eV)</u>
0.2864	0	0.12573
0.2846	1	0.09265
0.2641	2	-0.12162
0.2368	3	-0.27312
0.2108	4	-0.34688
0.1890	5	-0.37324
0.1716	6	-0.37856
0.1566	7	-0.37289
0.1442	8	-0.36350
0.1338	9	-0.35116
0.1249	10	-0.33789

$$* \quad \psi = N r e^{-gr} \cos \theta$$

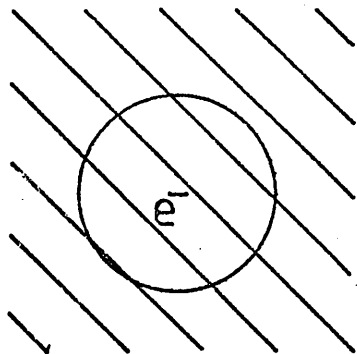
TABLE II. E.5

2p excited state of cavity continuum model. Effects of
cavity expansion on mean charge radius and % charge in cavity

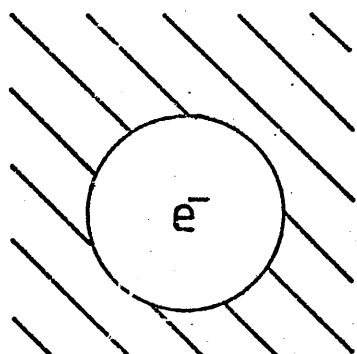
R_0 (Cavity Radius in A°)	\bar{r} (Mean Charge Radius in A°)	% Charge in Cavity
0	4.619	0
1	4.297	0.496
2	5.009	5.232
3	5.587	13.486
4	6.276	21.706
5	7.000	28.815
6	7.705	34.996
7	8.448	39.911
8	9.174	44.115
9	9.887	47.761
10	10.592	50.920

FIG. II. A.1

The Polaron Model

FIG. II. A.2

The Cavity Continuum Model

FIG. II. A.3

The Semicontinuum Model

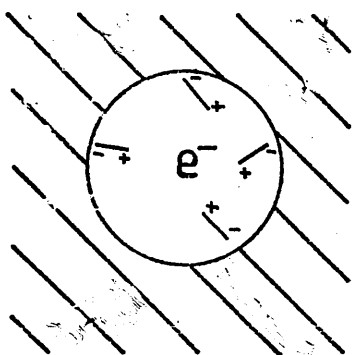
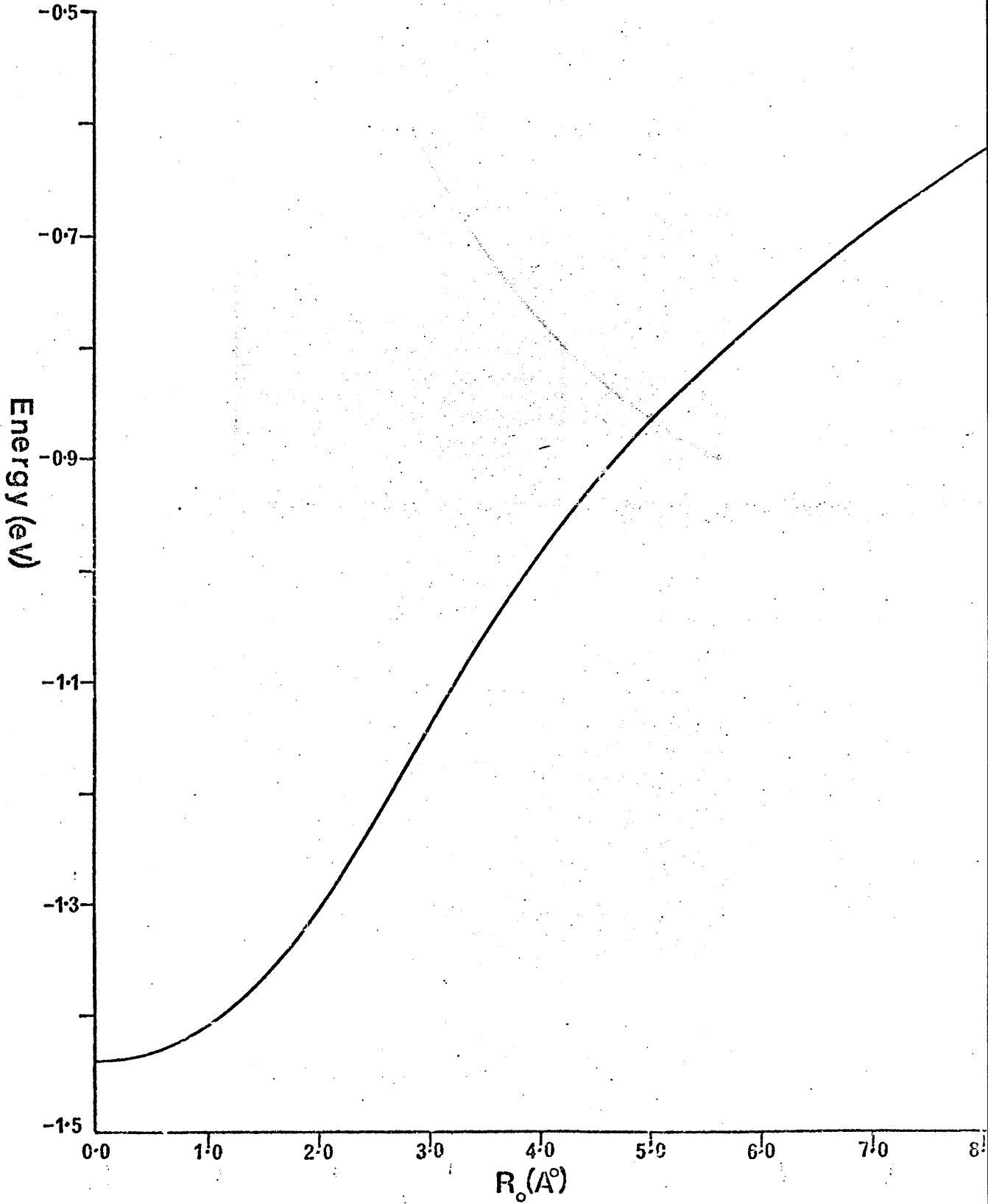
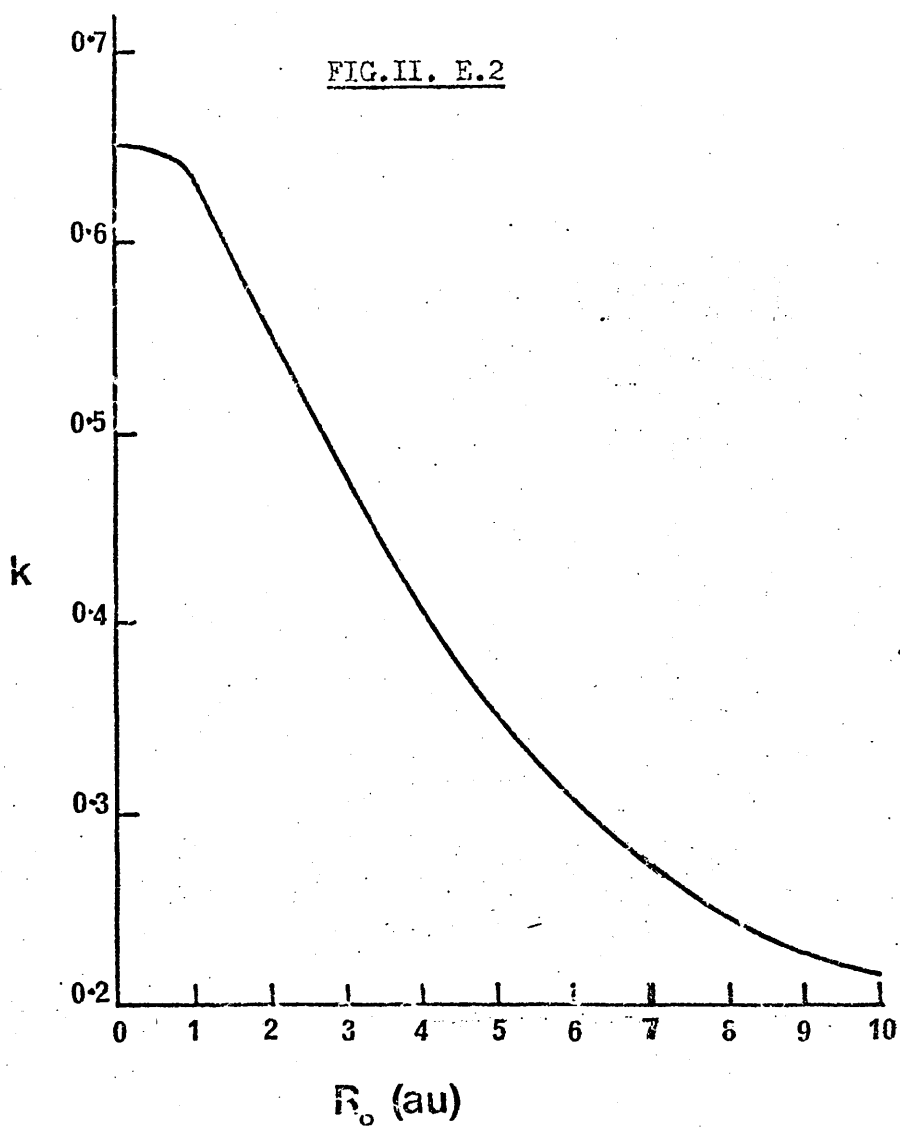


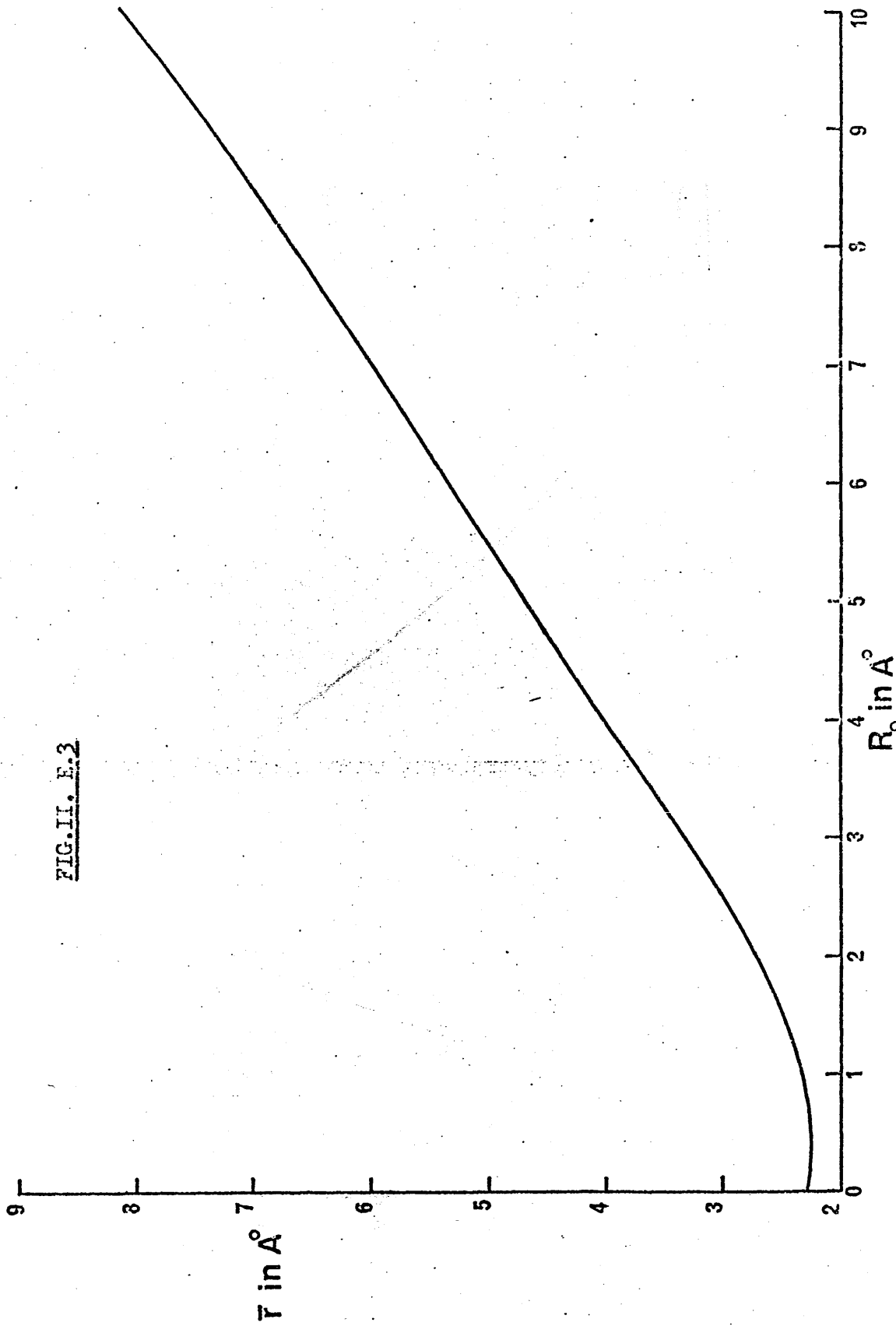
FIG. II. E.1

1s State of Cavity Continuum Model. Energy in eV Versus Cavity Radius in A° .



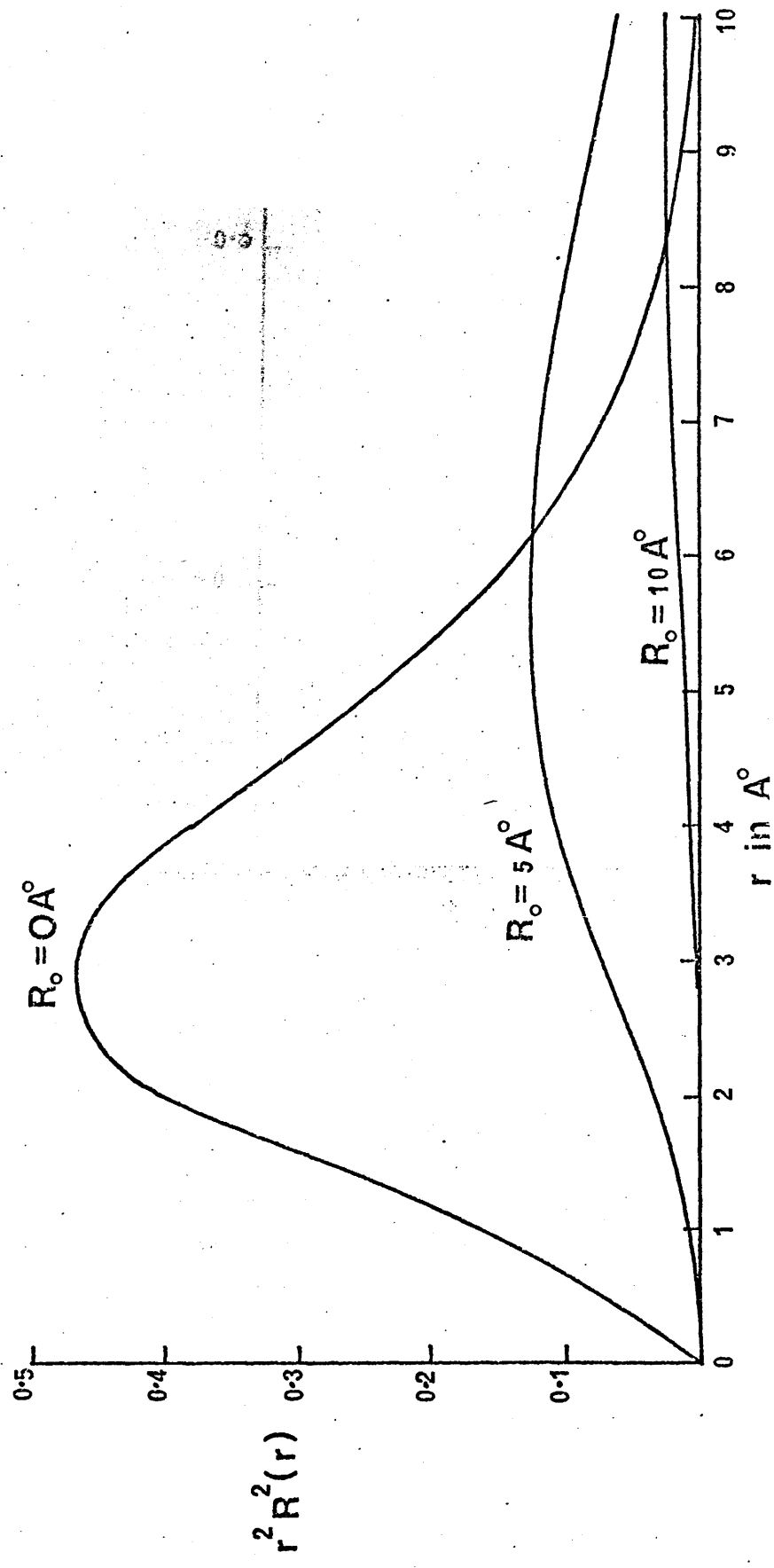


1s State of Cavity Continuum Model. k Versus R_0 .



1s State of Cavity Continuum Model. Mean Charge Radius (F) Versus Cavity Radius: (R_0)

FIG. II. E-4



1s Ground State of Cavity Continuum Model. $r^2 \times$ Radial Part of 1s Function Versus r for Different Cavity Radii.

FIG. II. E.5

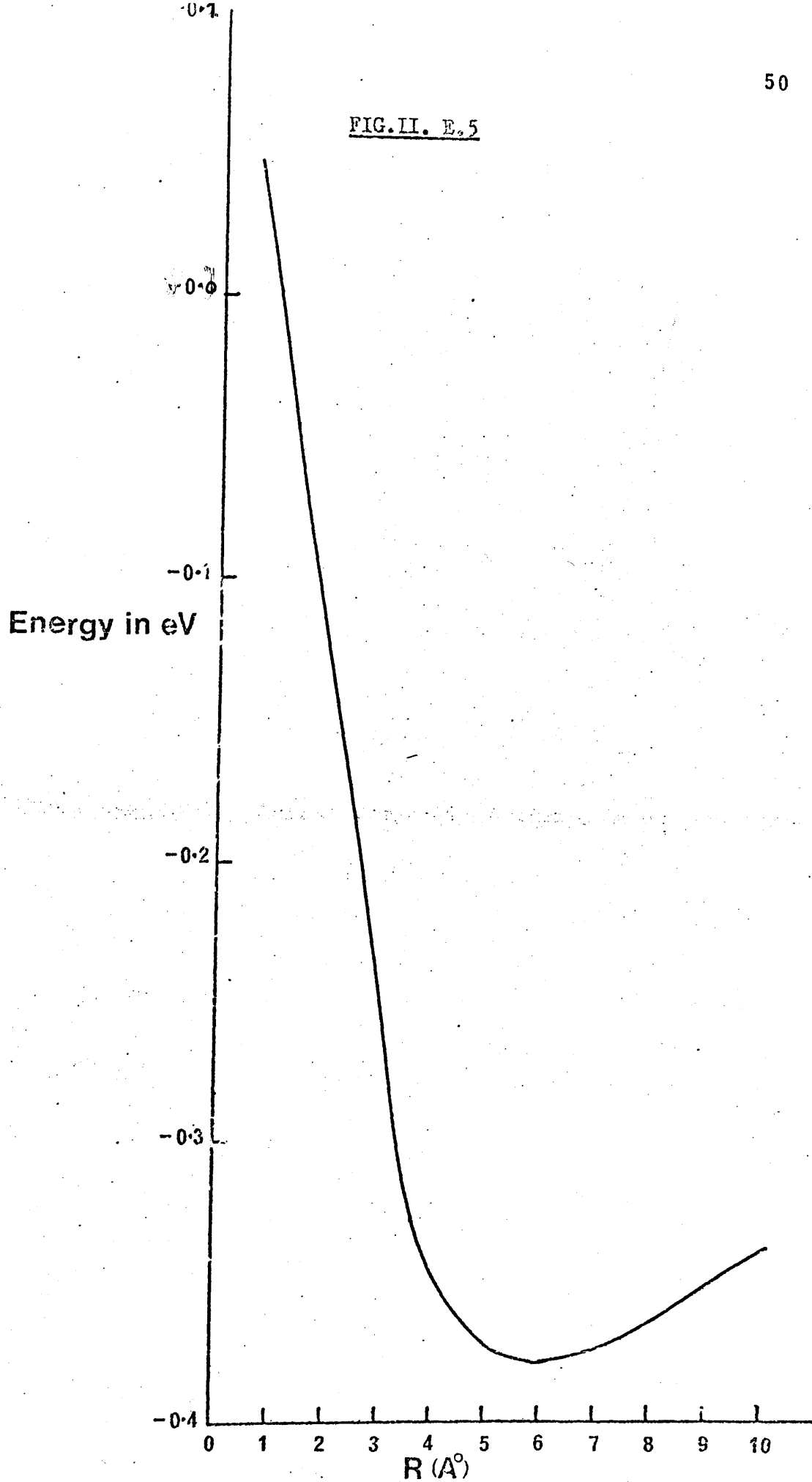
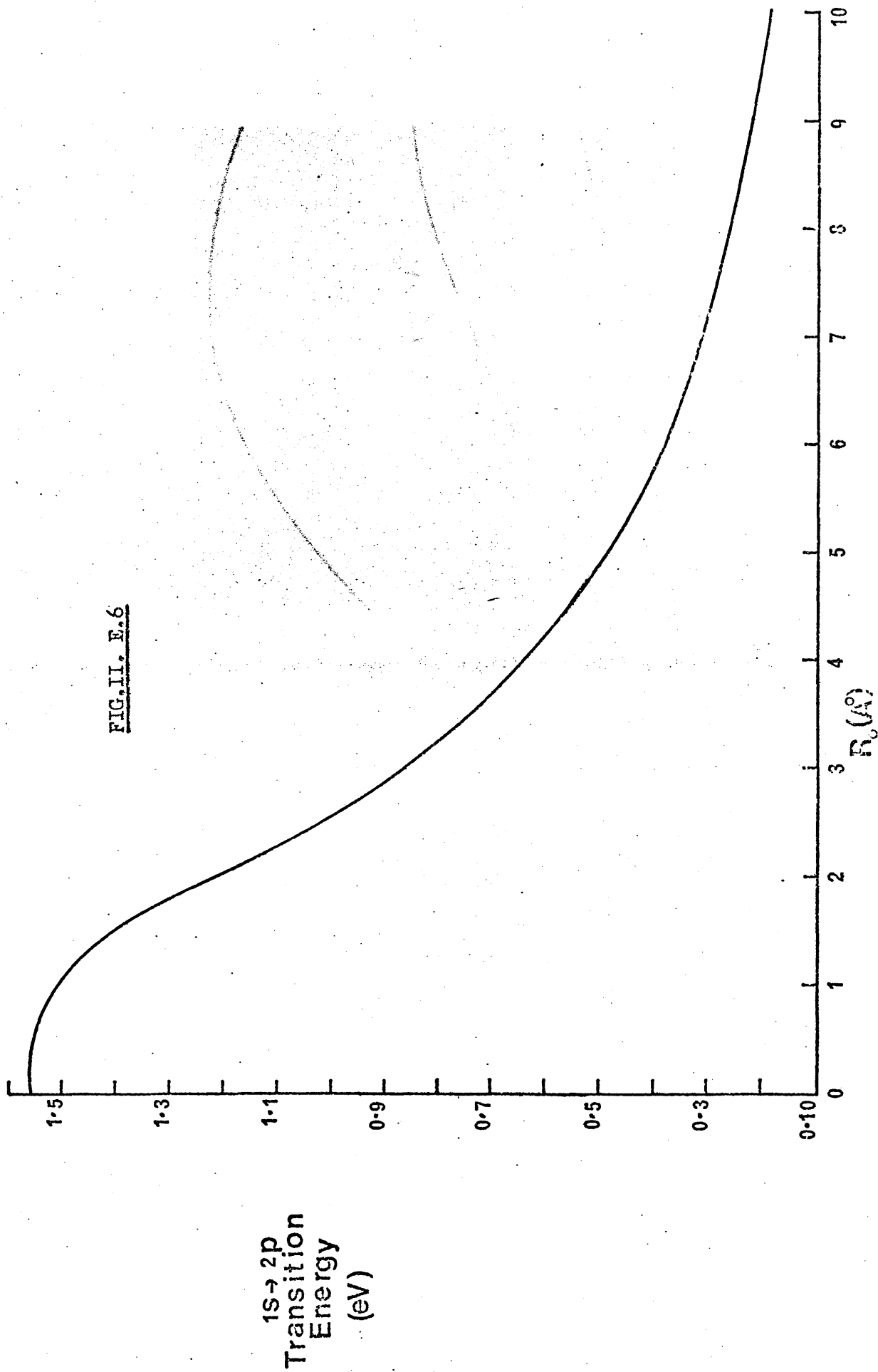
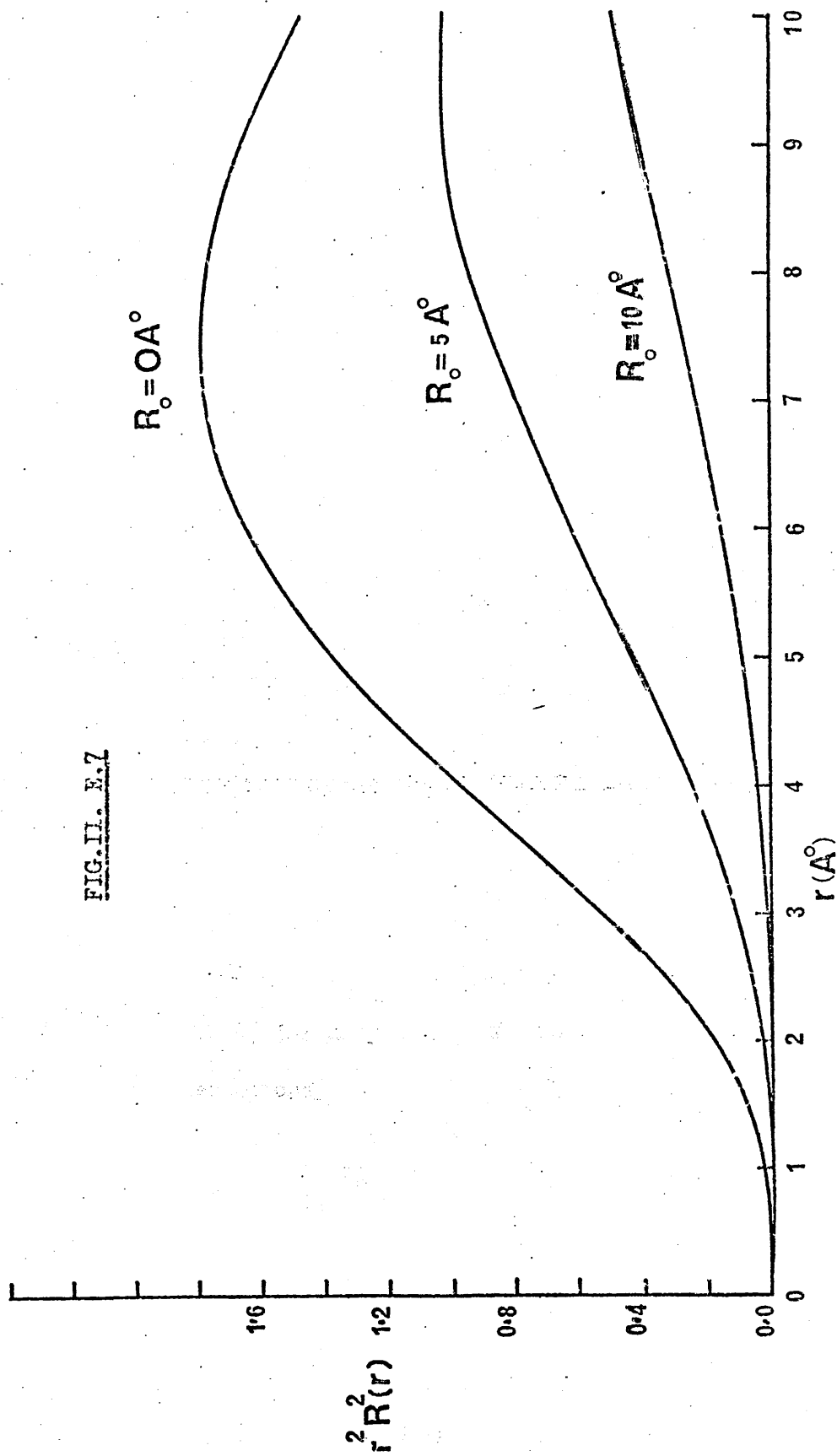
2p State of Cavity Continuum Model. Energy (eV) Versus Cavity Radius (\AA)

FIG. II. E. 6



1s → 2p
Transition
Energy
(eV)

R_0 (Å)



2p Excited State of Cavity Continuum Model. $r^2 \times$ Radial Part of $2p_z$ Function Versus r For Different Cavity Radii.

III

Self-Consistent Field Molecular Orbital TheoryA. Introduction

In order to prepare the way for the studies of short-range interactions via the structural models of the solvated electron, the general theory of ab initio and approximate SCF molecular calculations will be set out here. The study of open-shell cases will require some care and justification in its treatment.

B. Basic SCF Theory. The Hartree-Fock Method for Closed Shells

Solution of the Schrödinger equation (1),

$\mathcal{H}\Psi = E\Psi$, for molecules requires the construction of a molecular Hamiltonian. Classically, for an assemblage of n interacting particles,

$$H = \sum_{i=1}^n \frac{p_i^2}{2m_i} + V(1, 2, \dots, i, \dots, j, \dots, n),$$

where p_i and m_i are the momentum and mass, respectively, of the i th particle, and V is the energy of the system due to the particles' positions (2). Thus, for a system of N nuclei and n electrons, with no relativistic interactions,

$$H = \sum_{\alpha=1}^N \frac{p_{\alpha}^2}{2M_{\alpha}} + \sum_{i=1}^n \frac{p_i^2}{2m_i} + \sum_{\alpha=1}^N \sum_{\beta=1}^N \frac{Z_{\alpha} Z_{\beta}}{R_{\alpha\beta}} e^2 + \sum_{i=1}^n \sum_{j=i+1}^n \frac{e^2}{r_{ij}}$$

$$- \sum_{i=1}^n \sum_{\alpha=1}^N \frac{Z_{\alpha} e}{R_{\alpha i}} \quad , \quad \text{taking coordinates from the centre of mass.}$$

The quantum-mechanical Hamiltonian may now be obtained (3)

by the transformation $\mathbf{p} \rightarrow -i\hbar\nabla$, giving

$$\mathcal{H} = - \sum_{\alpha} \frac{\hbar^2 \nabla_{\alpha}^2}{2M_{\alpha}} - \sum_i \frac{\hbar^2 \nabla_i^2}{2m_i} + \sum_{\alpha, \beta} \frac{Z_{\alpha} Z_{\beta} e^2}{R_{\alpha\beta}} + \sum_{i < j} \frac{e^2}{r_{ij}} - \sum_{i, \alpha} \frac{Z_{\alpha} e}{R_{\alpha i}},$$

or, in atomic units,

$$\mathcal{H} = - \sum_{\alpha} \frac{\nabla_{\alpha}^2 m_e}{2M_{\alpha}} - \sum_i \frac{\nabla_i^2}{2} + \sum_{\alpha, \beta} \frac{Z_{\alpha} Z_{\beta}}{R_{\alpha\beta}} + \sum_{i < j} \frac{1}{r_{ij}} - \sum_{i, \alpha} \frac{Z_{\alpha}}{R_{\alpha i}}$$

Application of the Born-Oppenheimer approximation allows separation of the nuclear and electronic terms to give (2)

$$\mathcal{H}^e = - \sum_i \frac{\nabla_i^2}{2} + \sum_{i < j} \frac{1}{r_{ij}} - \sum_i \sum_{\alpha} \frac{Z_{\alpha}}{R_{\alpha i}} \quad \text{--- (III. B.1)}$$

Choice of a suitable electronic wavefunction will then affect the level of accuracy obtainable, the ideal function being one which treats the probability of the position of each electron as a function of the positions of all the others. Computational impracticability generally leads to the postulation of a similar wavefunction, in which the positional probabilities of all the electrons are treated independently, i.e.,

$$\Psi(1, 2, \dots, n) = \sqrt{\frac{1}{n!}} \begin{vmatrix} \Psi_1(1) \Psi_2(1) \dots \Psi_n(1) \\ \vdots \\ \Psi_1(n) \Psi_2(n) \dots \Psi_n(n) \end{vmatrix}$$

where Ψ_i is a single electron molecular orbital wavefunction, and the requisite antisymmetry with respect to particle exchange of Fermions is provided by the properties of the determinant (2). Since the Hamiltonian in III. B.1 is non-relativistic, it is purely spatial, and electron spin is commonly introduced by writing (4)

$$\Psi_i(j) = \psi_i(j) \eta(j), \quad \text{where } \psi_i \text{ is a spatial and } \eta \text{ a spin}$$

function. If $m_s = +\frac{1}{2}$, $\eta = \alpha$ and if $m_s = -\frac{1}{2}$, $\eta = \beta$.

Thus if we constrain pairs of electrons of opposite spin to occupy the same spatial orbitals, we have, for a closed shell configuration, a Restricted Hartree-Fock wavefunction:

$$\bar{\Psi}_{\text{RHF}} = \frac{1}{(2n!)^{\frac{1}{2}}} \begin{vmatrix} \psi_1(1)\alpha(1) \psi_2(1)\beta(1) \dots \psi_n(1)\alpha(1) \psi_n(1)\beta(1) \\ \vdots \\ \psi_1(2n)\alpha(2n) \dots \psi_n(2n)\beta(2n) \end{vmatrix} \quad \text{--- (III. B.2)}$$

usually written

$$\bar{\Psi}_{\text{RHF}} = \frac{1}{(2n!)^{\frac{1}{2}}} |\psi_1(1)\alpha(1) \psi_1(2)\beta(2) \dots \psi_n(2n)\beta(2n)| \quad \text{--- (III.B.3)}$$

The most common way of finding the eigenvalues of \mathcal{H}^e is the Hartree-Fock Self-Consistent Field Method (2, 3, 4, 5, 6), in which the expectation of \mathcal{H}^e is minimised with respect to the MOs ψ_i under the constraint that these MOs remain orthonormal.

i.e., $\langle \bar{\Psi} | \mathcal{H}^e | \bar{\Psi} \rangle$ is minimised with respect to all ψ_i , subject to $\langle \psi_i | \psi_j \rangle = \delta_{ij}$. This leads to an energy expression in which each electron is assumed to move in the average potential due to all the others, i.e.,

$$\begin{aligned} \bar{E} = & - \sum_i \int \bar{\Psi}^* \frac{\nabla_i^2}{2} \bar{\Psi} d\tau_1 \dots d\tau_n + \sum_{i < j} \int \bar{\Psi}^* \frac{1}{r_{ij}} \bar{\Psi} d\tau_1 \dots d\tau_n \\ & - \sum_i \sum_{\alpha} \int \bar{\Psi}^* \frac{Z_{\alpha}}{r_{i\alpha}} \bar{\Psi} d\tau_1 \dots d\tau_n. \end{aligned}$$

Indistinguishability of electrons implies that we may replace the i and j labels by, e.g., 1 and 2, and

$$\begin{aligned} \bar{E} = & - (2n) \int \bar{\Psi}^* \frac{\nabla^2}{2} \bar{\Psi} d\tau_1 \dots d\tau_n + \frac{1}{2} 2n(2n-1) \int \bar{\Psi}^* \frac{1}{r_{12}} \bar{\Psi} d\tau_1 \dots d\tau_n \\ & - \sum_{\alpha} Z_{\alpha} 2n \int \bar{\Psi}^* \frac{1}{r_{1\alpha}} \bar{\Psi} d\tau_1 \dots d\tau_n \end{aligned}$$

$$\Rightarrow \bar{E} = (2n) \langle \Psi | \mathcal{H}^c | \Psi \rangle + n(2n-1) \langle \Psi | \frac{1}{r_{12}} | \Psi \rangle, \text{ where } \mathcal{H}^c$$

is the core Hamiltonian.

Expansion of the Slater determinant and use of orthogonality gives

$$\bar{E} = 2 \sum_i H_{ii} + \sum_{i,j} (2J_{ij} - K_{ij}), \text{ where}$$

$$H_{ii} = \langle \psi_i | \mathcal{H}^c | \psi_i \rangle, \quad J_{ij} = \langle \psi_i \psi_j | \frac{1}{r_{12}} | \psi_i \psi_j \rangle \text{ and}$$

$$K_{ij} = \langle \psi_i \psi_j | \frac{1}{r_{12}} | \psi_j \psi_i \rangle.$$

The Coulomb integral, J_{ij} , represents the averaged electrostatic repulsion between MOs i and j , but the exchange integral, K_{ij} , is non-classical, arising from the use of an antisymmetric determinant (equation III. B.2) instead of a simple orbital product. As has been shown by Slater ^(2b) this term corrects for (a) the term J_{ij} , which includes a contribution for an electron in its own averaged potential and (b) the fact that the close approach of two electrons is very unlikely, although this "Fermi Hole" correction only operates on electrons of parallel spin, whereas ideally one should also allow for a "Coulomb Hole" which also prevents electrons of opposite spin from approaching too closely.

Subsequent variation of \bar{E} under the orthonormality constraint, using Lagrange's Method of Undetermined Multipliers ⁽⁷⁾ gives

$$F \psi_i = \sum_j \epsilon_{ij} \psi_j \quad \text{--- (III. B.4), where } \epsilon_{ij} \text{ is}$$

the matrix of undetermined multipliers, $\{\psi_k\}$ the MOs and F the Fock matrix, where

$$F = \left[\mathcal{H}^c + \sum_j (2J_j - K_j) \right], \quad \text{--- (III. B.5)}$$

and $J_j \psi_i = J_{ji}$, $K_j \psi_i = K_{ji}$.

Thus the problem can be reduced to a one-electron operator one, and equation II. B.4 is normally operated on via a unitary transformation (2, 6), which preserves the determinant III. B.2, since (8)

$$|U^{-1}AU| = |U^{-1}||A||U| = |U^{-1}||U||A| = |U^{-1}U||A| = |A|$$

This gives

(2b) $U^{-1}FU\psi_i = U^{-1}\epsilon U\psi_i$, and since ϵ is Hermitian by supposition there exists a unitary transformation which diagonalises it, giving

$$F\psi_i = \epsilon_i \psi_i, \quad \text{--- (III. B.6)}$$

the common form of the pseudo-eigenvalue Hartree-Fock equations.

It should be noted that an extra restriction is imposed on the transformation: since it is of the form

$$\Psi'_i = \sum_j c_{ij} \Psi_j, \quad \text{--- (III. B.7)}$$

where Ψ_j are spin-orbitals of the form $\psi_j(k)\zeta(m_k)$, then all the Ψ_j in B.7 must have $\zeta = \alpha$ or $\zeta = \beta$ if Ψ'_i is to be of the same form, i.e. the spin function must factorise out (9), and separate transformations for α and β spin orbitals, which do not mix orbitals of opposite spin, must be used.

In the closed-shell Hartree-Fock case this presents no problem, but in general such unitary transformations do not exist for open-shell RHF wavefunctions (10, 21) and the off-diagonal Lagrangian multipliers cannot be made to disappear.

Techniques employed to circumvent this include (i) ignoring the ϵ_{ij} (10, 11) (ii) the introduction of coupling operators (6b) and (iii) the Unrestricted Hartree-Fock Method (12, 4), which will be described later in this chapter.

C. The Roothaan-Hall Equations for Closed Shells

The solution of the Hartree-Fock equations may be performed numerically, but in the case of molecular systems it is more usual to express the MOs as linear combinations of complete sets of orthonormal basis functions ⁽⁶⁾, i.e.,

$$\psi_i = \sum_{\mu=1}^{\infty} C_{\mu i} \varphi_{\mu}, \text{ where } \langle \varphi_{\mu} | \varphi_{\nu} \rangle = \delta_{\mu\nu}, \text{ and as}$$

long as the conditions are satisfied, any complete set will suffice.

Impracticability constrains us to the use of partial summations of non-orthogonal functions, however, e.g.,

$$\psi_i = \sum_{\mu=1}^n C_{\mu i} \varphi_{\mu} \text{ ——— (III. C.1), and in this case the}$$

choice of functions is critical.

Substitution of III. C.1 into III. B.3 ^(3, 4, 6) and minimisation of \bar{E} with respect to each $C_{\mu i}$, under the constraints $\langle \psi_i | \psi_j \rangle = \delta_{ij}$, using the same methods, leads to

$$\sum_{\nu} (F_{\mu\nu} C_{\nu i} - \sum_j \epsilon_{ij} C_{\nu j} S_{\mu\nu}) = 0, \text{ ——— (III. C.2)}$$

$$\text{where } F_{\mu\nu} = H_{\mu\nu} + \sum_{\lambda\sigma} P_{\lambda\sigma} \left\{ (\mu\nu | \lambda\sigma) - \frac{1}{2} (\mu\lambda | \nu\sigma) \right\}, \text{ ——— (III. C.2a)}$$

$$P_{\lambda\sigma} = 2 \sum_{i=1}^{\text{occ}} C_{\lambda i}^* C_{\sigma i}, \text{ ——— (III. C.2b)}$$

(where the summation is over the occupied orbitals only)

$$\text{and } (\mu\nu | \lambda\sigma) = \iint \varphi_{\mu}(1) \varphi_{\nu}(1) \frac{1}{r_{12}} \varphi_{\lambda}(2) \varphi_{\sigma}(2) dr_1 dr_2 \text{ ——— (III.C.2c)}$$

If we again assume a Unitary Transformation which diagonalises ϵ_i , we obtain

$$\sum_{\nu} (F_{\mu\nu} - \epsilon_i S_{\mu\nu}) C_{\nu i} = 0, \text{ ——— (III. C.3)}$$

the Roothaan-Hall equations ^(6a, 13), whose validity depends on the feasibility of the Unitary Transformation on the matrix $C_{\nu i}$.

Further transformation gives the pseudo-eigenvalue equations

$$F' C' = C' E \quad , \quad \text{--- (III. C.4)}$$

where $F' = S^{-\frac{1}{2}} F S^{\frac{1}{2}}$ and $C' = S^{\frac{1}{2}} C$. Solution of the secular equation

$$|F'_{\mu\nu} - \epsilon_i \delta_{\mu\nu}| = 0 \quad \text{--- (III. C.5)}$$

gives the eigenvalues of the occupied MOs, and the eigenvectors (as columns of C') are then found by solution of

$$\sum_{\nu} (F'_{\mu\nu} - \epsilon_i \delta_{\mu\nu}) C'_{\nu i} = 0 \quad \text{--- (III. C.6)}$$

for each ϵ_i . Generally, equation III. C.5 is solved by numerical diagonalisation of F' , and III. C.6 yields the required coefficients.

The whole process, after a suitable set of basis functions has been chosen, consists of calculation of the one and two electron integrals used in III. C.2, and the construction of a density matrix via III. C.2b. The resulting Fock matrix is then transformed and diagonalised as described above, new eigenvectors are found, and the process repeated until the energy converges to a self-consistent value.

D. Treatment of Open Shells - the UHF Wavefunctions (3, 4, 6, 12)

In general, open shell calculations, as will be necessary for the investigation of molecular clusters dressed with an excess electron, present more problems than closed shell ones. Spin and spatial symmetry considerations require that for singlet states of diradicals we use more than one Slater determinant; He in the $1s^2 2s^1$ 1S configuration requires a wavefunction of the form

$$\Psi(1,2) = \frac{1}{\sqrt{2}} \left\{ 1s(1)2s(2) + 1s(2)2s(1) \right\} \left\{ \alpha(1)\beta(2) - \beta(1)\alpha(2) \right\} ,$$

i.e.,

$$\frac{1}{\sqrt{2}} \left\{ |1s(1)\alpha(1)2s(2)\beta(2)| + |1s(1)\beta(1)2s(2)\alpha(2)| \right\} .$$

However, any configuration with one electron outside closed shells (e.g., the excess electron molecular cluster models) will require only one Slater determinant.

Another disadvantage of the open-shell RHF wavefunction is that no valid Unitary Transformation preserving the RHF wavefunctions exists which may be used on equation III. A.4 to remove the off-diagonal Lagrangian multipliers (9), as was mentioned at the end of section III.B. Again, however, this difficulty does not arise with Unrestricted Hartree-Fock wavefunctions, where separate HF equations are solved for α and β electrons.

In the UHF method, the space parts of the wavefunctions are no longer constrained to be identical, and Ψ_{UHF} is written as

$$\Psi_{\text{UHF}} = |\psi_1^\alpha(1)\alpha(1)\psi_1^\beta(2)\beta(2)\dots\psi_n^\alpha(2n-1)\alpha(2n-1)|, \quad \text{--- (III.D.1)}$$

for a single excess electron. This leads (4, 12) to the equations

$$\sum_{\nu} (F_{\mu\nu}^\alpha - \epsilon_i^\alpha \sum_{\nu} S_{\mu\nu}) C_{\nu i}^\alpha = 0 \quad \text{--- (III. D.2)}$$

$$\sum_{\nu} (F_{\mu\nu}^\beta - \epsilon_i^\beta \sum_{\nu} S_{\mu\nu}) C_{\nu i}^\beta = 0 \quad \text{--- (III. D.3)}$$

where $F_{\mu\nu}^\alpha = H_{\mu\nu} + \sum_{\lambda\sigma} \left[P_{\lambda\sigma}^\alpha(\mu\nu|\lambda\sigma) - P_{\lambda\sigma}^\alpha(\mu\sigma|\lambda\nu) \right]$
 $F_{\mu\nu}^\beta = H_{\mu\nu} + \sum_{\lambda\sigma} \left[P_{\lambda\sigma}^\beta(\mu\nu|\lambda\sigma) - P_{\lambda\sigma}^\beta(\mu\sigma|\lambda\nu) \right],$
 which are solved as before.

The UHF method suffers from the disadvantage that the wavefunction is not an eigenfunction of S^2 , where $\underline{S} = S_{x\underline{i}} + S_{y\underline{j}} + S_{z\underline{k}}$ is the total electronic spin operator (14, 15), but it remains an eigenfunction of S_z . Although this may appear serious, the effect judged on ab initio computations by the present author, has been slight, values of ~ 0.76 instead of 0.75 being obtained for $\langle S^2 \rangle$.

E. Choice of Basis Sets

The truncated basis sets used in LCAO calculations should be chosen carefully, and many such sets have been developed, the criteria being that they give energy values sufficiently near the Hartree-Fock

limit and that they reproduce quite well properties such as spin and charge densities, dipole moments, bond lengths and angles, etc. Most basis sets are of the form $f(r)Y(\theta, \varphi)$, where $f(r)$ is a radial function, and $Y(\theta, \varphi)$ is a spherical harmonic; the form of $f(r)$ giving best results, namely the Slater function, ⁽¹⁶⁾ of form

$$f(r) = N r^{n-1} e^{-\zeta r} ,$$

does not give two-electron integrals capable of analytical evaluation, and more time-consuming numerical techniques must be employed.

Gaussian functions, of the form

$$f(r) = N r^n e^{-\alpha r^2}$$

with $Y(\theta, \varphi)$ sometimes written as $x^i y^j z^k$, where i, j and k are integers, were introduced by Boys ^(17, 18). These, although giving two electron integrals susceptible of analytical evaluation ^(17, 18, 19), require more functions, and hence many more integrals, to duplicate the effect of Slater functions.

Many other approaches have been used, such as the use of cusp functions ⁽²⁰⁾ and Floating Spherical Gaussians ^(21, 22), but the atom-centred Slater and Gaussian functions remain the most popular, and comparisons by Hosteny et al. ⁽²³⁾ on H_2O showed that the Slater-Type Orbitals (STOs) were suitable for the inner shells, while Gaussians were better for the valence shells, and hence for properties like potential surfaces, equilibrium geometries and excitation energies. Least-squares fitting of Gaussians to Slaters has also been tried by Pople et al. ⁽²⁴⁾ with marked success.

Most common in the literature is the optimised contracted basis set; this is derived from the ordinary optimised basis set of so-called primitive Gaussians ⁽²⁵⁾, which is normally unduly large for the SCF iteration procedure, and is usually contracted to a set of linear combinations of primitives ^(26, 27, 28) to reduce running time and

storage space. Choice of a basis set depends on balancing time considerations against accuracy, and even a very flexible basis set may give poor results for dipole moments and more esoteric properties (29).

Interwoven with the flexibility is the question of angular dependence. It has been shown, in the case of NH_3 , that the inversion barrier cannot be adequately predicted without the use of polarisation functions (30, 31, 32), and that bonding in some sulphur compounds (33) requires the consideration of d-orbitals. Care must therefore be taken to include polarisation functions in cases where the orbital hybridisation is likely to alter.

F. Approximate Methods - CNDO and INDO

(i) The CNDO scheme

The spectacular increase in availability of SCF *ab initio* methods in recent years has been offset by the vast demands such calculations make on computer resources, since the number of two-electron integrals required goes up as the fourth power of the number of basis functions.

Such problems have nurtured the semi-empirical methods, which simplify integrals by a combination of systematic neglect and semi-empirical parameterisation, enabling larger molecules to be tackled. In the wake of Parr's Zero Differential Overlap Approximation (34), Pople and co-workers produced various rotation-invariant approximation methods such as CNDO, INDO and NDDO, which increase in complexity as they do in usefulness.

Such methods rely basically on the neglect of two electron repulsion integrals involving overlap distributions over different atomic centres, and of the overlap integrals involved in normalisation of the MOs (35, 36). That is,

$$(\mu\nu|\lambda\sigma) = (\mu\mu|\lambda\lambda)\delta_{\mu\nu}\delta_{\lambda\sigma} \quad \text{--- (III. F.1)}$$

$$\text{and } \delta_{\mu\nu} = \delta_{\mu\nu} \quad \text{--- (III. F.2)}$$

where μ and ν must be on the same atom, and λ and σ must be on the same atom; in this way all three and four, and many two centre integrals may be removed. The one-electron integrals over the core Hamiltonian, which describe the bonding in the molecule, are constructed partly from experimental data.

Ideally, the observables obtained should be, as they are with the Roothaan equations, unchanged under a linear transformation of the basis set, that is, under rotation, hybridisation and symmetry combination, but the above expression does not guarantee this. Pople et al. have shown (35) that invariance under rotation and hybridisation can be assumed if equation (III. F.1) is written as

$$(\mu\nu|\lambda\sigma) = \delta_{AB}\delta_{\mu\nu}\delta_{\lambda\sigma} \quad \text{--- (III. F.3)}$$

$$\text{where } \delta_{AB} = (\mu_A \mu_A | \lambda_B \lambda_B) \quad \text{--- (III. F.4)}$$

is dependent only on atoms A and B, and not on the particular orbitals; it is an average repulsion term for electrons associated with atoms A and B.

Similar approximations are made for $H_{\mu\nu}$, namely (if μ and ν are both on atom A),

$$H_{\mu\nu} = \langle \mu | \mathcal{H}^c | \nu \rangle = \langle \mu | -\frac{\nabla^2}{2} - V_A | \nu \rangle - \sum_{B \neq A} \langle \mu | V_B | \nu \rangle, \quad \text{--- (III. F.5)}$$

where V_K is the potential due to the nucleus and core electrons of atom K.

$$\text{i.e., } H_{\mu\nu} = U_{\mu\nu} - \sum_{B \neq A} \langle \mu | V_B | \nu \rangle \quad \text{--- (III. F.6)}$$

$U_{\mu\nu} = 0$ by the spherical symmetry of V_A if the wavefunctions are non-hybrid unless $\mu = \nu$, and $\langle \mu_A | V_B | \nu_A \rangle$ is written, by analogy with III. F.4, as V_{AB} , the average potential on any valence electron of A due to the nucleus and core electrons of atom B.

$$\text{Thus } H_{\mu\nu} = U_{\mu\nu} \delta_{\mu\nu} - \sum_{B \neq A} V_{AB} \quad \text{--- (III. F.7)}$$

If μ and ν are on A and B, then some form of parameterisation is required, for

$$H_{\mu\nu} = \langle \mu | -\frac{\nabla^2}{2} - V_A - V_B | \nu \rangle - \sum_{C \neq A, B} \langle \mu | V_C | \nu \rangle \quad \text{--- (III. F.8)}$$

which, by the usual approximations, gives

$$H_{\mu\nu} = \langle \mu | -\frac{\nabla^2}{2} - V_A - V_B | \nu \rangle = \beta_{\mu\nu} \quad \text{--- (III. F.9)}$$

This, which requires empirical parameterisation, is a resonance integral (37) giving the energy of the two electrons in the field of the cores of A and B, and in the CNDO method, this is written as

$$\beta_{\mu\nu} = \beta_{AB}^0 S_{\mu\nu}, \quad \text{--- (III. F.10)}$$

where β_{AB}^0 is a solely atom-pair dependent parameter, this being simplified further via

$$\beta_{AB}^0 = \frac{1}{2}(\beta_A^0 + \beta_B^0). \quad \text{--- (III. F.11)}$$

Finally, these single-atom bonding parameters are fitted using *ab initio* calculation results with a minimal basis set.

Since the adjustable parameters, namely $U_{\mu\mu}$, V_{AB} , γ_{AB} and β_{AB}^0 may be specified in various ways, different schemes such as CNDO/1 and CNDO/2 have arisen, but neither of these directly concern the present work.

(ii) The INDO scheme

In studying excess electrons, one wishes to account for properties dependent on excess spin densities, and to allow for effects due to parallel and opposing spins. Since the two-electron exchange integral ($\mu\nu|\mu\nu$) is neglected in the CNDO schemes, spin densities in inner orbitals and separate states due to spin differences cannot be accounted for in this method.

In the INDO formulation, all the main approximations of CNDO are included, with parameterisation as in CNDO/2 with the exception that monatomic differential overlap in one-centre integrals is now retained (38, 39); that is, $(\mu\nu|\mu\nu)$ is retained, provided that μ and ν reside on the same atomic centre. The extra integrals are then evaluated in terms of Slater-Condon parameters (2) , which are obtained empirically, with the exception of F^0 , corresponding to γ_{AA} , this being evaluated analytically as it is in the CNDO/2 approximation. Similarly, Slater-Condon parameters also appear in the $U_{\mu\mu}$ expressions.

(iii) Extensions to the INDO scheme for solvated electron models

Since excess electron states prove to be fairly loosely bound and diffuse (40, 41) it is desirable to introduce some facility for including linear combinations of diffuse orbitals as extensions to the less than minimal INDO basis set. The present author has made alterations to the basic INDO programme of Pople and Beveridge, to enable floating spherical Slaters (FSS) to be used, as follows:

(a) Extra data on the new floating Slater are stored in the unused array space reserved for He atoms.

(b) γ_{AB} , evaluated in the INDO approximation as

$$\iint \psi_{s_A}^2(1) \frac{1}{r_{12}} \psi_{s_B}^2(2) d\tau_1 d\tau_2$$

is evaluated as usual if A, (or B, or both) is a floating spherical Slater.

(c) Since the FSS has only one 1s orbital, the integral such as $(sp_x | sp_x)$, which involve higher Slater-Condon parameters than F^0 , do not require computation for the FSS. Only $(ss | ss) = F^0 = \gamma_{AA}$ is used.

(d) V_{AB} , the potential on an electron of A when affected by the core of B, given in INDO as

$$V_{AB} = Z_B \int \psi_{s_A}^2(1) \frac{1}{r_{1B}} d\tau, \text{ is evaluated as usual, the } Z \text{ of the}$$

FSS being set to zero.

(e) $U_{\mu\mu}$, the energy of an electron in the field of its own core, is not set to zero, since the FSS electron possesses kinetic energy, but no nucleus.

Thus

$$U_{\mu\mu} = \langle \mu | -\frac{\nabla^2}{2} | \mu \rangle$$

$$\text{i.e., } U_{\mu\mu} = \frac{\gamma^3}{2},$$

where $\psi(r) = \frac{(2\gamma)^{3/2}}{2} e^{-\gamma r}$ is the FSS.

(f) by IV.F. 9, 10, 11,

$$H_{\mu\nu} = \langle \mu | -\frac{\nabla^2}{2} - V_A - V_B | \nu \rangle, \text{ when } \mu \text{ and } \nu \text{ are on different}$$

centres, and

$$H_{\mu\nu} = \beta_{\mu\nu} \approx \beta_{AB}^0 S_{\mu\nu} \approx \frac{1}{2}(\beta_A^0 + \beta_B^0) S_{\mu\nu};$$

it will be assumed, for want of a better criterion, that each β^0 atomic term involves about half the KE plus its own potential. Thus, for the floating Slater, we parameterise β_x^0 as

$$\frac{\gamma^3}{4}, \text{ which is probably slightly on the pessimistic side for}$$

bonding purposes, but we wish to avoid introducing non-existent strong bonding in calculations designed to adduce which structures are likely to trap an excess electron.

With these extra refinements, a set of floating Slaters, all with the same exponent, can be introduced into a cluster to examine the effects of greater diffuseness and flexibility of basis sets.

The study of excited open-shell states is also basic to solvated electron theory, and since Koopman's Theorem is in general invalid for

open-shell cases (3), a more rigorous evaluation of excitation energies was carried out; further modifications by the author were made to the INDO programme to allow SCF calculations on promoted electron states via reordering of MOs before the first calculation of the density matrix. The next chapter will include calculations using the above technique, as an aid to the study of short-range interactions.

Slater, J.C., *The Electronic Structure of Atoms*, Addison-Wesley, Reading, 1974.

and D.L. Beveridge, *Approximate Molecular*, McGraw-Hill, N.Y., 1970.

Slater, J.C., *Quantum Theory of Solids*, McGraw-Hill, N.Y., 1967.

Slater, J.C., *Quantum Theory of Solids*, McGraw-Hill, N.Y., 1967.

Slater, J.C., *The Principles of Physics*, Vol. 1, D. Van Nostrand, Princeton, N.J., 1950.

Slater, J.C., *Quantum Mechanics*, McGraw-Hill, N.Y., 1969.

Slater, J.C., *Quantum Theory of Solids*, McGraw-Hill, N.Y., 1967.

Slater, J.C., *Quantum Theory of Solids*, McGraw-Hill, N.Y., 1967.

Slater, J.C., *Quantum Theory of Solids*, McGraw-Hill, N.Y., 1967.

References III

1. (a) E. Schrödinger, Ann. Physik., 79 (1926) 361, 489, 734.
 (b) E. Schrödinger, Ann. Physik., 80 (1926) 437.
 (c) E. Schrödinger, Ann. Physik., 81 (1926) 109.
2. (a) J.C. Slater, Quantum Theory of Atomic Structure, Vol.I, McGraw-Hill, New York, 1960.
 (b) Vide supra, Vol.II.
 (c) J.C. Slater, Quantum Theory of Molecules and Crystals, Vol.I, McGraw-Hill, New York, 1963.
3. H.F. Schaefer III, The Electronic Structure of Atoms and Molecules, Addison-Wesley, Reading, 1972.
4. J.A. Pople and D.L. Beveridge, Approximate Molecular Orbital Theory, McGraw-Hill, N.Y., 1970.
5. R. McWeeny and B.T. Sutcliffe, Methods of Molecular Quantum Mechanics, Academic Press, London, 1969.
6. (a) G.C.J. Roothaan, Rev. Mod. Phys., 23 (1951) 69.
 (b) G.C.J. Roothaan, Rev. Mod. Phys., 32 (1960) 179.
7. H. Margenau and G. Murphy, The Mathematics of Physics and Chemistry, Vol.I, D. Van Nostrand, Princeton, N.J., 1956.
8. L.I. Schiff, Quantum Mechanics, McGraw-Hill, N.Y., 1949.
9. W.J. Hunt, T.H. Dunning Jr., W.A. Goddard III, Chem. Phys. Lett., 3 (1969) 606.
10. R.K. Nesbet, Proc. Roy. Soc., (Lon). A230 (1955) 312.
11. D.R. Hartree, The Calculation of Atomic Structures, John Wiley, 1957.
12. J.A. Pople and R.K. Nesbet, J. Chem. Phys., 22 (1954) 571.
13. G.G. Hall, Proc. Roy. Soc., (Lon). A205 (1951) 541.
14. A.J. Freeman and R.E. Watson, Magnetism, ed. G.T. Rada and H. Suhl, Academic Press, New York, 1965.

15. J.I. Musher, Chem. Phys. Lett., 7 (1970) 397.
16. J.C. Slater, Phys. Rev., 36 (1930) 57.
17. S.F. Boys, Proc. Roy. Soc., (Lon)., A200 (1950) 542.
18. S.F. Boys, Proc. Roy. Soc., (Lon)., A258 (1960) 402.
19. I. Shavitt, in Methods in Computational Physics Vol.II (1963)
eds. B. Alder, S. Fernbach and M. Rotenberg.
20. E. Steiner and B.C. Walsh in Quantum Chemistry - The State of the
Art, p.151, eds. V.R. Saunders and J. Brown.
21. A.A. Frost, J. Chem. Phys., 47 (1967) 3707.
22. S.Y. Chu and A.A. Frost, J. Chem. Phys., 54 (1971) 764.
23. R.P. Hosteny, R.R. Gilman, T.H. Dunning, A. Pipano, I. Shavitt,
Chem. Phys. Lett., 7 (1970) 325.
24. N.J. Hehre, R.F. Stewart and J.A. Pople, J. Chem. Phys., 51 (1969)
2657.
25. S. Huzinaga, J. Chem. Phys., 42 (1965) 1293.
26. J.L. Whitten, J. Chem Phys., 44 (1966) 359.
27. T.H. Dunning, J. Chem. Phys., 53 (1970) 2823.
28. T.H. Dunning, J. Chem. Phys., 55 (1971) 716.
29. M. Dixon, T.A. Claxton, J.A.S. Smith, J. Chem. Soc., Far. Trans.II
12 (1972) 2158.
30. R.G. Body, D.S. McClure and E. Clementi, J. Chem. Phys., 49 (1968)
4916.
31. A. Rauk, L.C. Allen and E. Clementi, J. Chem. Phys., 52 (1970) 4133.
32. R.M. Stevens, J. Chem. Phys., 55 (1971) 1725.
33. D.W.J. Cruickshank, B.C. Webster and M.A. Spinnler, Int. Jour.
Quant. Chem., 15 (1967) 225.
34. R.G. Parr, J. Chem. Phys., 20 (1952) 1499.
35. J.A. Pople, D.P. Santry, G.A. Segal, J. Chem. Phys., 43 (1965)
S129.

36. J.A. Pople, G.A. Segal, J. Chem. Phys., 43 (1965) S136.
37. Ref.4, p.59 ff.
38. J.A. Pople, D.L. Beveridge and P.A. Dobosh, J. Chem. Phys., 47 (1967) 2026.
39. R.N. Dixon, Mol. Phys., 12 (1967) 83.
40. M. Weissmann and N.V. Cohan, J. Chem. Phys., 59 (1973) 1385.
41. B.C. Webster, J. Chem. Soc., Faraday Trans.II, 73 (1977) 699.

of basis set requires equal caution. As

diffuse orbitals, which characteristically lower the

IV

Water Clusters - Short-Range InteractionsA. Introduction and Comments on Criteria for Solvation

Since the electron, in water and ice at least, is inferred to be localised on a few molecules, it may be valid to represent the short-range interactions by molecular SCF calculations, and the long-range ones by a continuous dielectric medium ⁽³⁴⁾. Short-range properties such as spin densities will then be mainly determined by the local structure, and long-range properties such as the total energy will be related to the medium polarisation field. For instance, a spherically disposed charge of one electron confined in a cavity of radius 3\AA in water will be stabilised to the extent of 1.1 eV by the optical polarisation alone, while total relaxation of the dielectric medium will yield 2.4 eV.

Thus a negative ion cluster may exceed the energy of its neutral species by up to 1.0 eV and still favour electron trapping; energetic criteria are therefore not an absolute measure of trapping ability, but may serve to grade clusters on a relative scale as possible trapping centres.

The choice of basis set requires equal caution. As has been pointed out by various workers ^(1, 2), a system which does not bind an excess electron will demonstrate a lowering in its energy as progressively more diffuse basis functions are added, approaching asymptotically from above the energy of the neutral state plus a free electron. In ab initio calculations on the solvated electron, the ideal should be to add to the basis set apposite to the neutral cluster a succession of diffuse orbitals, which invariably lower the energy of the negative ion state. If the energy of the excess electron state is below that of the neutral state, one may with caution infer a bound

stable state; if the converse is true, one may be observing either a drifting off of the electron or a stable but diffuse bound state; again, energetic criteria alone will not suffice.

However, if the eigenvalue of the excess electron MO is negative, or if its eigenvector does not possess its highest atomic orbital coefficient in the most diffuse MO, then we may tentatively assume binding. The spatial behaviour of the excess spin density, ρ^s , on addition of diffuse functions, may also provide a binding criterion. Similarly, fitting of calculations to experimental data such as solvation energies, optical absorption peaks^(1,3,4,5,7,17,22) and proton spin densities⁽¹⁰⁾ may be used as guides to a cluster's suitability, since these may be fairly insensitive to long-range effects. It should be noted that even a positive electron affinity, found with a flexible and adequate basis set, in a properly parameterised calculation, does not in itself imply solvation, since it may occur on a highly improbable part of the configuration curve for the cluster. Studies of energies versus configuration coordinates are more definitive than "single shot" evaluations.

B. Theoretical Models of Other Workers: Water Dimers and Larger Clusters

(i) Early models

Among the earlier and more approximate theoretical models are those of Raff and Pohl⁽⁶⁾, who considered H_2^+ perturbed by two hydroxyl ions, and McAloon and Webster⁽⁷⁾, who performed extended Hückel calculations on water and ammonia dimers. The latter results indicated that a dimer with Structure II (See Fig. IV. B.1) gave reasonable excitation energies, and delocalised spin densities, but displayed a red shift on compression, contrary to experimental

evidence (8).

A structure similar to I also displayed reasonable excitation *energies and compressional shifts but retained all its spin density on one molecule.

The famous structural model of Natori and Watanabe (9) (Structure III in Fig.IV. B.1) was treated using a linear combination of the four inner hydrogen 1s functions in the potential due to the O and H atoms, giving $h\nu \approx 0.80$ eV, and an estimated heat of solvation of ~ -2.4 eV. This, however, includes a term for the removal of a central H₂O from Structure III, whereas the evidence (see Section I) suggests that such defects are formed prior to electron capture, and neglects the long-range medium polarisation.

The natural continuation of such work is through better semiempirical results to an ab initio level, cost permitting, and this has been the recent trend.

(ii) A Spin Density Optimised Calculation

The INDO minimal basis calculations of Kerr and Williams (10) are interesting in that they make no attempt to use energy as a criterion, relying instead on fitting calculated ρ^s values for water structures to experimental results (11,12). All possible (H₂O)₂⁻ dimer structures were thoroughly studied, bond lengths and angles being optimised at each stage. None of the ρ^s approached the experimental result of total ρ^s on all protons, $\rho^s_H \leq 0.08$ (11,12,27), but some structures gave markedly lower total ρ^s_H than others (~ 0.2) and these were assumed to be the optimal conformations. The disparity between theory and experiment was still large, but may have been due to lack of a suitably diffuse and

* For one of the orientations

flexible set of basis orbitals. The Dimer structure most favoured was almost identical to Structure II, which may be used for all practical purposes: an O...O distance of 3.3\AA , an O-H length of 1.2\AA and a bond angle of 105° gave inner and outer proton spin densities of 0.091 and 0.018 respectively, or a total protonic spin density of 0.218.

A tetramer structure gave a value of 0.383, but not all possible tetramer structures were investigated.

No other properties, such as optical transition energies, were calculated, but it is of interest that the optimum dimer configuration for the excess electron state agrees with that obtained by Naleway and Schwartz (13), using energetic criteria.

(iii) Ab Initio Studies on Dimers

The work of Naleway and Schwartz consists of a similarly thorough search through possible dimer orientations, with calculation of total energies and electronic transition energies. Ab initio calculations were performed using a flexible double zeta Gaussian basis set (obtained by splitting off the most diffuse function from a serviceable set of contracted Gaussians) and a fixed H_2O monomer geometry of $R(\text{O-H}) = 1.80882 \text{ au}$ (0.957167\AA) and $\hat{\text{H}}\text{OH} 104.52^\circ$ (14).

The neutral case of Structure I displayed the lowest energy, confirming the results of Del Bene and Pople (15), at an O...O distance of 5.67 au (3.00\AA). The energies of the neutral and excess electron species were calculated as -152.0186 au and -151.7974 au respectively, with a transition of 2.21 eV to an excess electron excited state. On the other hand, in support of Kerr and Williams' findings, the most favoured structure for the excess electron state is Structure II, with O...O distance 7 au (3.70\AA) and energies of -151.9999 au and -151.8495 for the neutral and excess electron state. The electronic transition energy from the excess electron state was 2.48 eV, yet

further from the experiment value of 1.72 eV ⁽¹⁶⁾. Assessment of the effects of geometrical relaxation was made by stretching of the inner O-H bond, which revealed that for one geometry the energy of the excess electron fell below that of the corresponding neutral one. This fact, unnoticed by Naleway and Schwartz, has been graphed by the present author (see Fig.IV. B.2); the relevant energy reversal occurs at $R(\text{O-H inner}) = 2.42 \text{ \AA}$ (1.28\AA°).

However, examination reveals that the energetic minimum for this stretching is well above that of the neutral state by about 1.6 eV, demonstrating the necessity of examining more than one point on the configuration curve before forming conclusions about stability.

The same workers have also examined the effect of more diffuse basis sets, such as 3s on oxygen and (3s, 3p) on oxygen plus 2s on hydrogen. Such additions lower the energy of the excess electron state, but no corresponding excitation energies are quoted. This very thorough study of the water dimer, though informative as to favoured structures, gives no idea of the spatial behaviour of the excess electron as geometry and basis set are varied, nor of the dependence of the excitation energy on basis.

(iv) INDO Calculations on Dimers and Tetramers

The H_2O dimer has also been treated at an INDO SUHF level, using a minimal valence basis, by Howat and Webster ⁽¹⁷⁾, who carried out an investigation of Structure II, obtaining energies, spin densities and excitation energies. Using a geometry of $R(\text{O-H}) = 0.958\text{\AA}^\circ$, $\hat{\text{H}}\text{OH} = 104.45^\circ$ ⁽¹⁷⁾, they kept the monomer geometry fixed, varying the intermolecular separation. As in the Naleway and Schwartz studies, a configurational minimum appears in the excess electron state, this time at an O...O separation of 3.116\AA° , with energies of -38.4953 au and -38.2787 au (neglecting oxygen 1s energies) for the neutral and excess

electron states respectively. In accord with the neglect of most multicentre differential overlap integrals in the INDO method ⁽¹⁸⁾, spin densities on the various nuclei are evaluated by summation of the diagonal elements of the spin density matrix pertaining to each nucleus, neglecting off-diagonal contributions. The results are encouraging: spin delocalises over the cluster to the extent of 0.28 on O, 0.18 on the inner hydrogens, and 0.04 on the outer ones. While this gives a total $\rho_{\text{H}}^{\text{S}}$ of 0.440, as against 0.218 for the specifically spin-optimised calculations of Kerr and Williams, and the experimental result of ≤ 0.08 , it nevertheless confirms that spin delocalisation can occur on clustering. An excitation energy of 1.98 eV, with the expected compressional blue shift ⁽¹⁹⁾ is in reasonable agreement with experiment, especially since the excited-state energies were calculated by a non SCF repopulation of the MOs optimised for the ground state. Cycling to self-consistency would have been expected to lower this energy closer to the experimental 1.72 eV. A slight shift of spin density to the peripheral hydrogens is observed on excitation, with ρ^{S} values of 0.22, 0.15 and 0.13 on oxygen and the inner and outer protons, respectively, but since the values were obtained from a non-SCF calculation, their value is limited.

Further calculations by the same investigators on a wurtzite-like structure plus excess electron, generally similar to Structure I, elucidated that its ground state spin density resided almost entirely on one molecule, shifting to the other on excitation, providing, they suggest, a possible mechanism for photoconduction.

However, the Structure I-like model has excitation energies upwards of 5 eV, and a lack of delocalisation, making it an unlikely candidate for an electron trap.

While dimer studies are useful in predicting general trends, the experimental evidence, as has been shown, points to larger molecules. Building on the work of Natori and Watanabe ⁽⁹⁾, Howat and Webster have also performed minimal valence basis INDO computations on tetramer defect clusters of type III (see Fig.IV.B.1) and its equivalent, IIIa, when both H atoms on each water molecule point towards the centre. Energy curves for these electron states once again display a configurational minimum in the symmetric breathing mode of the cluster, at $R(\text{centre}-O) = 1.918\text{\AA}^{\circ}$ for Structure III, where the neutral and excess electron states have energies of -77.008 au and -76.524 au respectively, and at $R(\text{centre}-O) = 1.677\text{\AA}^{\circ}$ for Structure IIIa, which is reported to be less stable. Spin densities and excitation effects are more illuminating.

Both forms have total $\rho_{\text{H}}^{\text{S}}$ of 0.32 and 0.36 for III and IIIa, a result still far from ≤ 0.08 , but less than the dimer result, showing a spin shift to the oxygen centre on clustering. However, structure III has an excitation energy of 2.08 eV with a blue shift on compression, while IIIa displays 0.86 eV and a red shift on compression. While this is slightly worse than the dimeric result, it is clear that the compressional blue shift, and the expected lowering of $h\nu$ on SCF treatment of the excited state, will favour Structure III over IIIa.

(v) CNDO/2 Results on Tetramers

Extra basis functions have been added to larger clusters in the CNDO/2 calculations of Weissmann and Cohan ^(1,3), who examined Structures III and IV (see Fig.IV. B.1), along with some five-molecule chains. Since each structure has been examined only at its experimentally observed neutral geometry, the magnitude of any electron affinity obtained is subject to change as the structure relaxes, but the fact that Structure III, with $R(\text{centre}-O) = 2.76\text{\AA}^{\circ}$ has -79.495 au and

-79.514 au for its neutral and excess electron states shows a strong apparent tendency to electron capture. Structure IV, similarly, displays energies of -99.410 au and -99.441 au. Since also the lowest occupied MO of the negative ion states of Structures III and IV has eigenvalues of -0.39 eV and -0.57 eV, it appears that the excess electron state is the energetically preferred one, even when evaluated at a geometry more favourable to the neutral state. Weissmann and Cohan take these results as implying that a regular icelike structure is the favoured trapping site, and estimate from the eigenvalues an excitation energy of ~ 1.9 eV. The excited negative ion state is further inferred to be bound, provided that long-range polarisation effects the ground and excited states equally, and unbound otherwise.

However, their solvation energies appear to be at variance with experimental and other theoretical data, in the following way. The calculations indicate spontaneous electron trapping on isolated clusters containing upwards of four water molecules, the icelike pentamer (Structure IV) being particularly favoured to the extent of ~ 0.8 eV.

Now a crude estimate of the additional energy obtained from electron /long-range dielectric medium interactions would be $\gg 2.5$ eV (see Chapter VI), leading to a solvation energy of over 3 eV, discounting the cluster relaxation. The observed heat of solvation for water is 1.7 eV. More concretely, favouring a regular ice structure as a trapping site would make the large decrease in solvated electron yield as temperature is lowered ⁽²¹⁾ difficult to explain; furthermore, the structure disrupting F^- ion greatly increases the trapping ability of pure crystalline ice ⁽²⁰⁾. A defect model, on the other hand, fits these data, and the observations of Section I, more aptly. If the calculated energy drop is not realistic, this may be because of the parameterisation

chosen, or because the extra orbitals added were specifically optimised to fit the e^- state rather than the neutral one. It would be difficult not to obtain "solvation" in such circumstances.

(vi) SUHF INDO Calculations on Four and Six-Membered Clusters

Similar results are obtained by Fukui et al. (22), who performed cluster calculations using some diffuse functions at an INDO SUHF rather than a CNDO/2 level, on tetramer Structures III and IIIa, and on octahedrally disposed water molecules. 1s, 2s and 2p orbitals are centred in the model, after suitable parameterisation of the γ s (the Slater exponents) and β^A , the partial resonance integrals (see Chapter III) for the functions; these are arranged empirically to fit the observed proton spin densities, ρ_H^S , and to fit the energy of the highest occupied orbital in the negative ion state to the observed solvation energy. As already discussed, the first criterion (ρ_H^S) is relevant, but there is no a priori justification for fitting the ionisation potential of the isolated cluster to the observed property of solvation energy. Furthermore, there is some dubiety about the idea of calculating spin densities using a method parameterised by means of these quantities, and the same argument applies to conclusions about solvation energies.

Results using the most flexible basis (extra 1s, 2s and 2p orbitals at the cluster centre) show values of -1.48 eV (Model III) and -1.54 eV (Model IIIa) for the energy difference ($E^- - E_{\text{neut}}$), with excitation energies of 1.42 eV and 1.51 eV, accompanying total ρ_H^S values of -0.0224 and -0.016 respectively. (The excitation energy is defined by an approximate first order perturbation method rather than an SCF-type calculation). The cluster geometry is based on the R (centre-O) distance of 2.92\AA deduced for H_2O (23,24). The octahedrally disposed clusters yield solvations energies > 2 eV, but all the models in which two or three extra functions are centred in the cavity

display a tendency for the excess electron spin density to concentrate in these extra orbitals, although Fukui et al. claim that sufficient total spin density extends outwards to warrant the inclusion of a second solvation shell. Ideally, one would place more extra orbitals outside the cluster to determine whether they were being preferentially occupied, but again this is time consuming.

They show also, from examination of the excess electron MO, that on excitation the excess electron is transferred from the 1s and 2s extra central orbitals to almost total occupation of the $2p_z$ orbital, and their spin density plots indicate an expansion of the excess electron density in the z direction, and slight reduction in other directions. Thus there is a slight tendency for spin density to shift outwards on excitation.

Thus the general behaviour of the excess electron on solvation and excitation has been examined by the preceding groups of workers, but the practice of parameterising the calculations in order to make the excess electron state lower than the neutral one may cast doubt on the subsequent calculated solvation energies, since one may have a negative electron affinity for an isolated cluster but still stabilise the system by means of long-range polarisation in the surrounding dielectric.

C. Investigation of The Hydrated Electron in Water and Ice - Methods and Results

(i) Introduction

The structural model studies reviewed in Section B indicate that disparities in calculations may occur for various reasons; the basis set used may be unsuitable; states may be examined only at a single geometry; different levels of approximation may be used, e.g., extended Hückel, CNDO/2, INDO and ab initio; the difficult problem of

parameterisation of semiempirical calculations for extra, diffuse functions may be biased in favour of the properties sought; the criteria for the existence of a solvation centre may be based on calculated energy differences for isolated clusters, and nothing else. It seems more reasonable to take spin densities and excitation energies into account.

The ideal calculation is clearly a CI treatment of a flexible, diffuse Hartree-Fock limit basis set at an ab initio level on a cluster in the presence of a large number of background molecules, but computational economies preclude this, although Clementi et al. have produced definitive papers on the rôle of water in solvation using large-scale calculations (25).

Even Hartree-Fock limit ab initio calculations with a basis set suitable for the excess electron are prohibitive, and at present more limited treatments are the norm. It was therefore decided to investigate the solvated electron in water and ice at several different levels, beginning with the water dimer.

(2) The Water Dimer - an Ab Initio Study

An ab initio minimal basis investigation of Structures I and II was essayed, in the manner of Naleway and Schwartz, but with more emphasis on the excited states, and calculation of Mulliken spin densities, in the hope of observing at an ab initio level what had hitherto been investigated using the INDO approximation (17).

(a) Method

The ab initio spin-unrestricted Hartree-Fock technique has been discussed in Section III. Since many geometrical configurations for neutral, excess electron and excited excess electron state were to be studied, it was decided to limit the basis set to a minimal valence

STO-4G one used by Del Bene and Pople ⁽¹⁵⁾ for studies of H-bonding in neutral dimers (Table IV. C.1). This will tend to place the energies of excess electron states too high, but should show how the energies of the states and their spatial spin distributions respond to configurational changes.

The monomer geometry of $R(O-H) = 0.9915A^\circ$, $\hat{H}OH = 100.053^\circ$ ⁽¹⁵⁾ was kept constant, the intermolecular geometry being varied for Structures I (C_s) and II (C_{2h}).

Mulliken spin densities were evaluated for each atomic centre A by

$$\rho_A^s = \sum_{\mu \text{ on } A} (P_{\mu\mu}^\alpha - P_{\mu\mu}^\beta) S_{\mu\mu}$$

for each AO, μ , associated with that centre; this method should demonstrate how spin is partitioned, provided that the basis sets on each centre are reasonably balanced.

The excited excess electron state was obtained by reoccupying the MOs for the corresponding ground state, and cycling to self-consistency. This was usually effective, but some states were difficult to obtain.

Finally, lest the UHF method produce eigenfunctions too far from the eigenfunctions of S^2 , the value of $\langle \Psi | S^2 | \Psi \rangle$ was monitored for each state, and found to be within 0.05 of the expected 0.75. $-\frac{V}{T}$ was also found to be within 0.02 of the Virial Theorem value of 2 for all cases studied.

(b) Results and Discussion

Ground state energies for Structure I are shown in Table IV. C.2.

In agreement with previous results, a shallow configurational minimum appears (see Fig. IV. C.1) at an equilibrium O...O separation of $2.73A^\circ$, corresponding to an energy of -150.975 au. Addition of an excess electron to give the ${}^2A'$ state preserves this minimum (see

Fig.IV. C.2), but contracts the structure to an O...O distance of 2.40\AA , with an energy of -150.498 au, a value 0.477 au, or 12.98 eV above the neutral state. Restricting structural relaxation during capture places the excess electron state 13.4 eV above the neutral. Structure I, favoured in the neutral state, does not appear to be a good electron trap, in accord with the results of other workers (17).

As can be seen from the results of Naleway and Schwartz (13), addition of further diffuse orbitals lowers this energy gap, but does not render it favourable to solvation.

Model II, with its opposing protons, is found to have no stable configurational minimum, as illustrated in Table IV. C.3, and Fig. IV. C.3, the tendency being for the molecules to drift apart, or possibly rearrange until the more stable H-bonded Structure I is obtained. The corresponding excess electron state displays an energetic minimum, however (see Fig.IV. C.4) at an H...H separation of 1.15\AA , with an energy of -150.570 au, rendering it more favourable to an excess electron than Structure I.

Examination of excess electron Mulliken spin distributions gives results as shown in Fig.IV. C.3, where over 95% of ρ^s is on the right hand water molecule of Structure I, with a large part on the protons. Since we may infer that greater delocalisation of e^- over the molecular structure implies greater stabilisation, such asymmetry does not favour Structure I as a trapping site. This is reinforced by the observation that relaxation towards the e^- state equilibrium geometry ($O...O = 2.4\text{\AA}$) increases the asymmetrical distribution.

Structure II shows both a delocalisation of spin density over the two molecules, and also a lowering of the spin on the hydrogens towards the experimental result of 0.16 per proton for alkaline ice (27a). A tendency for almost all the ρ_H^s to collect on the inner protons can

also be noticed; this is in qualitative agreement with the INDO calculations of Howat and Webster (17).

Excitation produces interesting results. The excited states of Structure I reveal two interesting states, of ${}^2A''$ and ${}^2A'$ symmetry, respectively, with energies as shown in Table IV. C.4. Plotting the energies of these states against $O\dots O$ separation (Fig. IV. C.5) reveals an unbound state (${}^2A'$) and a state with an energetic minimum of ~ -150.340 au at $R(O\dots O) = 2.37A^0$ (${}^2A''$). Although extrapolation from such a model is speculative, this behaviour agrees with attempts by some workers to fit the e^-aq optical spectrum to a combination of bound/bound and bound/free state transitions (28): it should be emphasised, however, that the e^- ground state of Structure I has been deemed less favourable than that of Structure II. For completeness, the energy of the bound-bound transition has been evaluated on a Franck-Condon basis from the SCF data (see Table IV. C.5 and Fig. IV. C.6), showing two opposing trends: ${}^2A' \rightarrow {}^2A''$ transitions show a blue shift on expansion, while the strictly symmetry-forbidden ${}^2A' \rightarrow {}^2A'$ ones reveal a red shift, the latter being in accord with experiment (29). At the e^- ground state equilibrium geometry of $\sim 2.4A^0$, however, this leads to an excitation energy of ~ 4.9 eV as against 2.7 eV for the former ${}^2A' \rightarrow {}^2A''$ transition. The observed peak value for the transition is 1.72 eV with a peak width of ~ 0.92 eV (30).

Structure II, with the more favoured ground state for e^- , exhibits a non-binding excited state (see Table IV. C.6 and Fig. IV. C.7), which is in accord with suggestions by some workers (31) that the optical spectrum of e^-aq has a photoionisation efficiency profile. A Franck-Condon transition from the ground state would require about 5.8 eV, and a compressional blue shift is indicated.

Such a crude but broad-ranging semiempirical calculation cannot be expected to give results of quantitative accuracy. However, some new qualitative results have emerged. In neither model does the energy of the negative ion state fall below that of the neutral, but this is not expected, since, (a) the basis set was not sufficiently flexible and diffuse to describe the more diffuse negative ion state and (b) it is probable that long range polarisation fields are the principal factors determining whether solvation can ultimately occur.

Although there are thus disparities between calculated and measured solvation energies, and optical spectra, it has been established that Structure II possesses a configurational minimum in the e^- state, making it a better candidate for trapping than the regular H-Bonded dimer. This vindicates to some extent the speculations from experimental data on trapping in crystalline ice (see Section I) that defect sites may favour electron trapping.

The excitation energies are high, probably for reasons detailed in (a) above, but are qualitatively interesting: it might be conjectured that the crossed ${}^2A'$ and ${}^2A''$ states of Structure I could give rise to a complex optical spectrum, blending bound-bound and bound-quasifree transitions, as suggested by Delahay et al. (32). On the other hand, the excess electron ${}^2A'$ ground state for Structure I is configurationally unstable, and Structure II is the more likely electron trap. The latter has the correct spectral shift on compression, and its excited state has no configurational minimum, reinforcing the idea of bound-quasifree transitions. Improvement of the basis set and addition of diffuse functions is expected to lower all the energy levels, affecting the more diffuse excited states to a greater extent; a reduction in $h\nu$ on improvement of basis set is thus expected, towards the experimental value of 1.72 eV for water. The limitation that Structure II must excite

to an unbound state is not a serious one: not all modes of relaxation have been explored; an improved basis set may preferentially lower another excited state; a dimer unit may be too small to model accurately all the short-range interactions. It is also possible that the observed spectrum does not involve bound-bound transitions at all.

Mulliken spin densities for Structure I are shown in Fig.IV.C.9. The ${}^2A'$ e^- ground state has most of its spin density concentrated on the right-hand molecule, and the delocalisation which Kerr and Williams stipulate for stabilisation is absent. Nor does excitation improve matters: the ${}^2A''$ state retains the same type of distribution, and in the ${}^2A'$ state the disposition is reversed, spin having transferred to the other molecule. (Similar behaviour was noted in the Howat and Webster INDO calculations on a Wurtzite-type arrangement).

The Structure II results are more reassuring: (Fig.IV. C.8) the excess electron appears to reside in the interior of the dimer, and is distributed over both molecules, giving a total ρ_H^S of 0.38, as against Kerr and Williams' specifically spin-optimised INDO result of 0.208⁽¹⁰⁾. Excitation transfers spin to the outside of the dimer, as shown, but leaves it symmetrically distributed, so that Structure II may be inferred, from spin distributions, to be the better trap.

Again, the limited basis used, and the use of Mulliken distributions rather than direct evaluation of ρ^S at points in space, leaves the actual figures obtained open to question, but indicates the H-bonded structure of water to be less favourable to electron trapping than defect centres of the Structure II type.

D. Water Multimers

If the solvated electron in water is indeed localised on some defect structure, it is of interest to investigate the extent of its localisation: Kawabata's evidence (see Section II) suggests that the region is not macroscopically significant, and NMR results indicate that in both crystalline ⁽²⁷⁾ and glassy ⁽¹¹⁾ ice the electronic hyperfine interaction is with 4, 6 or 8 protons, and line shape analyses suggest $g \pm 2$ ⁽¹²⁾. Various structures containing from 4 to 12 H₂O molecules were examined at the INDO level, using the INDO programme of Pople and Beveridge ⁽³³⁾, specially modified by the author to handle excited states and use spherical floating Slater's (see Section III.F).

For the basic H₂O unit, a minimal valence basis set with orbital exponents as optimised by Pople and Beveridge was used ⁽¹⁸⁾, the molecular geometry being fixed at $R(O-H) = 0.958 \text{ \AA}$, $\hat{O}H = 104.45^\circ$, as used by Howat and Webster ⁽¹⁷⁾. Data obtained in the monomer calculation are shown in Table IV. D.1. H₂O⁻ itself is clearly unstable with respect to the neutral molecule plus a free electron. One significant point is the tendency for the spin density to shift outward to the protons on the ${}^2A_1 \rightarrow {}^2B_1$ excitation.

(i) The Effect of Environment on a Small Cluster-Solvation Shells

In this study, an attempt was made to simulate the addition of solvation shells to (H₂O)₄. The basic unit (Fig. IV. D.1) was a D_{2d} (H₂O)₄ cluster, where 4 protons pointed towards the centre, while the remaining 4 were disposed outside. Data on the neutral and excess electron states are displayed in Table IV. D.2. The energy of the charged (H₂O)₄ cluster is above that of the neutral one with the same geometry, but all long-range medium polarisation has been neglected. Spin shifts have been large: 75.6% of the excess spin now lies on the oxygens, as against 39.01% in the monomer, and the total spin density

on the central protons is 0.196; in fact, the total proton spin density of 0.244 is approaching Kerr and Williams' carefully optimised result of 0.208 (10).

Four more water molecules were then placed tetrahedrally round the cluster at a distance of $3R$ from the centre, where R was the centre to vertex distance in the inner cluster ($R = 1.918\text{\AA}$) and a similar shell was again added at $5R$ to give a $3(\text{H}_2\text{O})_4$ structure. Energies, and spin densities at O, central and outer protons in the inner cluster are displayed in Table IV. D.2, so that the effects of a solvation shell can be assessed. The changes are not great; the excess spin remains firmly in the inner cluster, and the faintest spin shift towards the oxygens is noted; clustering has had little effect on the inner water tetramer.

Alternative solvation shells at $2R$ and $2R + 4R$ were tried, and although calculations on the latter did not converge, results from the former are included in Table IV. D.2. Here a slight shift of the inner cluster spin is noted, from 1.000 to 0.994, and a slight decrease in $\rho_{\text{Hi}}^{\text{S}}$ confirms this small outward trend, but the solvation shell has little effect on the spin distribution. With these indications of the localised nature of the trapped electron, it was decided to investigate a possible trapping site on another structure which might exist in water.

(ii) An H-bonded Double Ring Structure

For this model, 2 H-bonded $(\text{H}_2\text{O})_6$ chair rings were stacked as sketched in Fig. IV. D.2, with the H_2O molecules in each ring in a quasi-random orientation, to simulate a possible H-bonded water fragment. Coordinates were evaluated using a programme written by the author. Three oxygen molecules in the upper ring were H-bonded to three in the lower, the H_2O geometry being as detailed in Section IV. D(i), and the

upper O-H-lower O distance was 2.76\AA . INDO calculations were performed on the neutral and excess electron states of this cluster, firstly with the regular INDO minimal basis set as specified by Pople and Beveridge (18), and secondly with a variable exponent floating spherical 1s Slater orbital at the centre of the structure, utilising various values of \mathcal{J} , some of which did not yield iterative convergence.

The same geometry was maintained throughout.

Table IV. D.3 shows the energies obtained with various values of \mathcal{J} . (It was not possible to force convergence to any excited excess electron states). Increasing contraction of the central orbital leads to a drop in the neutral state energy with a corresponding charge shift out of the centre of the cluster, whereas the excess electron state has a minimum at $\mathcal{J} = 0.1$, coupled with retention of 99% of the spin density in the central orbital. (A full set of data obtained is set out in Table IV. D.3). Once again it appears that the excess electron is best described as being quite well localised on the cluster.

References IV

1. M. Weissmann and N.V. Cohan, *J. Chem. Phys.*, 59 (1973) 1385.
2. E. Clementi and A.D. McLean, *Phys. Rev.*, 133A 419 (1964).
3. M. Tachiya, Y. Tabata and K. Oshima, *J. Phys. Chem.*, 77 (1973) 263.
4. M. Weissmann and N.V. Cohan, *Chem. Phys. Lett.*, 7 (1970) 445.
5. N.V. Cohan, G. Finkelstein and M. Weissmann, *Chem Phys. Lett.*, 26 (1974) 93.
6. L. Raff and H.A. Pohl, *Adv. Chem. Ser.* 50 p.173, Washington, Am. Chem. Soc., 1965.
7. B.J. McAloon and B.C. Webster, *Theor. Chim. Acta.*, 15 (1969) 385.
8. Farhataziz, L.M. Perkey and R.R. Hentz, *J. Chem. Phys.*, 60 (1974) 4383.
9. M. Natori and T. Watanabe, *J. Phys. Soc. Jap.*, 21 (1966) 1573.
10. C.M.L. Kerr and F. Williams, *J. Phys. Chem.*, 76 (1972) 3838.
11. K. Ohno, I. Takemura and J. Sohma, *J. Chem. Phys.*, 56 (1972) 1202.
12. B.G. Ershov and A.K. Pikaev, *Radiat. Res. Rev.*, 2 (1969) 1.
13. C.A. Naleway and M.E. Schwartz, *J. Phys. Chem.*, 76 (1972) 3905.
14. G. Herzberg, *Electronic Spectra of Polyatomic Molecules*, Van Nostrand, New York 1966.
15. J. Del Bene and J.A. Pople, *J. Chem. Phys.*, 52 (1970) 4858.
16. W.C. Gottschall and E.J. Hart, *J. Phys. Chem.*, 71 (1967) 2102.
17. G. Howat and B.C. Webster, *J. Phys. Chem.*, 76 (1972) 3714.
18. J.A. Pople and D.L. Beveridge, *Approximate Molecular Orbital Theory*, McGraw-Hill, N.Y., 1970.
19. R.R. Hentz, Farhataziz and E.M. Hansen, *J. Chem. Phys.*, 55 (1971) 4974.
20. K. Kawabata, *J. Chem. Phys.*, 55 (1971) 3672.
21. I.A. Taub and K. Eiben, *J. Chem. Phys.*, 49 (1968) 2499.

22. S. Ishimaru, H. Kato, T. Yamabe and K. Fukui, *Chem. Phys. Lett.*, 17 (1972) 264.
23. J. Morgan and B.E. Warren, *J. Chem. Phys.*, 6 (1938) 666.
24. G.W. Brady and W.J. Romanov, *J. Chem. Phys.*, 32 (1960) 306.
25. e.g., H. Kistenmacher, H. Popkie and E. Clementi, *J. Chem. Phys.*, 59 (1973) 5842.
26. B.C. Webster, *J. Chem. Soc., Faraday Trans. II*, 73 (1977) 1699.
27. (a) J.E. Bennet, B. Mile and A. Thomas, *J. Chem. Soc., A* (1967) 1393.
(b) J.E. Bennet, B. Mile and A. Thomas, *J. Chem. Soc., A* (1969) 1502.
28. R. Lugo and P. Delahay, *J. Chem. Phys.*, 57 (1972) 2122.
29. B.D. Michael, E.J. Hart and K.H. Schmidt, *J. Phys. Chem.*, 75 (1971) 2798.
30. E.J. Hart and W.C. Gottschall, *J. Phys. Chem.*, 71 (1967) 2102.
31. (a) G.A. Kenney and D.C. Walker, *J. Chem. Phys.*, 53 (1970) 1282.
(b) G. Kenney-Wallace and D.C. Walker, *J. Chem. Phys.*, 55 (1971) 447.
32. B. Baron, P. Delahay and R. Lugo, *J. Chem. Phys.*, 55 (1971) 4180.
33. J.A. Pople and D.L. Beveridge, Ref.18, Appendix.
34. For a theoretical treatment, in general terms, of an electron in dilute molecular solutions, see J. McHale and J. Simons, *J. Chem. Phys.*, 67 (1977) 389.

TABLE IV. C.1.

Slater exponents (STO-4G) for minimal basis ab initio water dimer calculations

Atomic Orbital	Exponent
Oxygen ζ_1	7.66
Oxygen ζ_2	2.23
Hydrogen ζ_1	1.23

TABLE IV. C.2.

Ab initio minimal basis (STO-4G) calculations on the Structure I geometry of the H₂O dimer. Neutral and open shell ground states

O...O Separation (Å ^o)	¹ A' Neutral State Energy(au)	² A' e ⁻ State Energy (au)
1.5	-149.52477025	-149.13645527
1.7	-150.46790078	-150.06226250
1.8	-150.66743131	-150.25293669
1.9	-150.78817243	-150.36462280
2.0	-150.86278673	-150.4301987
2.1	-150.90930660	-150.46750880
2.2	-150.93816182	-150.48733145
2.3	-150.95569714	-150.49604078
2.35	-150.96154051	-150.4985942
2.39	-150.96516140	-150.49785331
2.4	-150.96594090	-150.49780415
2.5	-150.97152496	-150.49538559
2.6	-150.97418866	-150.49063039
2.73	-150.97512250	-150.48290492
2.8	-150.97495033	-150.47855224
2.9	-150.97427958	-150.47249124
3.0	-150.97336878	-150.46684491
3.1	-150.97239850	-150.46174499
3.2	-150.97147025	-150.45723700
3.3	-150.97063455	-150.45331621
3.5	-150.96929643	-150.44708671

TABLE IV. C.3.

Ab initio minimal basis (STO-4G) calculations on the Structure II geometry of the H₂O dimer. Neutral and open shell ground states.

H...H Separation (Å°)	¹ A _g Neutral State Energy (au)	² A _g e ⁻ State Energy (au)
1.0	-150.92030086	-150.56004661
1.1	-150.93374778	-150.56830966
1.15	-150.93876636	-150.56999840
1.2	-150.94292034	-150.57038627
1.3	-150.94922627	-150.56801197
1.4	-150.95359195	-150.56243457
1.5	-150.95663620	-150.55460008
1.6	-150.95877600	-150.54525669
2.0	-150.96275483	-150.50342564
2.5	-150.96413362	-150.46204877
3.0	-150.96460308	-150.43923518

TABLE IV. C.4.

Ab initio minimal basis (STO-4G) calculations on the Structure I geometry of the H₂O dimer. Excited open shell states

O...O Separation (Å°)	2A'' Excited State (au)	2A' Excited State (au)
1.5	-149.09476821	
1.7	-149.99927003	
1.8	-150.18164121	
1.9	-150.28649978	
2.0	-150.34640269	
2.1	-150.37922907	
2.2	-150.39529095	
2.3		-150.29335048
2.4	-150.40007950	-150.31880701
2.5	-150.39553946	-150.33783119
2.6	-150.38906596	-150.35219602
2.73	-150.37966186	-150.36596481
2.8	-150.37465224	-150.37171836
2.9	-150.36793916	-150.37847649
3.0		-150.38393174
3.1	-150.35680369	
3.3		-150.39537928

TABLE IV. C.5.

Ab initio minimal basis (STG-4G) calculations on the Structure I geometry of the H₂O dimer. Excitation energies to the two excited states

O...O Separation (Å°)	$h\nu$ (eV) $2_{A'} \rightarrow 2_{A''}$	$h\nu$ (eV) $2_{A'} \rightarrow 2_{A'}$
1.5	1.13	
1.7	1.71	
1.8	1.94	
1.9	2.13	
2.0	2.28	
2.1	2.40	
2.2	2.50	
2.3		5.52
2.4	2.66	4.87
2.5	2.72	4.29
2.6	2.76	3.77
2.72	2.81	3.18
2.8	2.83	2.91
2.9	2.84	2.56
3.0		2.26
3.1	2.86	
3.3		1.58

TABLE IV. C.6.

Ab initio minimal basis (STO-4G) calculations on the Structure II of the water dimer. Excited state energies

H...H Separation (\AA)	2B_u Excited State Energy (au)	$h\nu$ (eV) ${}^2A_g - {}^2B_u$
1.0	-150.32777688	6.32
1.1	-150.34276521	6.14
1.15	-150.34852322	6.03
1.2	-150.35340103	5.90
1.3	-150.36112657	5.63
1.4	-150.36690920	5.32
1.5	-150.37141118	4.98
1.6	-150.37509177	4.63
2.0	-150.38666742	3.18
2.5	-150.40026434	1.68
3.0	-150.41107686	0.77

TABLE IV. D.2.

INDO calculations on $(\text{H}_2\text{O})_4$ clusters with solvation shells: neutral and excess electron states

Model	Energy (au)	ρ^{So}	ρ^{Si}	ρ^{Ho}	Total ρ^{S} in inner cluster
$(\text{H}_2\text{O})_4$ neutral	-76.0500889783				
$(\text{H}_2\text{O})_4$ excess electron	-75.8232230134	0.756	0.196	0.047	1.000
$(\text{H}_2\text{O})_4 + 4$ at 3R neutral	-152.1061633423				
" " " e^-	-151.8868808744	0.757	0.196	0.047	1.000
$(\text{H}_2\text{O})_4 + 3\text{R} + 5\text{R}$ neutral	-228.1628089095				
" " " e^-	-227.9435694118	0.758	0.195	0.047	1.000
$(\text{H}_2\text{O})_4 + 2\text{R}$ neutral	-152.1079220855				
" " " e^-	-151.8974464775	0.756	0.190	0.048	0.994

TABLE IV. D.1

INDO calculations on H₂O monomer: neutral (¹A₁), excess electron (²A₁) and excited (²B₁) states

State	Energy(au)	ρ_c^s	ρ_{Hi}^s	Total ρ_H^s
Neutral ¹ A ₁	-19.0142			
Excess Electron ² A ₁	-18.7282	0.390	0.305	0.610
Excited Excess Electron ² B ₂	-18.4852	-0.242	0.6211	1.242

TABLE IV. D.3.

(H₂O)₁₂ H-bonded structure with Central Slater 1s Orbital

ENERGY (A.U.)	ξ (CENTRAL ORBITAL)	ρ_c^s (CENT. OR.)	ρ_c (CENT. OR.)	
-228.0058939315	—	—		Neutral
-227.8067282688	—	—		Excess Electron
-228.0335911250	0.1	—	0.0182	Neutral
-227.9859261951	0.1	0.9902	1.0090	Excess Electron
-228.1127817914	0.3	—	0.0670	Neutral
-227.9561857347		0.7677	0.8392	Excess Electron
-228.138168586	0.5	—	0.0819	Neutral
-227.9611713895	0.5	0.1169	0.2087	Excess Electron

Structure

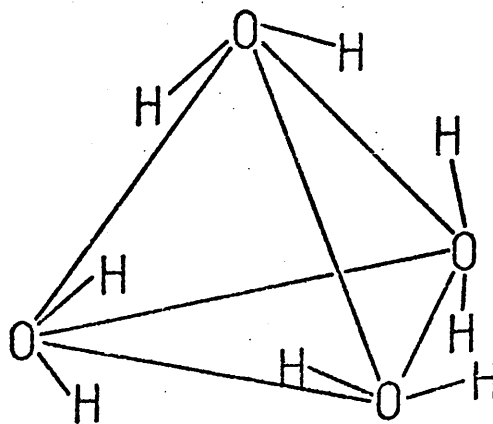
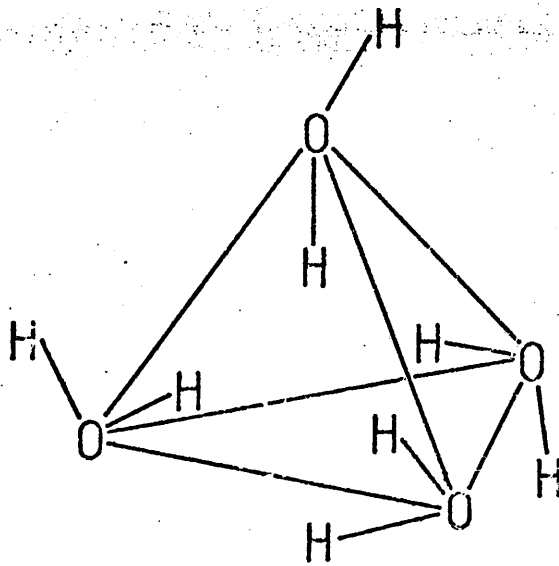
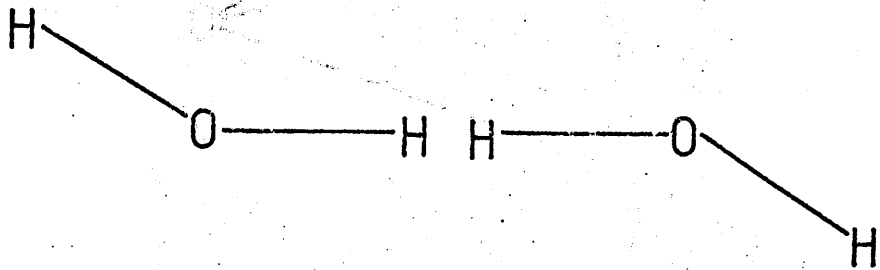
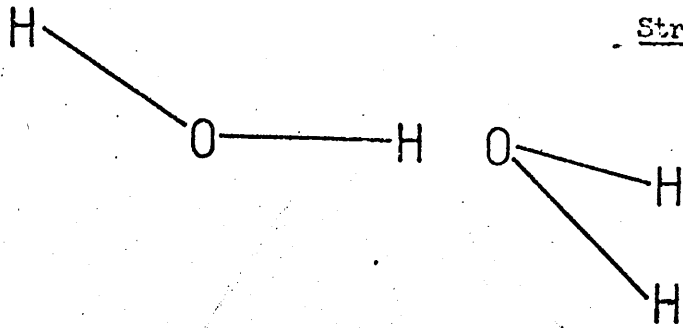


FIG. IV. B.1 (Contd.)Structure

IV

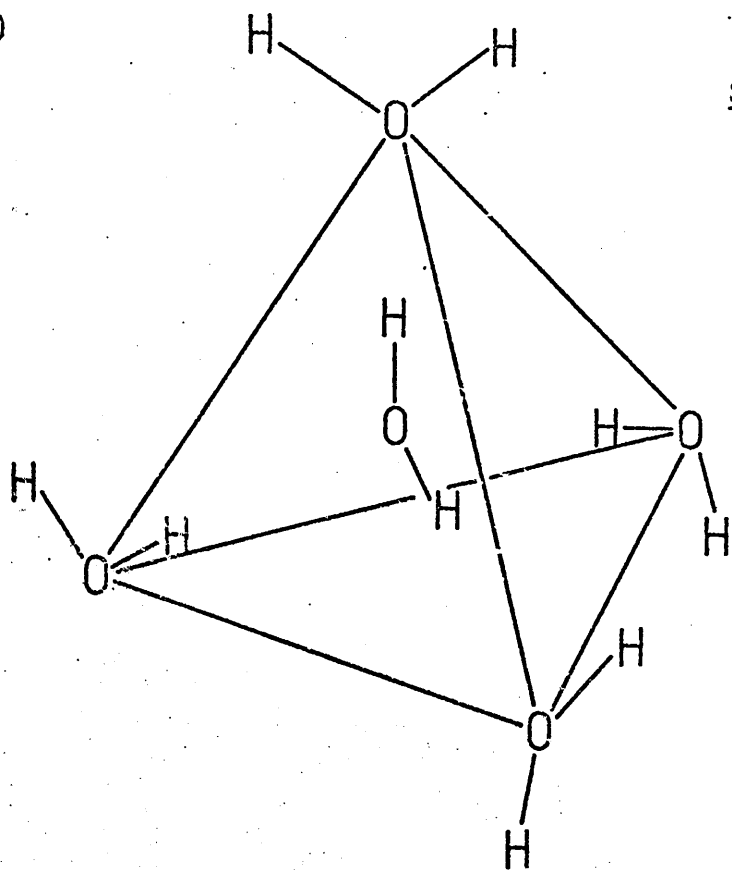
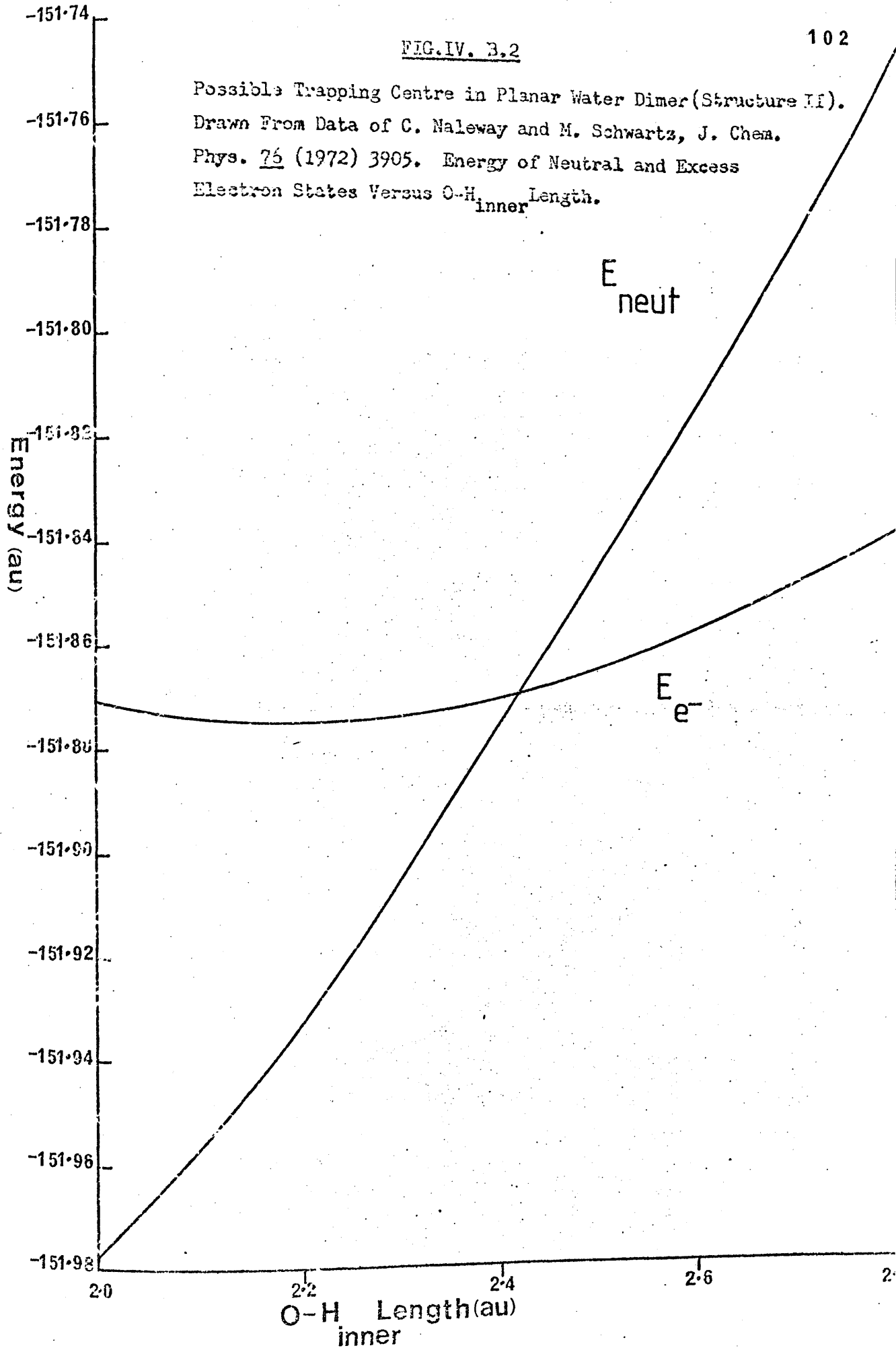
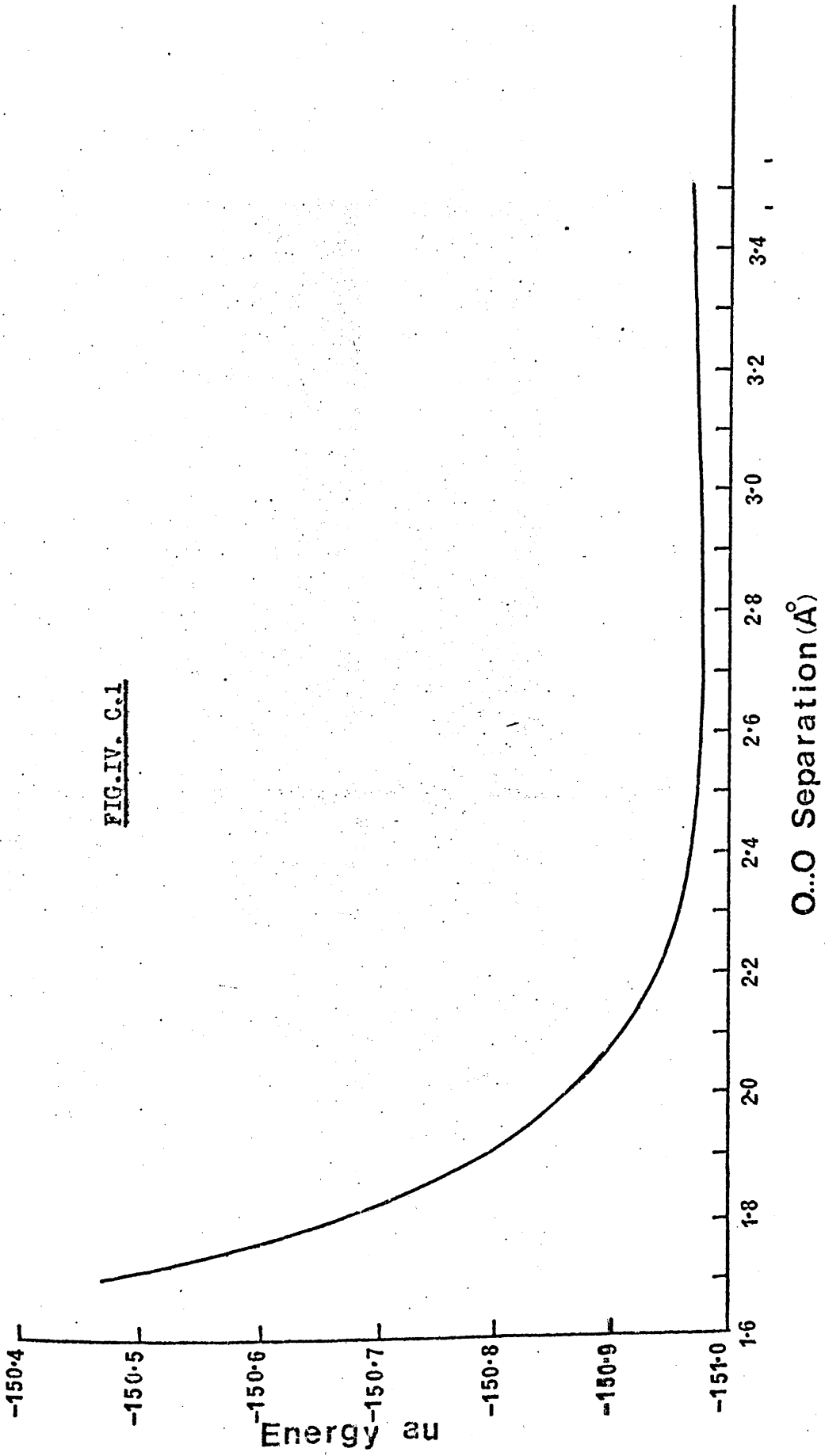


FIG. IV. 3.2

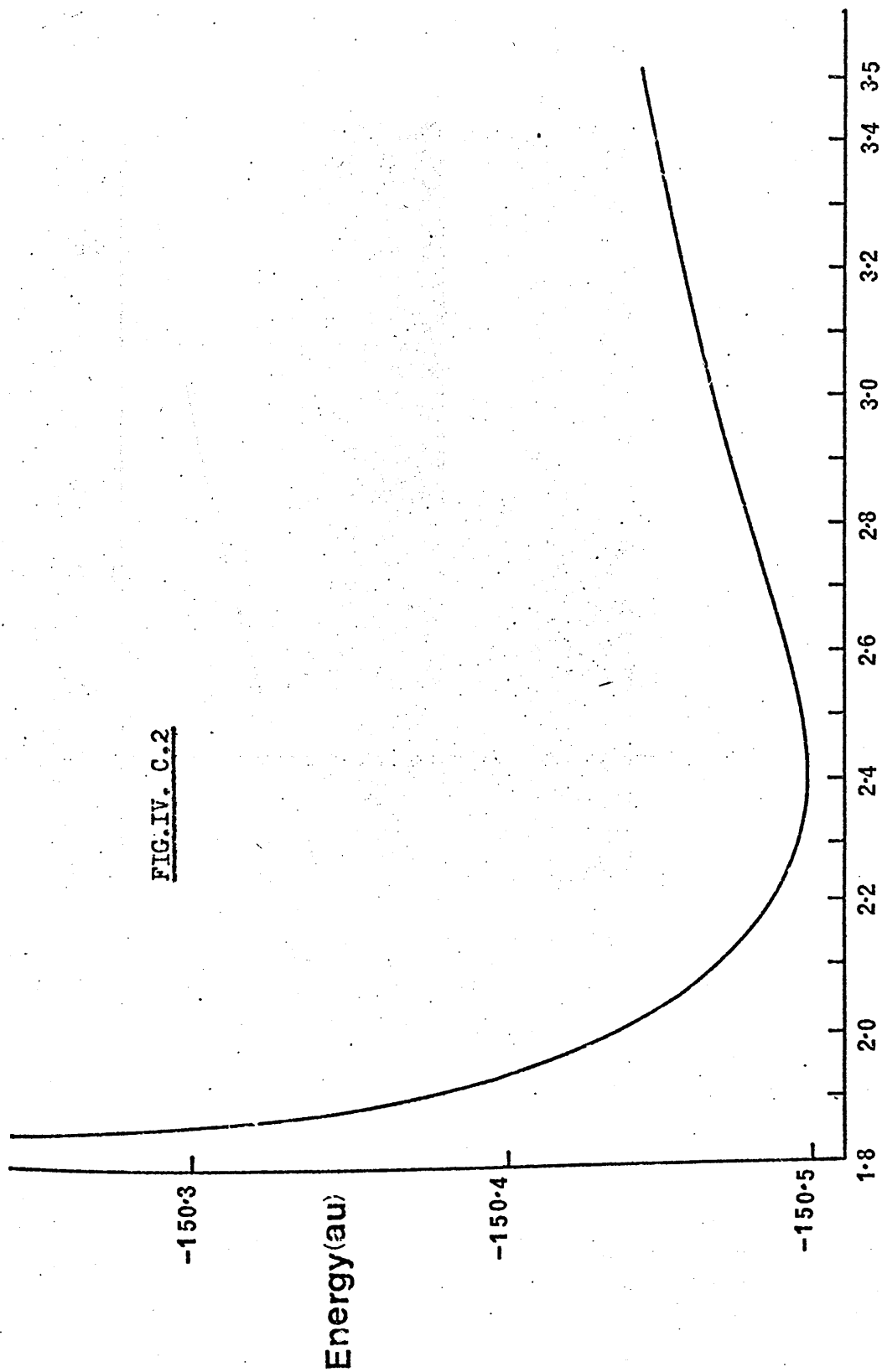
Possible Trapping Centre in Planar Water Dimer (Structure II).
Drawn From Data of C. Naleway and M. Schwartz, J. Chem.
Phys. 76 (1972) 3905. Energy of Neutral and Excess
Electron States Versus O-H_{inner} Length.





Water Dimer Structure I (Non-Planar). Neutral State ($^1A'$). Energy Versus Monomer Separation.

FIG. IV. C.2

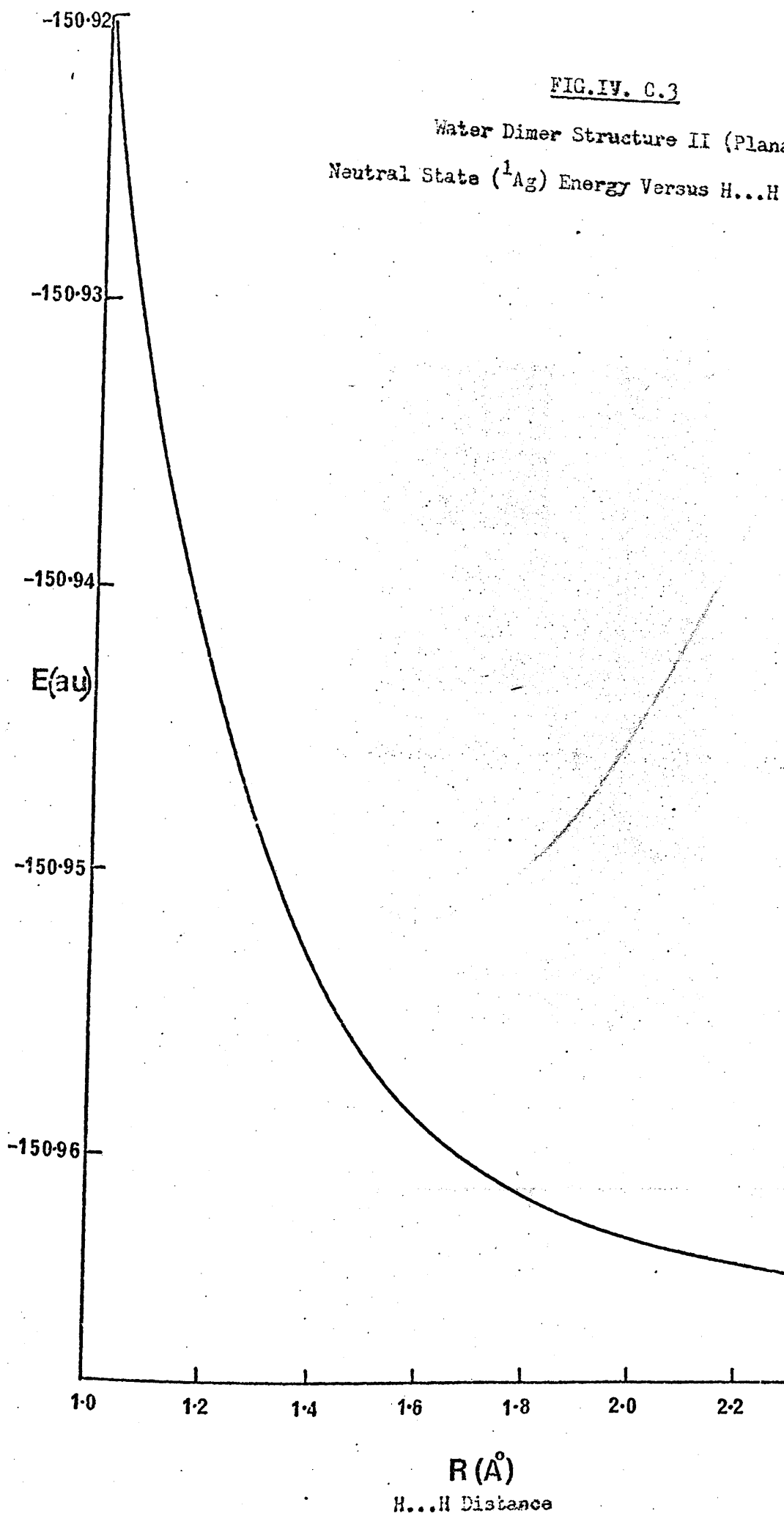


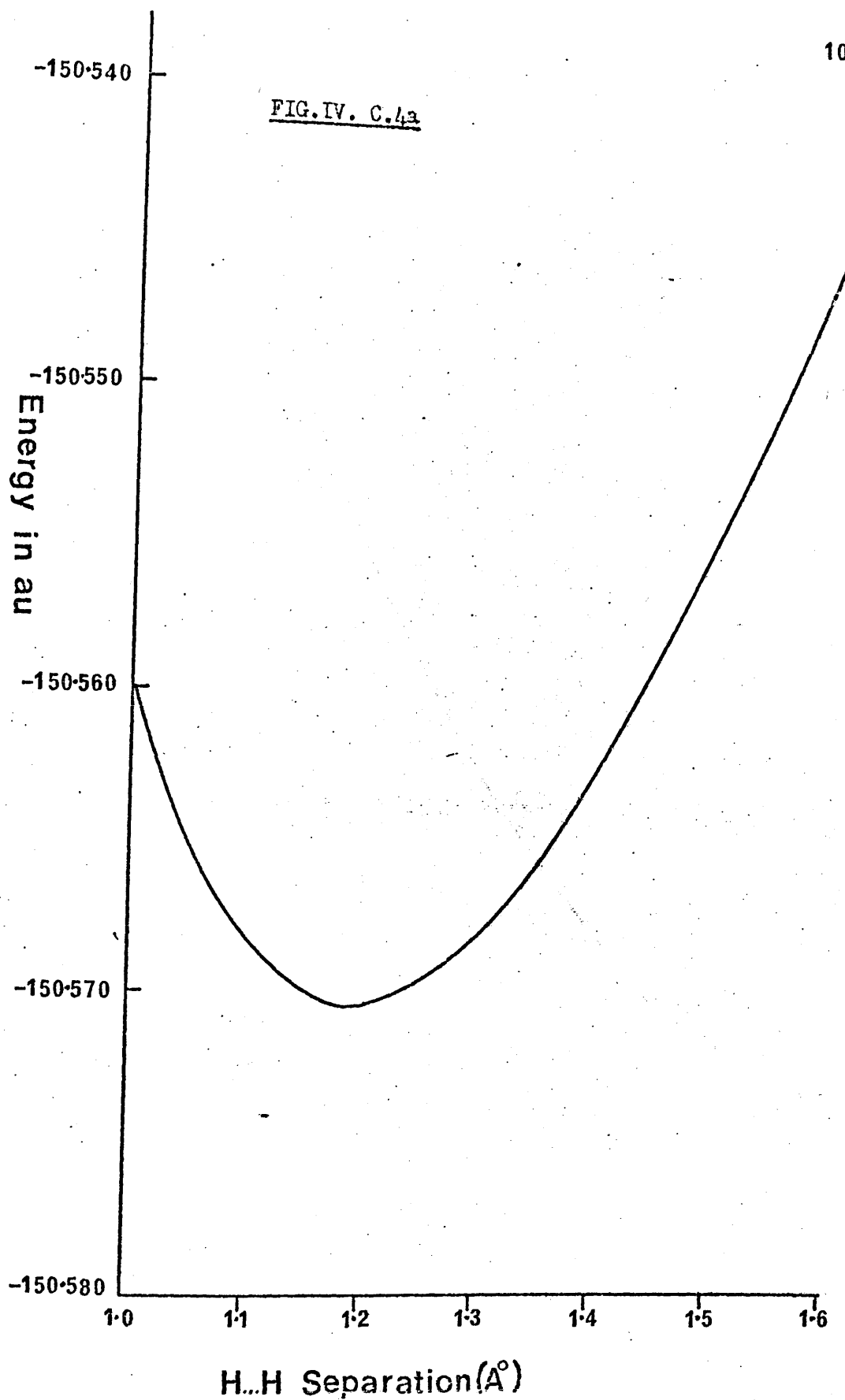
O..O Separation (A°)

Water Dimer Structure I (Non-Planar). Excess Electron State (²A'). Energy Versus Monomer Separation.

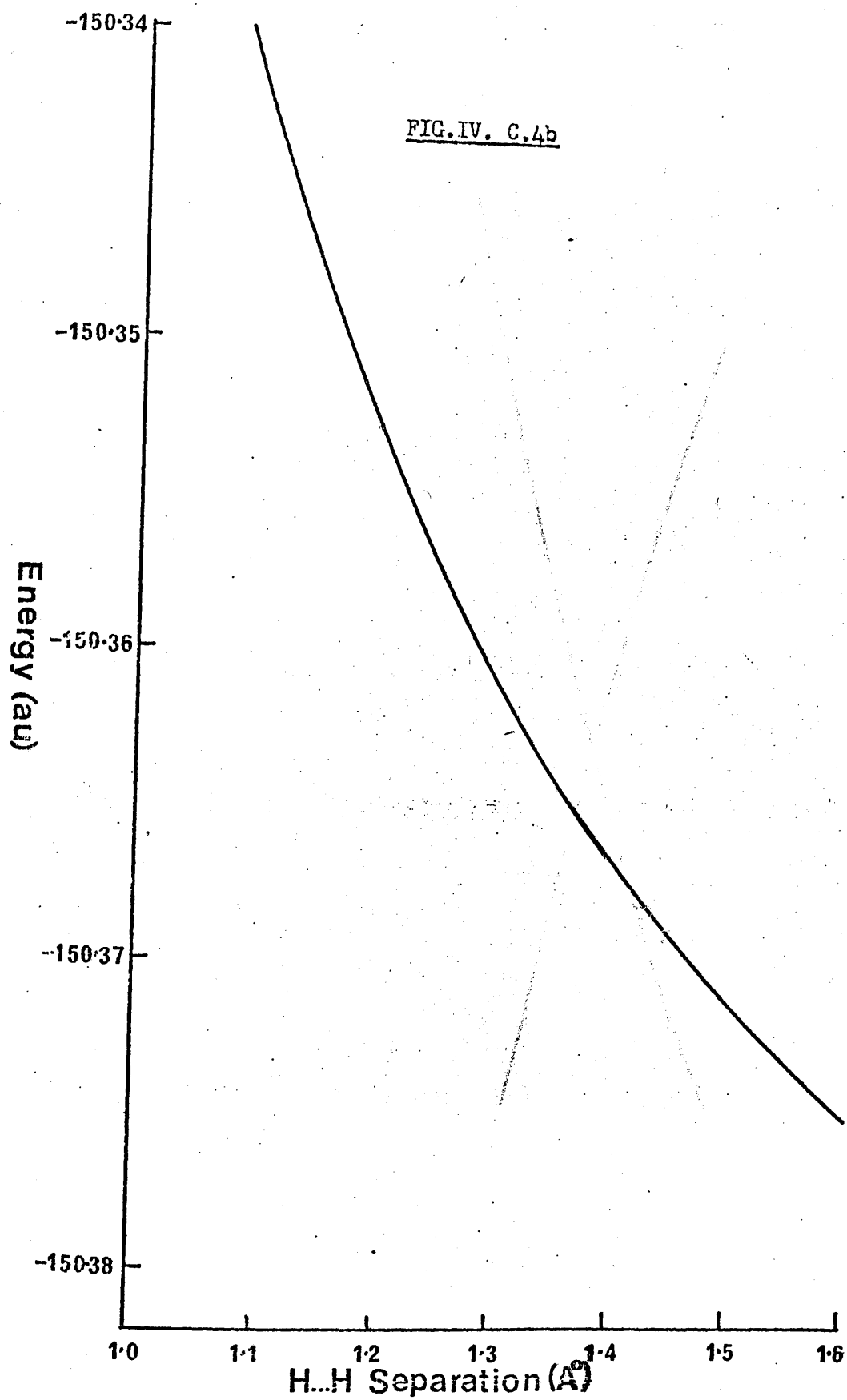
FIG. IV. C.3

Water Dimer Structure II (Planar)
Neutral State (1A_g) Energy Versus H...H Separation





Water Dimer Structure II (Planar). Excess Electron State (2A_g)
Energy Versus H...H Separation.



Water Dimer Structure II (Planar). Excess Electron Excited State (2B_u). Energy Versus H...H Separation.

Structure I Water Dimer (Non-Planar).
 e^{-*} states.

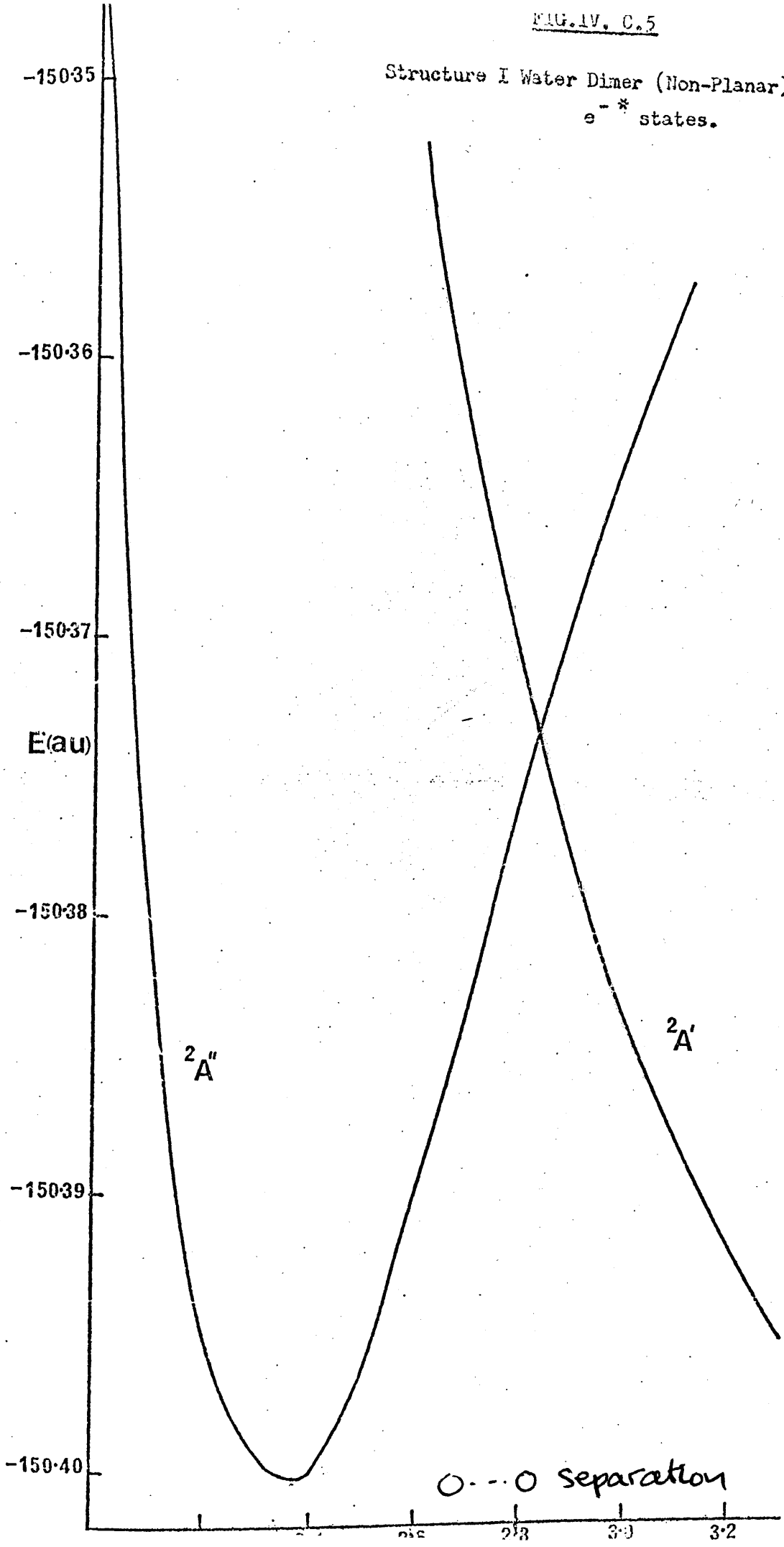


FIG. IV. C.6

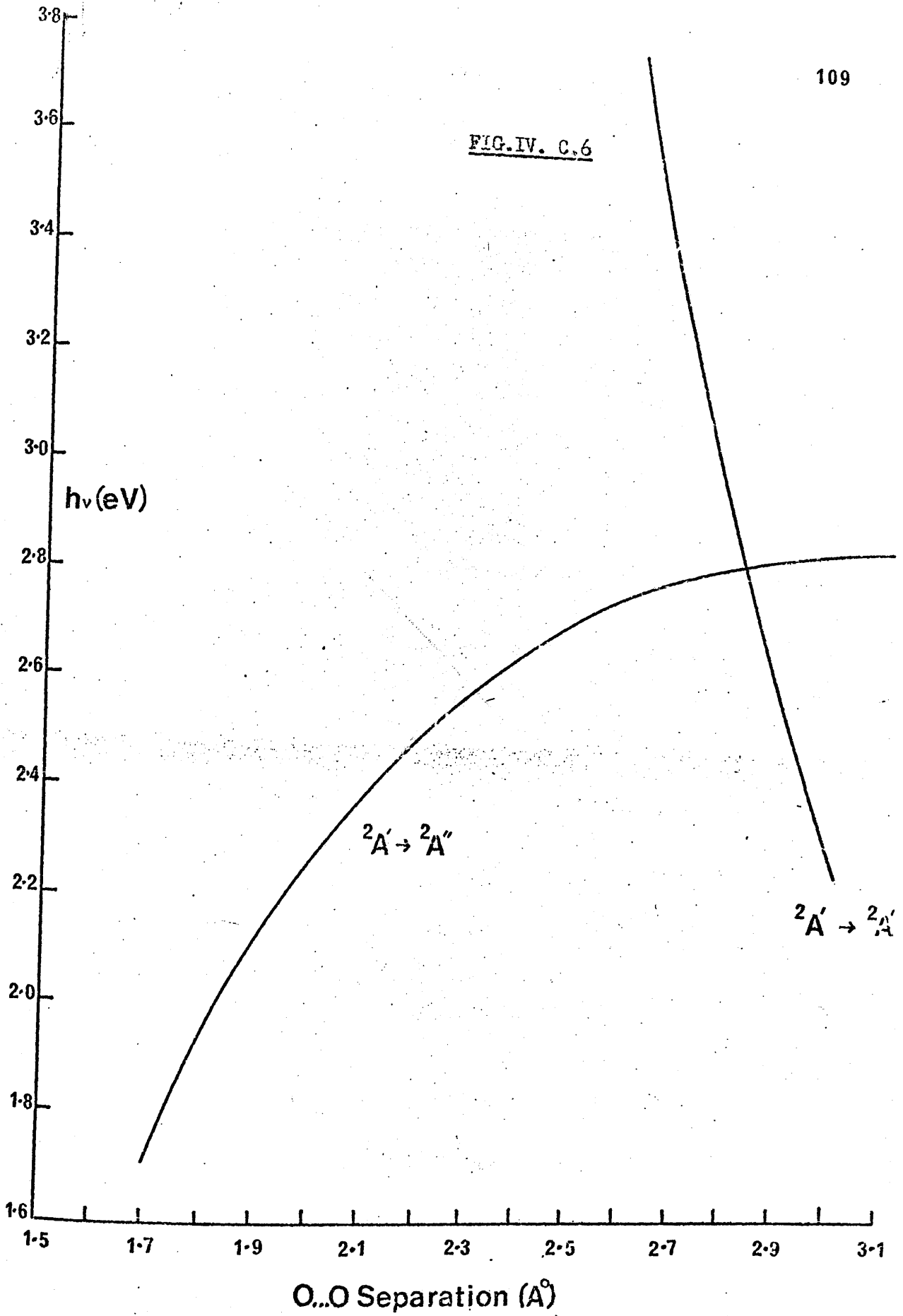
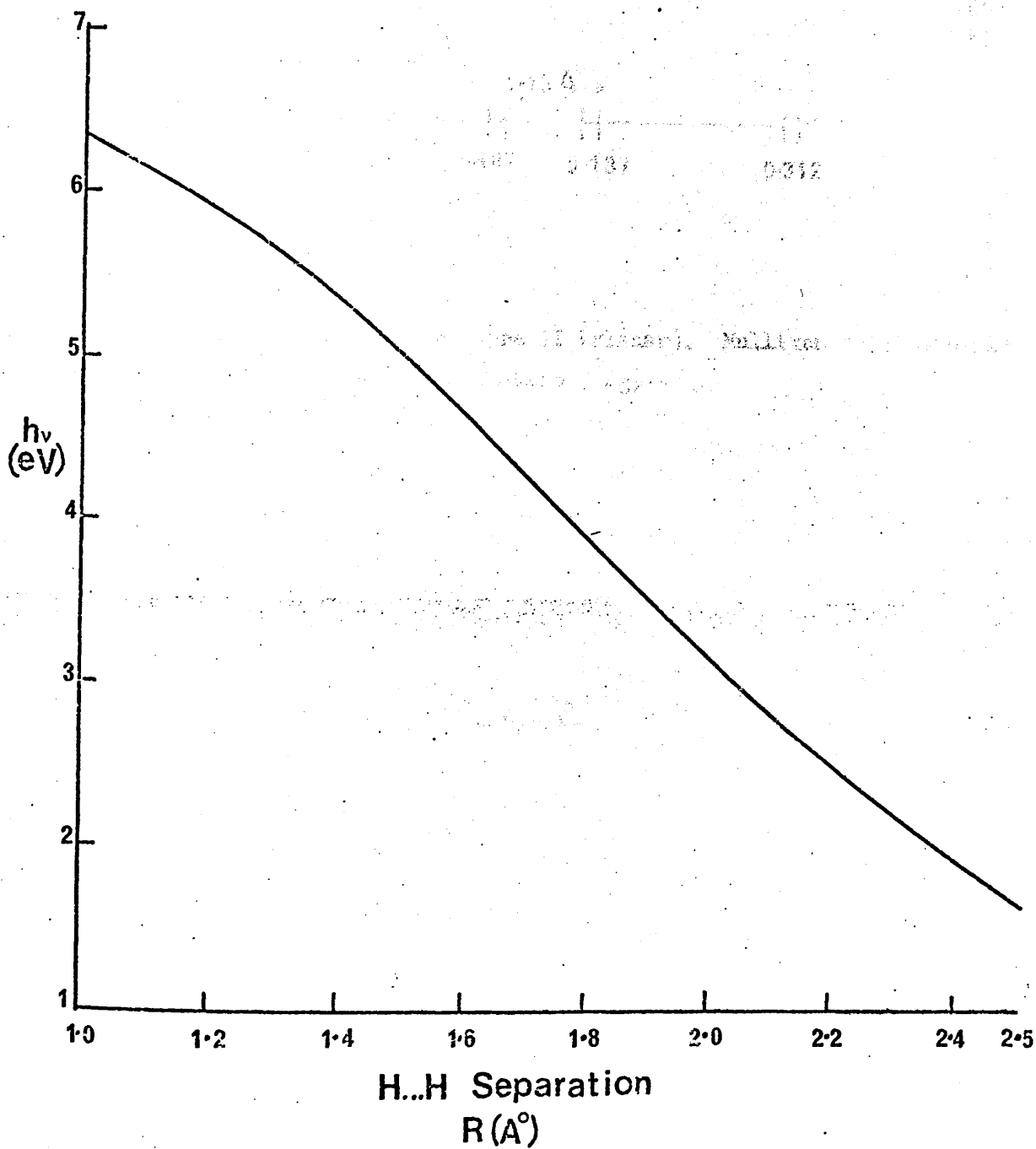
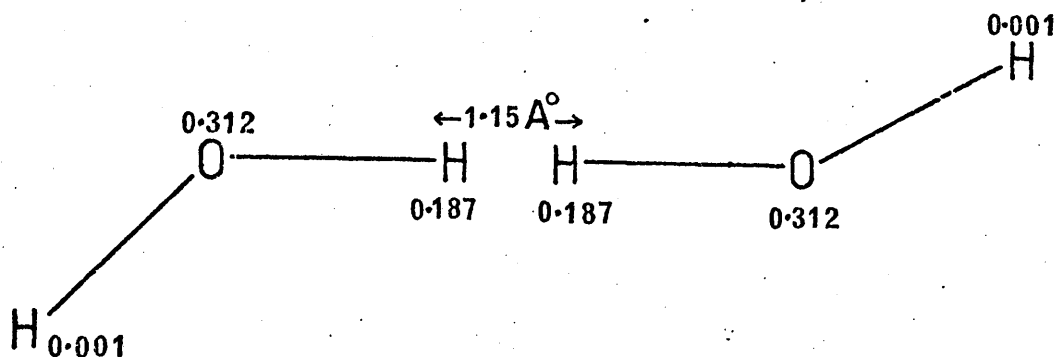
Structure I Water Dimer. $h\nu$ Versus O...O Separation (Å⁰).

FIG. IV. C.7

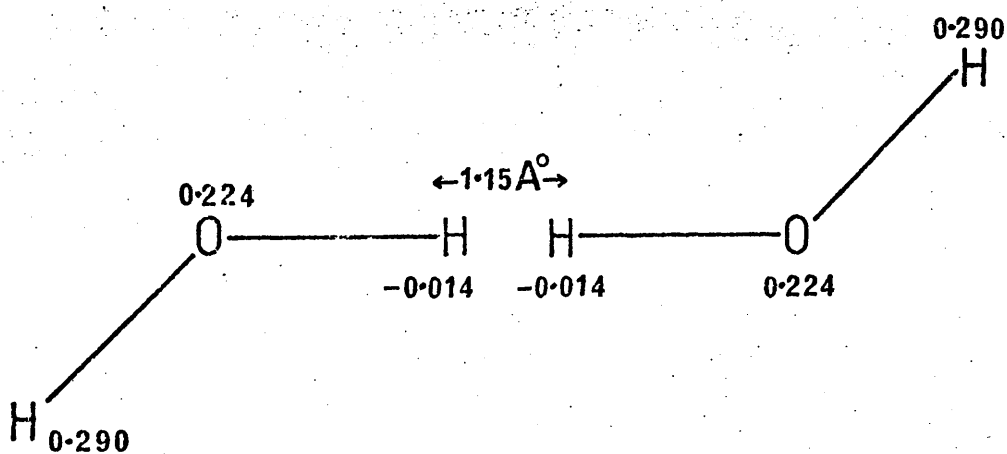


Water Dimer Structure II (Planar) ${}^2A_g \rightarrow {}^2B_u$ Transition.
 $h\nu$ (eV) Versus H...H Separation.

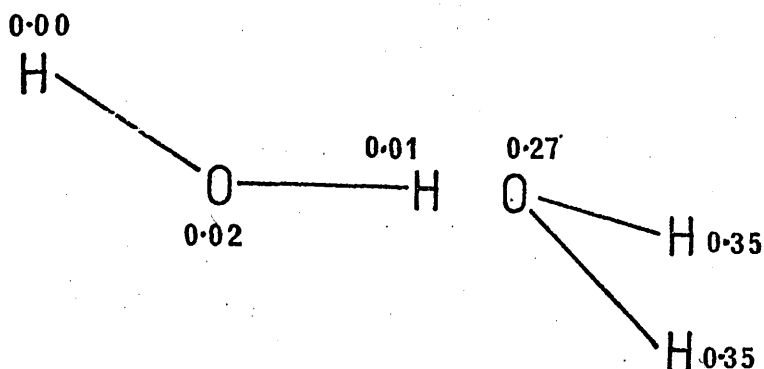
FIG. IV. C.8



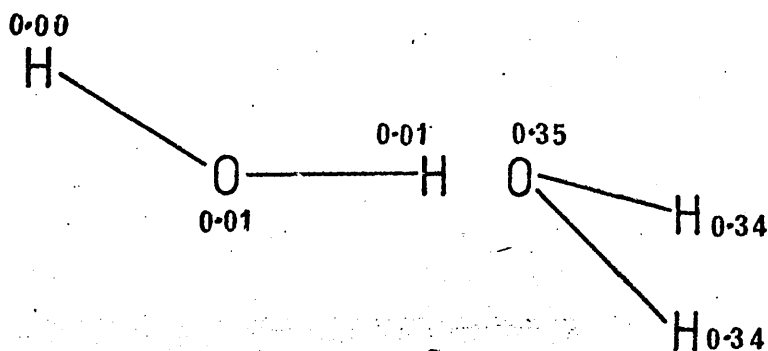
The Water Dimer. Structure II (Planar). Mulliken spin Densities For The Ground Excess Electron State (2A_g).



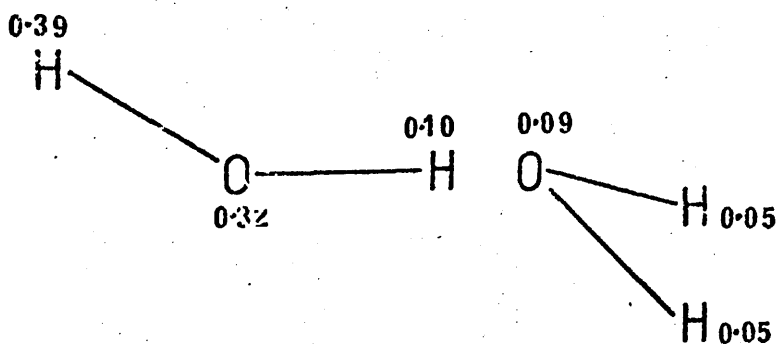
The Water Dimer. Structure II (Planar). Mulliken Spin Densities For The Excited Excess Electron State (2B_u).



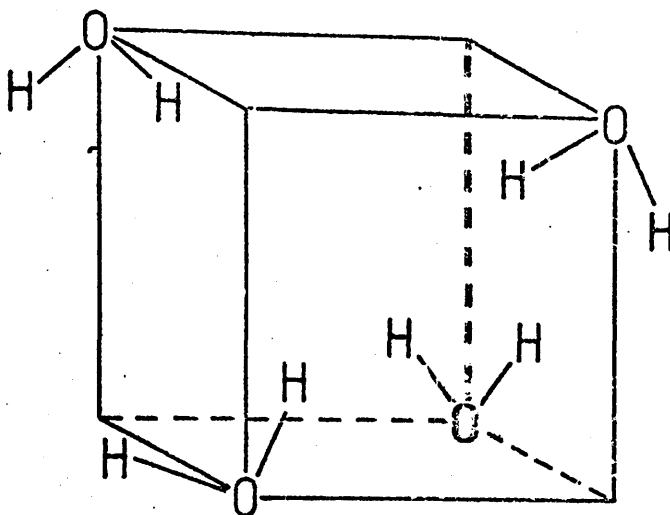
The Water Dimer. Structure I (Non-Planar) Mulliken Spin Densities for the Ground Excess Electron State ($^2A'$) ($O...O = 2.4 \text{ \AA}$)



Mulliken Spin Densities for the $^2A''$ Excess Electron Excited State. ($O...O = 2.4 \text{ \AA}$).

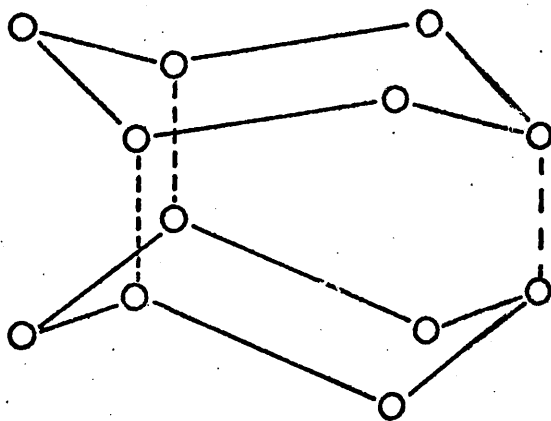


Mulliken Spin Densities for the $^2A'$ Excess Electron State. ($O...O = 3.0 \text{ \AA}$).



D_{2d} Structure for $(H_2O)_4$

FIG. IV. D.2



Double Chair Structure For $(H_2O)_{12}$

V

Methanol and Ammonia - Short-Range Interactions

No study of the solvated electron would be complete without reference to its trapping in alcohols and ammonia, since a great amount of information is available on these (1, 2). In the case of alcohols, it was decided to restrict calculation to a small methanol cluster, examining the effect of cluster size, and the addition of extra orbitals, at an INDO level. The ammonia studies were carried out at an ab initio level on monomers and dimers, to determine the effects of geometry and basis size and flexibility on the energies and spin distributions of the species studied.

A. The Methanol Tetramer - an INDO Study

The cluster studied was a D_{2d} $(\text{MeOH})_4$ arrangement, as depicted in Fig. V. A.1., with the hydroxyl protons pointing towards the centre, round which the oxygen atoms are tetrahedrally disposed. The CH_3OH geometry was kept fixed at that optimised by Pople and Beveridge (3). The cluster, imagined to be situated tetrahedrally in a cube, was examined with floating Spherical Slaters placed centrally on the cube faces, and one at the cube centre, or various combinations of these, the orbitals all having the same Slater exponent.

Energies, eigenvectors and spin and charge densities were evaluated using the modified INDO programme described in Section III.F, with the tetramer radius, R_0 (the distance from the centre to an O atom) initially set at 2.5\AA .

The floating Gaussian exponent, γ , was raised in steps of 0.1 au from 0.1 to 0.5, and comparisons of the negative ion energies were made between clusters with extra orbitals on the cube face only and those with the Slaters on the cube faces and the centre.

Energies and exponents are listed in Table W. A.1. Both sets of results show a preferential lowering of the energy at $\zeta = 0.3$, with the cube faces plus centre set of orbitals giving lower energies throughout. This set is used in the remaining calculations, since either the extra flexibility of the set with the central orbital, or of this orbital's location, favours the e^- state.

Optimisation of the cluster radius, using the above basis set, was carried out in such a way that the "cube face" Slaters always remained on the faces of the cube delineated by the tetrahedrally disposed O atoms.

Energies using the full basis, and using no extra orbitals at all are compared in Table V. A.2. (neutral state) and V. A.3. (excess electron state). Although the data are incomplete*, two conclusions emerge: the e^- state displays an optimum cavity radius at $\sim 2\text{\AA}$ on the minimal basis calculation, and in each case the addition of the diffuse basis lowers the energy levels considerably.

One expects, as shown in Table V. A.3., that the e^- state with the diffuse basis will also show such a configurational minimum, but at more negative energies than the minimal basis calculations.

However, the energy of the excess electron state still remains above the neutral state in each case, although addition of the diffuse basis narrows the gap: for instance, at $R_0 = 1.5\text{\AA}$, and a minimal valence basis, the gap is 2.9 eV, whereas addition of 7 $\zeta = 0.3$ Slaters reduces this to 1.8 eV. If other criteria for electron-trapping are studied, we obtain similar results.

Preferential stabilisation of the e^- state might be expected to

* Convergence was unobtainable in some of the cases, especially when extra floating Slaters were added.

yield a negative eigenvalue for the excess α spin MO; these were examined, the results being listed in Table V. A.4. In each case, the magnitude of the eigenvalue is reduced by the diffuse basis, but remains positive. Finally, the excess Mulliken spin distributions were examined for the two bases at several cluster radii, as shown in Table V. A.5. Here, the results seem to indicate some tendency towards excess electron capture: the minimal basis cluster, on expansion from $R_0 = 1.5A^0$, experiences a spin density shift to the four central protons, this density, at the energetically optimal radius of $2A^0$, being 0.04 per proton; addition of the 7 extra orbitals magnifies this shift, since the total ρ^s associated with the central orbitals varies from 0.02 at $R_0 = 1.5A^0$ to 0.83 at $2.5A^0$.

Thus, although theoretical results indicate some localisation of the excess electron, no definite evidence of trapping on a lone $(CH_3OH)_4$ cluster has yet been adduced. Several improvements might be made in the above study:

(a) the INDO calculations used possess by necessity some arbitrary parameterisation, which could be dispensed with in an ab initio calculation

(b) the diffuseness and flexibility of the basis set might be further improved

(c) if we are to use the excess spin density round the molecule as a trapping criterion, the Mulliken method is inadequate; a spatial plot of $\langle \hat{\Psi} | \hat{\rho}^s(\underline{R}) | \hat{\Psi} \rangle$, where $\hat{\rho}^s(\underline{R})$ is the spin density operator at the point \underline{R} , is required. This is tried in Section V.C.

With these ideas in mind, work was begun on a small cluster, namely $(NH_3)_2$, using a fairly flexible and diffuse basis set, at an ab initio level.

B. An Ab Initio Study of Possible Electron Trapping on an $(\text{NH}_3)_2$ Cluster: The Effect of Basis Diffuseness

The geometrical configuration used is depicted in Fig. V. B.1., where the N-H H-N bonds are linear, and the dimer lies in the staggered conformation (Point group C_{2h}). The experimentally observed geometry (4) of $\text{HNH} = 106.7^\circ$ and $R(\text{N-H}) = 1.9117$ au was used.

Since this calculation was to use a larger basis set, the dimer geometry was restricted to two cases having N...N separations of 5.4 au and 5.6 au respectively.

(1) Basis set

It was intended to make the basis set diffuse (to more easily accommodate a loosely bound electron) but flexible enough to avoid a spuriously high energy for the neutral species. Following the method of Naleway and Schwartz (5) a split double-zeta type Gaussian set was obtained as follows: a (N/7,3,1) 2s, 2p, 1d GTO basis set with a d-type polarisation function developed for NH_3 by Roos and Siegbahn (6a,6b) was "split" by removing the most diffuse Gaussian in the s and p contractions, and using these with the zetas unchanged (7). For hydrogen a polarisation set of GTOs by Dunning (8) was split in the same way. Full details of the basis set are in Table V. B.6., where it can be seen that the set for N comprised effectively 4 s orbitals (2 normal and 2 diffuse), 2 p orbitals (1 normal and 1 diffuse) and 1 d orbital: H, similarly, had 2 s orbitals (1 normal and 1 diffuse) and 1 p orbital. Calculations vindicate this basis, giving an energy of -56.145 au for the neutral NH_3 monomer (Virial coefficient 2.0044) as opposed to Roos and Siegbahn's -56.138 au for their original (N/7,3,1), (H/4,1) basis set.

However, since the excess electron may be a loosely bound species, this diffuse N basis was supplemented by four very diffuse GTOs with exponents 0.008, 0.005, 0.002 and 0.001 to form a hyperdiffuse basis set.

With this set, neutral NH_3 gave an energy of -56.146 au (Virial coefficient 2.0045) showing only a difference of 0.001 au over the diffuse set. For the excess electron state of NH_3 , the diffuse and hyperdiffuse sets gave energies of -55.978 and -56.145 au respectively. This difference of 0.167 au indicates the hyperdiffuse basis to be more apposite to such negative ion states.

(ii) Properties of the dimer and effect of the hyperdiffuse orbitals

(a) Energies. The energies for the dimer ground state (1A_g), excess electron ground state (2A_g) and excess electron excited state (2B_u) for both basis sets and both geometries are detailed in Tables V. B.1. and V. B.2. The most pertinent fact about stabilities is that the energy of $(\text{NH}_3)_2^-$ is higher than that of $\text{NH}_3 + \text{NH}_3^-$ with both basis sets, indicating either (1) that the $(\text{NH}_3)_2$ arrangement chosen will not stabilise an electron or (2) that the two geometries chosen lie on an unfavourable part of the configuration coordinate curve, as illustrated in Fig.V. B.2. The latter hypothesis is refuted by the diffuse basis results, where the 5.4 au negative dimer (-112.045 au) has an energy below that of the 5.6 au negative dimer (-111.963 au), but both are above the $\text{NH}_3 + \text{NH}_3^-$ energy of -112.123 : no possible fit can be made to a configuration curve. Improvement of the basis set to hyperdiffuse quality reverses the 5.4 au and 5.6 au energy levels (see again Fig.V. B.2), making a fit possible; it is conjectured that such orbitals may be vital in dealing with excess electronic states.

For the diffuse basis, the excess electron state in $(\text{NH}_3)_2$ lies 4.48 eV above the neutral state at the 5.4 au geometry, and 4.2 eV above it for the 5.6 au one, but the hyperdiffuse basis reduces both these gaps to 0.03 eV. Evidently any such energy difference is very basis-sensitive.

Similarly, Franck-Condon transitions between the 2A_g and 2B_u

states yield 1.26 eV and 0.924 eV for the diffuse basis, but 0.023 eV for both with the hyperdiffuse basis, as against the experimental observation of 0.80 eV (9). This energy lowering is clearly not in agreement, and suggests that the electron in $(\text{NH}_3)_2^-$ is in fact bound at these geometries, and that the favouring of hyperdiffuse functions indicates its tendency to leave the cluster altogether.

Since no more calculations on different N...N separations were essayed, no configuration curves which might have given indicators of the stabilities of these states was available. However, it can be concluded from the data on the hyperdiffuse set energies that a configurational minimum for the $(\text{NH}_3)_2^-$ calculation exists at $\text{N} \dots \text{N} > 5.6$ au, but that further diffuse functions may cause the electron to "drift off" completely. With this in mind, the other properties may be investigated.

(b) H.O.O. Eigenvalues. Table V. B.5. shows the eigenvalues of the highest occupied orbital for the 2A_g and 2B_u state in the two geometries and basis sets. Nowhere does this have the negative value which might denote electron capture, but the eigenvalues of the 5.6 au geometry are consistently the lower, and the hyperdiffuse basis lowers the eigenvalue significantly in all cases. (Again, whether more diffuse functions would lower the value below zero or merely nearer to zero cannot be decided).

(c) Mulliken Spin Distributions. These are shown in Table V. B.3. According to the diffuse basis results, little spin density resides on the inner protons, and much more on the outer ones, apparently refuting the qualitative notion that opposed protons act as a kind of electron trap (see also Section VI. E). Expanding the dimer from 5.4 au to 5.6 au causes an inward shift in spin density from the outer protons, so that the 5.6 au geometry has an outer proton spin density of 0.258, as

against 0.292 for the 5.4 au geometry. Excitation, however, reverses this effect: in both cases the spin is shifted outwards (cf the INDO water dimer calculations of Section IV), but the 5.6 au geometry acquires a spin density of 0.309 on its outer protons, while the other dimer has 0.304. This is consistent both with the concept that the excess electron expands on excitation, and that hyperdiffuse orbitals are required for an adequate simulation.

Addition of the hyperdiffuse orbitals has dramatic results: all the Mulliken spin density in both geometries and both states is now associated with the four hyperdiffuse s-type GTOs on the nitrogen atoms.

Of course, this does not suggest localisation of the excess electron on nitrogen: the Mulliken spin distribution merely indicates the partitioning of excess spin between the various orbitals, and since one set, namely the nitrogen s orbitals, has been grossly overloaded with hyperdiffuse functions which appear to describe the electron more accurately, the spin becomes associated with the nitrogen. The more equitable distribution of orbitals in the diffuse basis calculations should result in a better, but not satisfactory, reflection of the true partitioning. It was thus felt necessary to step beyond the limited applicability of the Mulliken analysis and compute the actual values of $\langle \Psi | \rho^s(\underline{R}) | \Psi \rangle$ at various points in space and at the nuclear centres.

(d) Actual Spin Density and Potential Calculations. Since calculation of actual spin densities and potentials, although useful, is expensive in terms of computer time and core (typically 20 min and 570K on an IBM 370/158 for one set of results on one such molecule) computation was limited to the hyperdiffuse case only, and to the N...N axis of the dimer. Properties at a set of points along this axis, and

at the nuclei, were evaluated using the ATMOL properties package (10). The data obtained for each case are listed in Tables V. B. 7-12.

Examination of net spin densities at points from the molecular centre up to 14 au along the N...N axis show the values to be negligibly small, the only nonzero value being one of 0.0003 au on nitrogen for the 2A_g state of both geometries, a scarcely significant value. The suggestion is (although the diffuse basis properties would be needed to verify it) that since, as seen in Section V. B., virtually all the excess spin density resides in the hyperdiffuse orbitals, the effective spin density in any small volume has been reduced to near zero: one is forced to conclude, especially from the nuclear spin densities, that the excess electron does not bind to the dimer, and that addition of further hyperdiffuse orbitals will merely remove the excess electron from the molecule, leaving $(NH_3)_2^+ e^-$. In this structure, therefore, any electron capture must be transient and loose.

Finally, in Fig.V. B.3. and Fig.V. B.4., total potentials for the neutral 1A_g 5.4 au and 5.6 au geometries are plotted along the N...N axis (graphs for the 2A_g and 2B_u , which were virtually indistinguishable, are not shown). The graphs, when considered as traps for a negative charge, have a deep potential well (+ 14.85 au) in the vicinity of the nitrogen nucleus, and a shallower one (~ -6 au) at the central protons; the outer protons have no discernible effect on the shape of the curve. If such combinations of deep and shallow wells exist in other molecules, they may serve as models for, e.g., the photo-shuttle effect (11) and other situations where different trap depths are observed (12, 13), such as selective photobleaching and time-dependent spectra.

(e) H.O.O. M.O. Coefficients. These confirm the tendency for the structure to lose the excess electron. The orbital coefficients of the highest occupied orbital were examined for all the excess electron

states, on the basis that if the coefficient of the most diffuse orbital did not predominate, then the electron was showing some tendency to remain in the vicinity of the cluster. The coefficients are shown in Table V. B.13., whence it can be seen that the most diffuse orbital is the greatest contribution in each case, and that excitation accentuates this tendency greatly.

(iii) Conclusions

It can be adduced from the above studies that the $(\text{NH}_3)_2$ cluster examined is not a likely candidate for electron trapping. Addition of more diffuse functions causes the excess electron to "drift" further off the cluster, as judged by a variety of criteria, and excitation accentuates the process. The partitioning of the electron, as measured by the Mulliken Analysis, is highly dependent on the nature and distribution of the basis set, and calculation of nuclear spin densities of excess electrons made in such a way (14, 15, 16) must be viewed in this light. Spatially evaluated spin densities in the molecule suffer a dilution due to the diffuseness of the electron but useful data should be obtainable in cases where the electron is bound to the cluster. The combination of deep and shallow potentials detected may serve as electron traps in more stable clusters, leading to preferential spectral bleaching, photo-shuttling and time-dependent variations in the optical spectra.

It may be that the most favourable trapping situation lies at a non-regular geometry of the molecule (17). With this in mind, a vibrating NH_3 molecule was chosen for study.

C. Non-Regular Geometries - the Umbrella Vibration of NH_3 and NH_3^-

(i) Geometry and Basis set

Calculations so far using $E(\text{neutral}) > E(\text{negative state})$ as the sole criterion for electron trapping, have failed to define any stable structures which preferentially capture electrons, although Webster (18) has postulated such capture from ab initio calculations on H_2O and H_2C . While long-range medium effects are obviously of importance in these studies, it may be that certain esoteric geometries (17) favour electron capture for long enough to allow stabilising relaxation processes to occur. This has led to the present ab initio study of the umbrella vibration of NH_3 and NH_3^- using the ATMOL suite of programmes.

The geometry chosen had a bond length as in Section V. B., but the lone-pair-N-H angle, θ , was allowed to vary from 90° to 130° in ten-degree steps (see Fig.V. C.1).

The basis set used was the diffuse set of Section V. B., although some results were obtained using the hyperdiffuse set. As is well known from attempts to calculate the inversion barrier in NH_3 (34-39), polarisation orbitals such as d on nitrogen and p on hydrogen are indispensable to describe adequately the planar D_{3h} transition state. Table V. B.6. shows the basis set used by the present author.

With this basis, the inversion barrier $E(D_{3h}) - E(C_{3v})$ is placed at 0.55 eV for the diffuse basis and 0.57 eV for the hyperdiffuse, comparing reasonably with the experimental value of 0.25 eV (19).

(ii) Change of Properties on Vibration

The energies and properties of the neutral state (${}^1A'_1$ for $\theta = 90^\circ$ and 1A_1 for $\theta \neq 90^\circ$) were evaluated in the standard manner, the excess electron state being calculated using a SUMF technique (20, 21, 22).

MO occupations were found to be as follows: for the D_{3h} geometry, neutral; $1a'_1(2)2a'_1(2)1e'(4)1a''_2(2); 3a'_1(0)\dots$, and excess electron;

$1a_1'(2)2a_1'(2)1e'(4)1a_2''(2)3a_1'(1) \vdots 2e'(0) \dots$; and for the C_{3v} geometries, neutral; $1a_1(2)2a_1(2)1e(4)3a_1(2) \vdots 4a_1(0)$ excess electron; $1a_1(2)2a_1(2)1e(4)3a_1(2)4a_1(1) \vdots 2e(0) \dots$. Thus promotion from the excess electron state is to a doubly degenerate MO in each case, and the excited state cannot be described by a single Slater determinant. For this reason only the neutral and excess electron states were studied.

(a) Energies. Energies obtained are shown in Table V. C.1. From a plot of the Neutral State Energy (Diffuse Basis) against θ (Fig. V. C.2), an energetic minimum in the region of $\theta \sim 116^\circ$ is apparent, as is the inversion barrier at $\theta = 90^\circ$. The excess electron state energy (Diffuse Basis) against θ (Fig. V. C.3), although higher in energy at each point than the neutral state ($E_e - E_{\text{neut}} \approx 4.6$ eV at $\theta = 112.1^\circ$) nevertheless displays an energetic minimum at 116° , forming a fairly shallow trap of depth ~ 0.5 eV. Comparison with the available hyperdiffuse results shows the same trend as the dimer calculations: the neutral states are barely affected by the extra orbitals, but the excess electron states drop to about 0.001 au above the neutral ones, suggesting again a tendency to formation of the neutral monomer plus a free electron. The H.O.O. eigenvalues in Table V. C.2. further confirm this.

(b) Mulliken Spin Densities. The Mulliken Spin Densities for the excess electron state (Diffuse Basis) are shown in Table V. C.3. The proton spin density is at a maximum for the planar form, decreasing as the hybridisation of N moves from sp^2 to sp^3 , while the nitrogen spin density is negative, becoming less so as the molecule differs from planarity: thus the net trend is for spin to shift to the centre upon bending. However, proton magnetic resonance data on sodium/ammonia solutions indicate a negative value for the proton spin density (23, 24, 25), in disagreement with the results of Table V. C.3. For a more

realistic description of the spin densities, it was decided to evaluate

$\langle \Psi | \rho^s(\underline{R}) | \Psi \rangle$ at various points.

(c) Spin Densities at the Nuclei - Negative Spin Densities on the Ammonia Proton

Spin and charge densities and potentials were evaluated at points along the C_3 axis of symmetry of the molecule, up to 9 au from the nitrogen atom in both directions, using the ATMOL properties programme.

The results for different values of θ are shown in Tables V. C.4. - V. C.8., where the properties at the nuclei are also shown. Now the general trend is seen to be reversed - as the molecule deviates from planarity, spin shifts away from the nitrogen nucleus. Even more striking is the negative proton spin density, which is emphasised as θ increases from 100° . Such a negative spin density has been suggested by r.m.r. observations on metal-ammonia solutions (23, 24, 25) and obtained theoretically by Ishimaru et al. (14, 26) and Newton (27, 28). However, the former used semi-empirical-type calculations, involving a Mulliken-type analysis. Since the present calculation involves no arbitrary parameters, and spin densities are evaluated at the nuclei, it is more comparable with that of Newton. At $\theta = 110^\circ$, the N and H spin densities are $+0.5115a_0^{-3}$ and $-0.0063a_0^{-3}$ respectively, compared with Newton's values of $+0.05a_0^{-3}$ and $-0.00063a_0^{-3}$ for his dipole-oriented $(NH_3)_4$ cluster surrounded by a polarised medium.

It would thus appear that constraining the electron to an isolated NH_3 molecule causes greater spin densities at the nuclei, with greater disparity between them.

A pointer to the behaviour of the excess electron in NH_3 is the fact that the spin densities at all the nuclei decrease as θ increases from 90° , suggesting a tendency for the species to move off the molecule.

D. Conclusions: the Nature and Scope of Short-Range Effects on Electron Solvation

Many data have been presented on the possibility of solvation. The inescapable conclusion for the models studied so far is that for a cluster of n molecules of X , (where X is a normal neutral molecule), $E(X\bar{n}) > E(X_n)$ both at an ab initio and reasonably parameterised JNDO level. The only case where the reverse obtains would appear to be in improbable molecular distortions, as mentioned in Section IV. B's comments on the unnoticed result of Naleway and Schwartz (5).

One can escape this dilemma either by redefinition of ΔE as $E(X\bar{n}) - E(nX+e^-)$ (26) or by recognising that this energy change is not the only factor defining solvation. Examination of other criteria, however, such as (a) the eigenvalue of the highest occupied orbital, (b) the coefficients of the most diffuse orbitals in the highest occupied M.O., (c) Mulliken spin distributions and (d) actual point spin densities in space, shows that although the excess electron states studied in these chapters may possess energetic configurational minima, the addition of more diffuse orbitals indicates a tendency for the electron to leave the molecule completely.

Several interesting points have been highlighted in the process. Neutral/excess electron states have energy differences which are critically dependent on the diffuseness of the basis set, and in the $(NH_3)_2$ and NH_3 studies, where exceptionally diffuse orbitals have been added, this difference tends to zero. Added flexibility can have its disadvantages, and the examination of some of the previous cluster calculations (14, 15, 29) with such orbitals added might lead to a drastic fall in reported negative ion state energies. Indeed, such an outcome is anticipated and well rationalised by Naleway and Schwartz, who regard very diffuse orbitals as being unrealistic for the liquid state, where other molecules would encroach on them.

Excitation energies, where available, appear to be dependent on the nature of the basis set, and any agreement obtained with more limited sets can be argued to be fortuitous.

Mulliken spin densities, used by other workers in such calculations, can be varied by shifting the weighting of orbitals on atomic centres, and, although useful for determining general trends in spin shift ⁽¹⁵⁾ should not be quantitatively related to e.s.r. spectra. The evaluation of actual spin densities at the nuclei is in principle preferable, but in this study has the disadvantage that Gaussians do not reproduce the cusp behaviour at the nucleus ⁽³⁰⁾, although cusped-Gaussian functions ⁽³¹⁾ could be used.

It would appear that clusters alone do not stabilise an excess electron, and that neither enlargement of the cluster size (Section IV.D) nor great flexibility of the basis set (Sections V. B and D) will alter this. For effective solvation, it seems that the surrounding medium and its concomitant long-range interactions cannot be neglected.

Small clusters, perhaps in some vibrationally distorted mode, could act as transient traps for the electron, localising it until long-range medium electronic and inertial polarisation fields have formed.

This picture of an electron loosely bound near some cluster in the liquid, but retained by long-range and more uniform polarisation fields, could go a long way towards explaining the similarity of shape in the optical spectra of the trapped electron ^(32, 33) regardless of the nature of the solvent.

References V

1. For alcohols, see:
 - (a) J.H. Baxendale and P. Wardman, Chem. Commun. (1971) 429.
 - (b) J.H. Baxendale and P. Wardman, J. Chem. Soc., Faraday Trans.I 69 (1973) 584.
 - (c) R.R. Hentz and G.A. Kenney-Wallace, J. Phys. Chem., 78 (1974) 514.
 - (d) J. Moan, Chem. Phys. Lett., 17 (1972) 565.
 - (e) H. Hase and T. Warashima, J. Chem. Phys., 59 (1973) 2152.
 - (f) T. Shida, S. Iwata and T. Watanabe, J. Phys. Chem., 76 (1972) 3683.
2. For ammonia, see:
 - (a) R.K. Quinn and J.J. Lagowski, J. Phys. Chem., 72 (1968) 1374.
 - (b) J.L. Dye: in J.J. Lagowski and M.J. Sienko (eds): Metal-Ammonia Solutions p.1 London, Butterworths, 1970.
 - (c) R. Catterall, *ibid.*, p.105.
 - (d) R.A. Pinkowitz and T.J. Swift, J. Chem. Phys., 54 (1971) 2353.
 - (e) Farhataziz, L.M. Perkey and R.R. Hentz, J. Chem. Phys., 60 (1974) 4383.
3. J.A. Pople and D.L. Beveridge, Approximate Molecular Orbital Theory, p.106, McGraw-Hill, New York 1970.
4. A. Rauk, L.C. Allen and E. Clementi, J. Chem. Phys., 52 (1970) 4133.
5. C.A. Naleway and M.E. Schwartz, J. Phys. Chem., 76 (1972) 3905.
6. (a) B. Roos and P. Siegbahn, Theor. Chim. Act., 17 (1970) 199.
(b) B. Roos and P. Siegbahn, Theor. Chim. Act., 17 (1970) 199.

7. An attempt was made to reoptimise the truncated linear combination of 6 Gaussians for the s functions by fitting it numerically to the function represented by the original 7, but the energies obtained in trial calculations were higher than those in the unoptimised truncated set.
8. T.H. Dunning, J. Chem. Phys., 53 (1970) 2823.
9. R.K. Quinn and J.J. Lagowski, J. Phys. Chem., 73 (1969) 2326.
10. I.H. Hillier and V.R. Saunders, Atlas Computer Laboratory, (1973).
11. F.S. Dainton, Ber. Bunsenges. Phys. Chem., 75 (1971) 608.
12. K. Kawabata, H. Horii and S. Okabe, Chem. Phys. Lett., 14 (1972) 223.
13. T. Higashimura, M. Noda, T. Warashina and H. Yoshida, J. Chem. Phys., 53 (1970) 1152.
14. S. Ishimaru, T. Yamabe, K. Fukui and H. Kato, Chem. Phys. Lett., 17 (1972) 264.
15. C.M.L. Kerr and F. Williams, J. Phys. Chem., 76 (1972) 3838.
16. G. Howat and B. Webster, J. Phys. Chem., 76 (1972) 3714.
17. See the comments in Section IV. on Ref.5.
18. B. Webster, J. Phys. Chem., 79 (1975) 2809.
19. J.D. Swallen and J.A. Ibers, J. Chem. Phys., 36 (1962) 1914.
20. J.C. Slater, Phys. Rev., 35 (1930) 210.
21. J.A. Pople and R.K. Nesbet, J. Chem. Phys., 22 (1954) 571.
22. All values of the Virial Coefficient for the excess electron state differed from 2 only in the 3rd decimal place, and all values of $\langle S^2 \rangle$ were close to 0.756.
23. T.R. Hughes, Jr., J. Chem. Phys., 38 (1963) 202.
24. D.E. O'Reilly, J. Chem. Phys., 41 (1964) 3736.
25. B.B. Wayland and W.L. Rice, J. Chem. Phys., 45 (1966) 3150.
26. S. Ishimaru, H. Kato, T. Yamabe and K. Fukui, J. Phys. Chem., 77 (1973) 1450.

27. M.D. Newton, J. Chem. Phys., 58 (1973) 5833.
28. M.D. Newton, J. Phys. Chem., 79 (1975) 2795.
29. M. Weissmann and N.V. Cohan, Chem. Phys. Lett., 7 (1970) 445.
30. R.P. Hosteny, R.R. Gilman, T.H. Dunning, A. Pipano and I. Shavitt, Chem. Phys. Lett., 7 (1970) 325.
31. E. Steiner and B.C. Walsh, Quantum Chemistry - the State of the Art: Atlas Symposium No.4, 1974, p.151.
32. T. Shida, S. Iwata and T. Watanabe, J. Phys. Chem., 78 (1972) 3683.
33. T. Shida, S. Iwata and T. Watanabe, *ibid.*, 78 (1972) 3691.
34. U. Kaldor and I. Shavitt, J. Chem. Phys., 45 (1966) 888.
35. E. Clementi, J. Chem. Phys., 46 (1967) 3851.
36. W.H. Fink and L.C. Allen, J. Chem. Phys., 46 (1967) 2276.
37. R.G. Body, D.S. McLure and E. Clementi, J. Chem. Phys., 49 (1968) 4916.
38. A. Rauk, L.C. Allen and E. Clementi, J. Chem. Phys., 52 (1970) 4133.
39. R.M. Stevens, J. Chem. Phys., 55 (1971) 1725.

TABLE V. A.1.

(CH₃OH)₄ Clusters - Excess Electron State Energies: R = 2.5 Å⁰

ζ	ENERGY OF e ⁻ STATE (au)	
	Slaters on Cube Faces Only	Slaters on Faces and Centre
0.1	-110.0044273861	-110.0289248104
0.2	-110.2016688202	-110.2625457388
0.3	-110.2658026045	-110.3422086751
0.4	-110.2179673142	-110.2968608103
0.5	-110.1216349625	-110.1812048919

TABLE V. A.2.

(CH₃OH)₄ Clusters - Neutral State Energies as Radius is Varied

R_0 (Å ⁰)	ENERGY OF NEUTRAL STATE (au)	
	With 7 Extra Floating Slaters ($\zeta=0.3$)	Minimal Valence Basis
1.5	-110.0101400676	-109.0908839785
2.0	-110.6289200934	-109.88871736855
2.5		-109.8880774757
3.0	-110.2587757730	

TABLE V. A.3.

(CH₃OH)₄ Clusters - e⁻ State Energies as Radius is Varied

R_0 Å ⁰	ENERGY OF e ⁻ STATE (au)	
	With 7 Extra Floating Slaters ($\zeta=0.3$)	Minimal Valence Basis
1.5	-109.9424004630	-108.9829430424
2.0	-110.5444328947	-109.7542213754
2.5	-110.3422086751	-109.7035179698
3.0		-109.6785470761

TABLE V. A.4.

(CH₃OH)₄ Clusters: Eigenvalues of the Excess α Spin MO

R_o (A ^o)	EIGENVALUE OF THE EXCESS α SPIN MO (au)	
	Diffuse Basis ($\zeta = 0.3$)	Minimal Valence Basis
1.5	0.0036	0.0431
2.0		0.0953
2.5	0.0783	0.1638
3.0		0.1952

TABLE V. A.5.

(CH₃OH)₄ Clusters: Mulliken Spin Densities

R_o (A ^o)	EXCESS SPIN DENSITIES FOR EXTRA BASIS CALCULATIONS				EXCESS SPIN DENSITIES FOR VALENCE BASIS		
	ρ_O^s	ρ_H^{s*}	ρ_C^s (Central Orbital)	ρ_T^s **	ρ_O^s	ρ_H^{s-}	$\rho_{\text{inner H}}^s$
1.5	0.27	0.01	0.02	0.03	0.29	-0.02	-0.05
2.0	0.00	0.00	0.83	1.00	0.20	0.00	0.04
2.5	0.00	0.00	0.83	1.00	0.13	0.01	0.10
3.0					0.09	0.01	0.11

* Average ρ^s on the 3 Methyl Protons** Total ρ^s on the 7 Diffuse Orbitals

TABLE V. B.1.

Ab Initio (NH₃)₂ Cluster: Comparison of Ground State Energies for the Diffuse and Hyperdiffuse

Basis at the 5.4 au Geometry

	DIFFUSE BASIS: ENERGY (au)	HYPERDIFFUSE BASIS: ENERGY (au)
Neutral Ground State (¹ A _g)	-112.20990309	-112.21209845
Excess Electron Ground State (² A _g)	-112.04519111	-112.21095775
Excess Electron Excited State (² B _u)	-111.99882039	-112.21010692

TABLE V. B.2.

Ab Initio (NH₃)₂ Cluster: Comparison of Ground State Energies for the Diffuse and Hyperdiffuse

Basis at the 5.6 au Geometry

	DIFFUSE BASIS: ENERGY (au)	HYPERDIFFUSE BASIS: ENERGY (au)
Neutral Ground State (¹ A _g)	-112.11856925	-112.23737419
Excess Electron Ground State (² A _g)	-111.96261400	-112.23623616
Excess Electron Excited State (² B _u)	-111.92866667	-112.23537627

TABLE V. B.3.

Ab Initio (NH₃)₂ Cluster: Comparison of Mulliken Spin Densities for the Diffuse and Hyperdiffuse Basis Set at the 5.4 au Geometry

		DIFFUSE BASIS: ρ^S	HYPERDIFFUSE Basis: ρ^S
Ground State (² A _g)	Excess Electron	Ns (DIFFUSE)	0.000
		Ns (HYPERDIFFUSE)	0.500
		N (TOTAL)	-0.212
		H INNER	0.128
		H OUTER	0.292
Excited State (² B _u)	Excess Electron	Ns (DIFFUSE)	0.000
		Ns (HYPERDIFFUSE)	0.500
		N (TOTAL)	-0.158
		H INNER	0.051
		H OUTER	0.304

TABLE V. B.4.

Ab Initio (NH₃)₂ Cluster: Comparison of Mulliken Spin Densities for the Diffuse and Hyperdiffuse Basis Set at the 5.6 au Geometry

STATE	ORBITAL	DIFFUSE BASIS ρ^s	HYPERDIFFUSE BASIS ρ^s
Excess Electron Ground State (² A _g)	N _s (DIFFUSE)	-0.146	0.000
	N _s (HYPERDIFFUSE)		0.500
	N (TOTAL)	-0.146	0.500
	H INNER	0.130	0.000
	H OUTER	0.258	0.000
Excess Electron Excited State (² B _u)	N _s (DIFFUSE)	-0.206	0.000
	N _s (HYPERDIFFUSE)		0.500
	N (TOTAL)	-0.198	0.500
	H INNER	0.081	0.000
	H OUTER	0.309	0.000

TABLE V. B.5.

Ab Initio (NH₃)₂ Cluster: Comparison of Eigenvalues of Highest Occupied
Orbital for Diffuse and Hyperdiffuse Basis set at the 5.4 au and 5.6 au
Geometries

GEOMETRY	STATE	DIFFUSE BASIS	HYPERDIFFUSE BASIS
5.4 au	Excess Electron Ground State (² A _g)	0.1583005	0.0011406
	Excess Electron Excited State (² B _u)	0.2065548	0.0019914
5.6 au	Excess Electron Ground State (² A _g)	0.1477628	0.0011380
	Excess Electron Excited State (² B _u)	0.1850785	0.0019979

TABLE V. B.6.

Diffuse double-zeta set used in NH₃ ab initio calculations

<u>Atom/Orbital</u>	<u>Coefficient</u>	<u>Zeta</u>
N (s)	0.0044790	2038.41
	0.0345810	301.689
	0.1642630	66.463
	0.4538980	17.8081
	0.4689790	5.30452
	0.0380390	0.764993
N (s)	1.0	0.2344240
N (s)	-0.0009810	2038.41
	-0.007822	301.689
	-0.037808	66.463
	-0.128928	17.8081
	-0.197084	5.30452
	0.513598	0.764993
N (s)	1.0	0.2
N (p)	0.119664	5.95461
	0.474629	1.23292
N (p)	1.0	0.286752
N (d)	1.0	0.95
H (s)	0.03283	13.3615
	0.23121	2.0133
	0.81724	0.4538
H (s)	1.0	0.1233
H (p)	1.0	0.789

TABLE V. B.7.

Ab Initio (NH₃)₂ Cluster: Hyperdiffuse Basis: N...N 5.4 au: Potential,
and Spin and Charge Densities: Neutral ¹A_g State

Distance along N...N axis (au)	ρ	V (au)
0	0.1252	- 9.7044
1	0.3910	-16.1638
2	0.5056	-16.7844
3	3.7796	-38.9400
4	0.1466	- 8.6580
5	0.0140	- 5.3844
6	0.0012	- 4.0638
7	-	-3.2994
8	-	-2.7892
9	-	-2.4220
10	-	-2.1438
11	-	-1.9254
12	-	-1.7486
13	-	-1.6026
14	-	-1.4796
N	185.9316	14.8540
H inner	0.4126	- 6.4026
H outer		- 4.8868

TABLE V. B.8.

Ab Initio (NH₃)₂ Cluster: Hyperdiffuse Basis: N...N 5.4 au: Potential,
 and Spin and Charge Densities: Excess Electron ²A_g State

Distance along N...N axis (au)	$\rho^{\alpha + \beta}$	$\rho^{\alpha - \beta} = \rho^s$	V (au)
0	0.1252	0	- 9.67
1	0.3910	-	-16.1294
2	0.5056	-	-16.7501
3	3.7796	-	-38.9055
4	0.1466	-	- 8.6237
5	0.1400	-	- 5.3500
6	0.0012	-	- 4.0295
7	0	-	- 3.2649
8	-	-	- 2.7549
9	-	-	- 2.3878
10	-	-	- 2.1098
11	-	-	- 1.8914
12	-	-	- 1.7148
13	-	-	- 1.5690
14	-	-	- 1.4462
N	185.9317	0.0003	14.8863
H inner	0.4126	-	- 6.3681
H outer	0.3800	-	- 4.8524

TABLE V. B.9.

Ab Initio (NH₃)₂ Cluster: Hyperdiffuse Basis: N...N 5.6 au; Potential,
and Spin and Charge Densities: Excess Electron Excited ²B_u State

Distance along N...N axis (au)	$\rho^{\alpha} + \beta$	$\rho^{\alpha} - \beta = \rho^s$	V (au)
0	0.1252	0	- 9.6779
1	0.3910	-	-16.1373
2	0.5056	-	-16.7579
3	3.7796	-	-38.9134
4	0.1466	-	- 8.6315
5	0.0140	-	- 5.3578
6	0.0012	-	- 4.0371
7	-	-	- 3.2723
8	-	-	- 2.7620
9	-	-	- 2.3946
10	-	-	- 2.1163
11	-	-	- 1.8976
12	-	-	- 1.7206
13	-	-	- 1.5744
14	-	-	- 1.4512
N	185.9316	-	14.8805
H inner	0.4126	-	- 6.3759
H outer	0.38	-	- 4.8602

TABLE V. B.10

An Initio $(\text{NH}_3)_2$ Cluster: Hyperdiffuse Basis: N...N 5.6 au: Potential,
 and Spin and Charge Densities: Neutral 1A_g State

Distance along N...N Axis (au)	$\rho^{\alpha} + \beta$	V (au)
0	0.0940	- 9.0374
1	0.4136	-24.2702
2	0.4678	-14.8468
3	13.2042	-60.1402
4	0.1858	- 9.2462
5	0.0174	- 5.5174
6	0.0016	- 4.1186
7	-	- 3.3290
8	-	- 2.8074
9	-	- 2.4342
10	-	- 2.1524
11	-	- 1.9316
12	-	- 1.7534
13	-	- 1.6062
14	-	- 1.4826
N		14.9062
H inner		- 6.2104
H outer		- 4.9246

TABLE V. B.11.

Ab Initio $(\text{NH}_3)_2$ Cluster: Hyperdiffuse Basis: N...N 5.6 au: Potential,
 and Spin and Charge Densities: Excess Electron 2A_g State

Distance along N...N axis (au)	$\rho^{\alpha+\beta}$	$\rho^{\alpha-\beta} = \rho^s$	V (au)
0	0.0940	-	- 9.0029
1	0.4136	-	-24.2357
2	0.4678	-	-14.8123
3	13.2042	-	-60.1059
4	0.1858	-	- 9.2118
5	0.0174	-	- 5.4829
6	0.0016	-	- 4.0842
7	-	-	- 3.2944
8	-	-	- 2.7731
9	-	-	- 2.4000
10	-	-	- 2.1183
11	-	-	- 1.8976
12	-	-	- 1.7195
13	-	-	- 1.5726
14	-	-	- 1.4491
N		0.0003	14.9407
H inner		-	- 6.1759
H outer		-	- 4.8901

TABLE V. B.12.

Ab Initio $(\text{NH}_3)_2$ Cluster: Hyperdiffuse Basis: N...N 5.6 au: Potential,
 and Spin and Charge Densities: Excess Electron 2A_1 State

Distance along N...N axis (au)	$\rho^{\alpha+\beta}$	$\rho^{\alpha-\beta}$	V (au)
0	0.0940	-	- 9.0109
1	0.4136	-	-24.2437
2	0.4678	-	-14.8203
3	13.2042	-	-60.1137
4	0.1858	-	- 9.2196
5	0.0172	-	- 5.4907
6	0.0016	-	- 4.0918
7	-	-	- 3.3020
8	-	-	- 2.7803
9	-	-	- 2.4069
10	-	-	- 2.1249
11	-	-	- 1.9039
12	-	-	- 1.7255
13	-	-	- 1.5781
14	-	-	- 1.4542
N	185.9396	-	14.9328
H inner	0.4088	-	- 6.1838
H outer	0.3896	-	- 4.8980

TABLE V. B.13.

Ab Initio (NH₃)₂ Cluster: Hyperdiffuse Basis: Coefficients of the H.O.O.

Geometry and State		Orbital ξ			
N...N		0.008	0.005	0.002	0.001
5.4 au	Excess Electron ² Ag	-0.2097	0.4356	-0.8414	1.0586
	Excess Electron ² Bu	-0.4298	-1.2474	4.4431	-9.9875
N...N					
5.6 au	Excess Electron ² Ag	0.2102	-0.4371	0.8420	-1.0587
	Excess Electron ² Bu	-0.4186	1.2110	-4.3107	9.6545

TABLE V. C.1.

An Initio NH₃: Umbrella Vibration: Energies of Neutral and Excess Electron States

Lone pair NH (θ) (degrees)	Diffuse Basis		Hyperdiffuse Basis	
	Neutral State Energy(au)	Excess Electron State Energy(au)	Neutral State Energy(au)	Excess Electron State Energy(au)
90	-56.1251	-55.9619	-56.1252	-56.1240
100	-56.1319	-55.9674	-56.1322	-56.1311
110	-56.1437	-55.9766	-	-
112.1	-56.1453	-55.9778	-56.1462	-56.1451
120	-56.1439	-55.9768	-	-
130	-56.1164	-55.9556	-	-

TABLE V. C.2.

Ab Initio NH₃: Umbrella Vibration: Highest Occupied Orbital Eigenvalues

Lone pair NH (θ) (degrees)	Diffuse Basis		Hyperdiffuse Basis	
	Neutral State H.O.O. Eigenvalue	Excess Electron State H.O.O. Eigenvalue	Neutral State H.O.O. Eigenvalue	Excess Electron State H.O.O. Eigenvalue
90	0.1680001	0.1576784	0.0011377	0.0011377
100	0.1703001	0.1581062	0.0011353	0.0011353
110	0.1744529	0.1591953	-	-
112.1	0.1750889	0.1592543	0.0011297	0.0011297
120	0.1757106	0.1577410	-	-
130	0.1712992	0.1496762	-	-

TABLE V. C.3.

Ab Initio NH₃: Umbrella Vibration: Excess Electron State: Variation
of Mulliken Spin Densities with Angle: Diffuse Basis

Lone pair-N-H (θ) (degrees)	$\rho_{N_s}^s$	$\rho_N^s(\text{TOTAL})$	$\rho^s(\text{H})$
90	-0.4973	-0.5992	0.5331
100	-0.4768	-0.5423	0.5141
110	-0.4280	-0.4465	0.4822
112.1	-0.4154	-0.4285	0.4762
120	-0.3650	-0.3713	0.4571
130	-0.2984	-0.3115	0.4372

TABLE V. C.4.

Ab Initio NH₃: Diffuse Basis: Excess Electron State: Charge and Spin
Densities and Potentials for the $\theta = 90^\circ$ Case

Distance up C ₃ Axis R (au)	$\rho^{\alpha+\beta}$	$\rho^{\alpha-\beta} = \rho^s$	V (au)
-9	0	0	- 0.4450
-8	"	"	- 0.5008
-7	"	"	- 0.5725
-6	"	"	- 0.6681
-5	"	"	- 0.8021
-4	"	"	- 1.0030
-3	0.0043	-0.0001	- 2.8901
-2.6	0.0121	-0.0001	- 3.8828
-2.2	0.0288	0.0	
-1.8	0.0661	0.0009	- 4.7386
-1.4	0.1643	0.0045	- 6.1716
-1.0	0.3778	0.0146	- 9.0427
-0.6	0.6981	0.0225	-16.5774
-0.2	14.0593	0.0340	-58.0387
N	186.0452	0.6296	
H	0.3578	0.0012	

TABLE V. C.5.

Ab Initio NH₃: Diffuse Basis: Excess Electron State: Charge and SpinDensities and Potentials for the $\theta = 100^\circ$ Case

Distance up C ₃ Axis R (au)	$\rho^\alpha + \beta$	$\rho^\alpha - \beta = \frac{1}{r^3}$	V (au)
-9	0	0	- 1.0043
-8	-	-	- 1.1297
-7	-	-	- 1.2905
-6	-	-	- 1.5044
-5	0.0002	0.0002	- 1.8024
-4	0.0008	0.0006	- 2.2469
-3	0.0037	0.0001	- 2.9777
-2.6	0.0098	-0.0002	- 3.4203
-2.2	0.0241	0.0001	- 4.0224
-2.0	0.0373	0.0009	- 4.4163
-1.8	0.0587	0.0027	- 4.9039
-1.4	0.1527	0.0133	- 6.3536
-1.0	0.3575	0.0401	- 9.2210
-0.6	0.6668	0.0648	-16.7146
-0.2	13.3866	0.0066	-58.0882
0.2	13.3274	0.0714	-57.9803
0.6	0.7108	-0.0004	-16.4810
1.0	0.3881	-0.0015	- 8.9177
1.4	0.1704	-0.0012	- 6.0435
1.8	0.0707	-0.0005	- 4.6196
2.0	0.0473	-0.0003	- 4.1511
2.2	0.0321	-0.0001	- 3.7783
2.6	0.0142	0	- 3.2199
3	0.0054	-	- 2.8174
4	0.0002	-	- 2.1561
5	-	-	- 1.7452
6	-	-	- 1.4646
7	-	-	- 1.2611
8	-	-	- 1.1071
9	-	-	- 0.9864
N	186.0976	0.5890	17.0724
H	0.3615	-0.0021	2.9338

TABLE V. C.6.

Ab Initio NH₃: Diffuse Basis: Excess Electron State: Charge and Spin
 Densities and Potentials for the $\theta = 110^\circ$ Case

Distance up C ₃ Axis R (au)	$\rho^{\alpha+\beta}$	$\rho^{\alpha-\beta}$	V (au)
-9	0	0	- 1.0128
-8	"	"	- 1.1404
-7	"	"	- 1.3044
-6	0.0001	0.0001	- 1.5230
-5	0.0005	0.0005	- 1.8294
-4	0.0019	0.0017	- 2.2933
-3	0.0046	0.0042	- 3.0737
-2.6	0.0091	0.0001	- 3.5487
-2.2	0.0213	-0.0003	- 4.1872
-2.0	0.0336	0.0004	- 4.5989
-1.8	0.0541	0.0027	- 5.1020
-1.4	0.1456	0.0172	- 6.5688
-1.0	0.3438	0.0546	- 9.4214
-0.6	0.6388	0.0928	-16.8586
-0.2	13.3954	-0.0016	-58.1399
0.2	13.2997	0.0725	-57.9934
0.6	0.7030	0.0002	-16.4273
1.0	0.3845	-0.0025	- 8.8478
1.4	0.1687	-0.0011	- 5.9701
1.8	0.0705	-0.0001	- 4.5487
2.0	0.0475	0.0001	- 4.0829
2.2	0.0325	0.0001	- 3.7133
2.6	0.0148	0.0002	- 3.1623
3.0	0.0059	0.0001	- 2.7676
4	0.0002	0.0	- 2.1227
5	0.0	"	- 1.7223
6	"	"	- 1.4480
7	"	"	- 1.2486
8	"	"	- 1.0972
9	"	"	- 0.9785
N	186.1965	0.5115	17.0631
H	0.3685	-0.0063	2.9588

TABLE V. C.7.

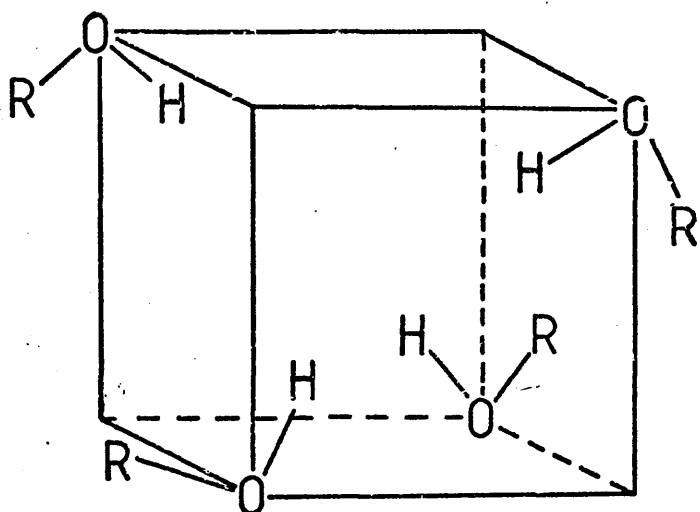
Ab Initio NH₃: Diffuse Basis: Excess Electron State: Charge and Spin
 Densities and Potentials for the $\theta = 120^\circ$ Case

Distance up C ₃ Axis R (au)	$\rho^{\alpha+\beta}$	$\rho^{\alpha-\beta}$	V (au)
-9	0	0	- 1.0215
-8	"	"	- 1.1515
-7	"	"	- 1.3189
-6	0.0001	0.0001	- 1.5427
-5	0.0010	0.0010	- 1.8585
-4	0.0040	0.0036	- 2.3462
-3	0.0075	0.0037	- 3.1926
-2.6	0.0113	0.0015	- 3.7115
-2.2	0.0233	-0.0005	- 4.3995
-2.0	0.0360	-0.0004	- 4.8343
-1.8	0.0573	0.0015	- 5.3561
-1.4	0.1507	0.0169	- 6.8337
-1.0	0.3442	0.0584	- 9.6459
-0.6	0.6208	0.1030	-16.9994
-0.2	13.3947	-0.0021	-58.1834
0.2	13.2777	0.0979	-57.9799
0.6	0.6862	0.0062	-16.3941
1.0	0.3738	0.0008	- 8.8084
1.4	0.1625	0.0009	- 5.9297
1.8	0.0675	0.0007	- 4.5093
2.0	0.0454	0.0006	- 4.0446
2.2	0.0310	0.0006	- 3.6762
2.6	0.0141	0.0003	- 3.1282
3.0	0.0057	0.0001	- 2.7365
4	0.0003	0.0001	- 2.0994
5	0	0	- 1.7051
6	"	"	- 1.4350
7	"	"	- 1.2385
8	"	"	- 1.0892
9	"	"	- 0.9719
N	186.2787	0.4427	17.058
H	0.3732	-0.0074	3.0105

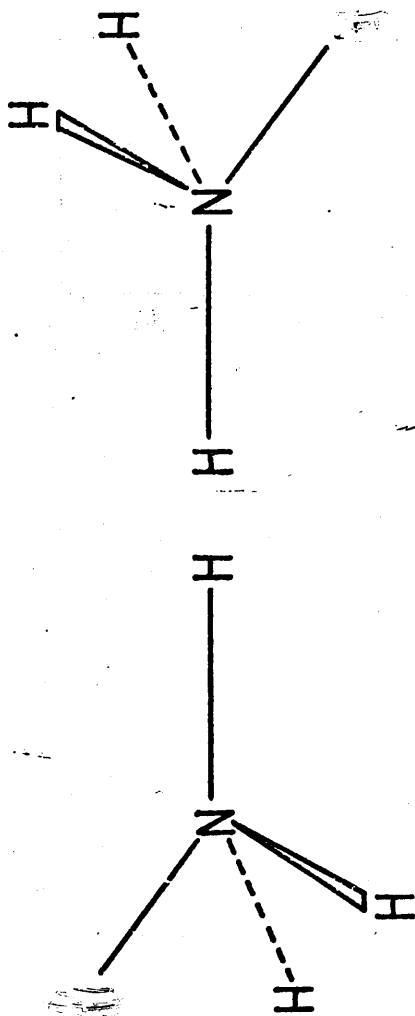
TABLE V. C.8.

Ab Initio NH₃: Diffuse Basis: Excess Electron State: Charge and Spin
 Densities and Potentials for the $\theta = 130^\circ$ Case

Distance up C ₃ Axis R (au)	$\rho^{\alpha+\beta}$	$\rho^{\alpha-\beta}$	V (au)
-9	0	0	
-8	"	"	
-7	"	"	
-6	0.0002	0.0002	
-5	0.0018	0.0018	
-4	0.0066	0.0062	- 2.4192
-3	0.0127	0.0071	- 3.3646
-2.6	0.0183	0.0037	- 3.9515
-2.2	0.0341	-0.0001	- 4.7173
-2.0	0.0497	-0.0011	- 5.1870
-1.8	0.0744	0.0	- 5.7337
-1.4	0.1732	0.0154	- 7.2049
-1.0	0.3591	0.0593	- 9.9229
-0.6	0.6075	0.1075	-17.1465
-0.2	13.3891	-0.0007	-58.2202
0.2	13.2542	0.0986	-57.9657
0.6	0.6642	0.0116	-16.3715
1.0	0.3590	0.0040	- 8.7862
1.4	0.1539	0.0025	- 5.9086
1.8	0.0629	0.0015	- 4.4889
2.0	0.0418	0.0012	- 4.0245
2.2	0.0284	0.0010	- 3.6564
2.6	0.0128	0.0004	- 3.1089
3.0	0.0051	0.0001	- 2.7179
4	0.0002	0.0	- 2.0834
5	0.0	"	- 1.6922
6	"	"	- 1.4248
7	"	"	- 1.2303
8	"	"	- 1.0824
9	"	"	- 0.9664
N	186.3441	0.3861	
H	0.3710	-0.0064	

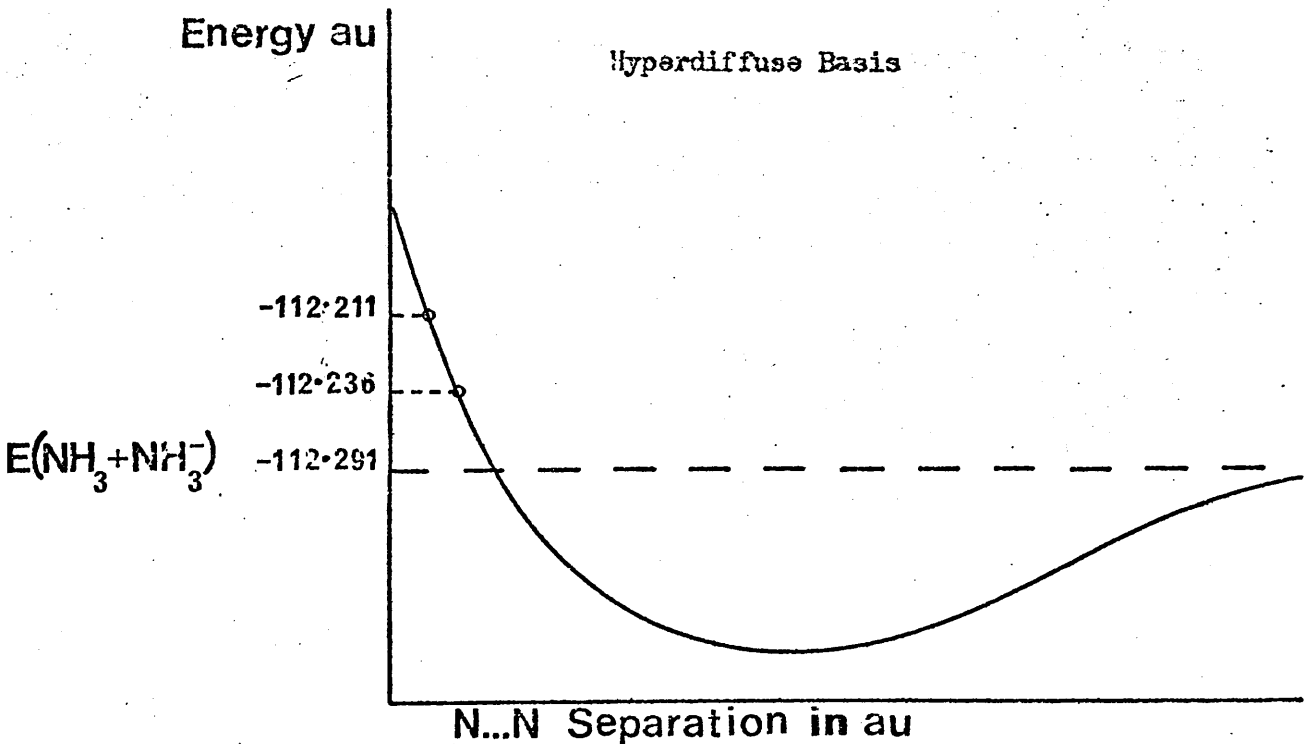
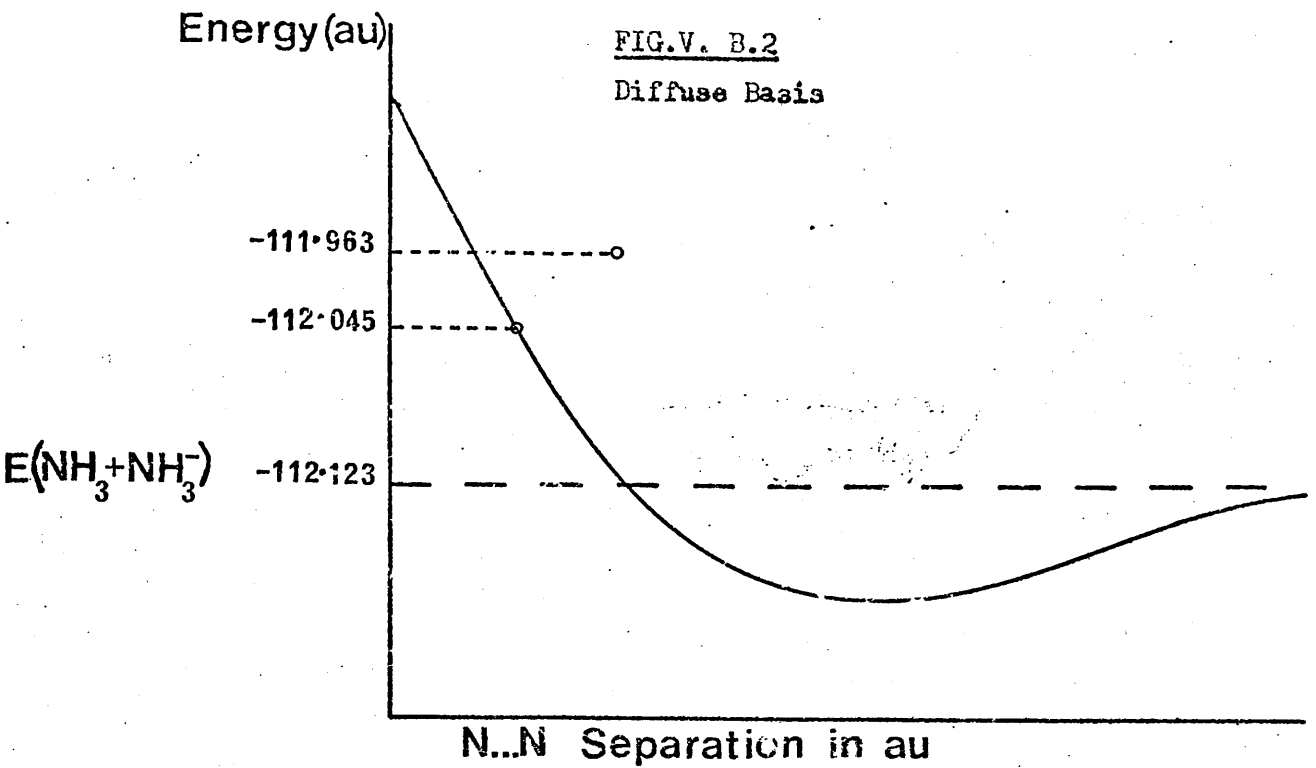
FIG.V. A.1

" D_{2d} " $(CH_3OH)_4$ Cluster Geometry. (R = CH_3)

FIG. V. B.1

NH_3 Dimer Calculations. Geometry Used.

... of ... and ... relative ... relative ...
 ... of ... at ... of ...
 ... of ...



Ab Initio $(\text{NH}_3)_2^-$ Cluster Calculations. Suggested Relative Locations Of The 5.4 au and 5.6 au (N...N Separations) On a Hypothetical Configuration Coordinate Curve.

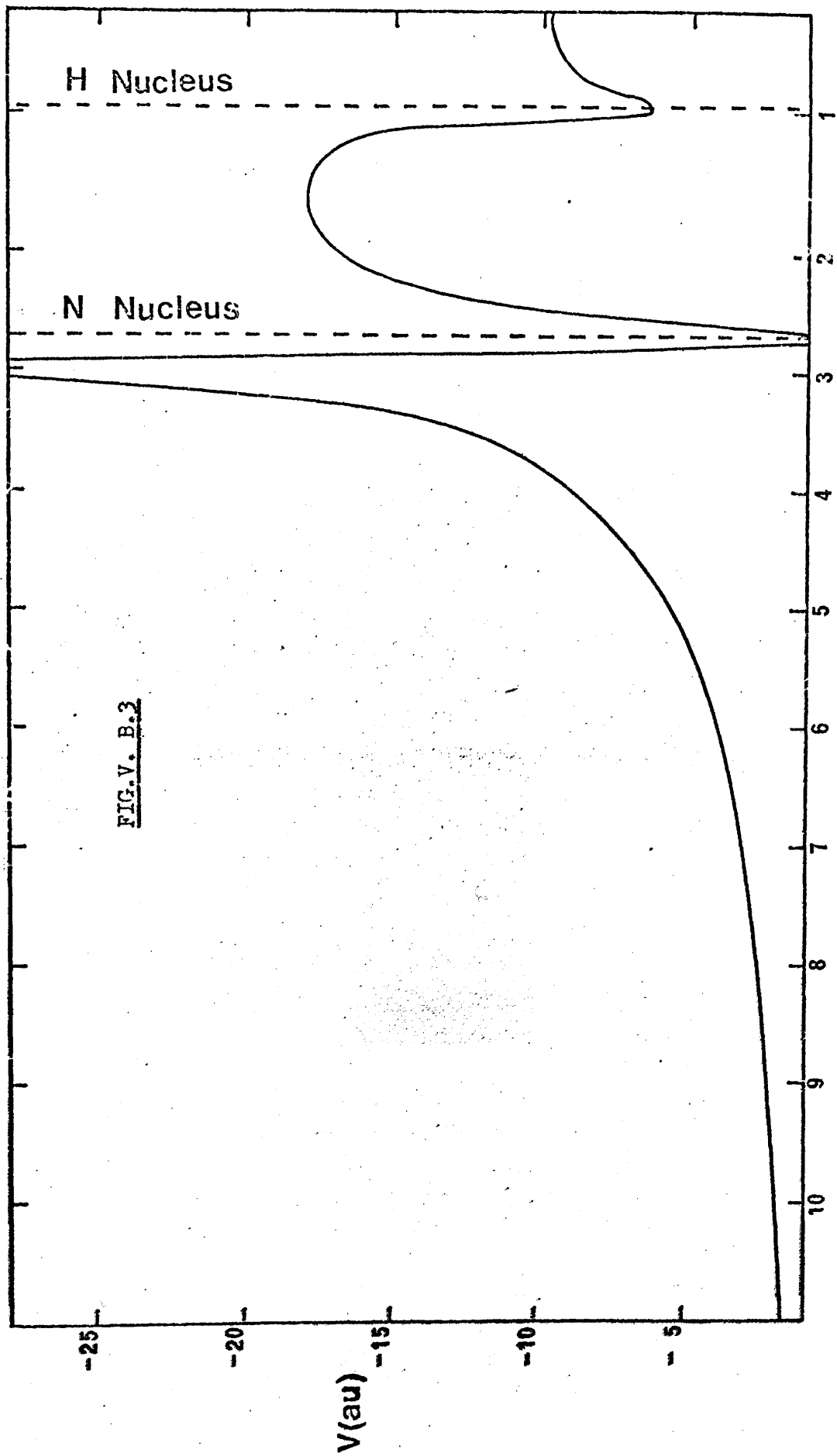


FIG. V. B.3

Distance from Centre of Molecule Along N-H...H-N Axis (au). Ab Initio Calculations on $(\text{NH}_3)_2$ cluster, $N...N = 5.4$ au. Hyperdiffuse Basis (^1Ag State). Potential Versus Distance from Centre of Cluster Along N-H...H-N Axis.

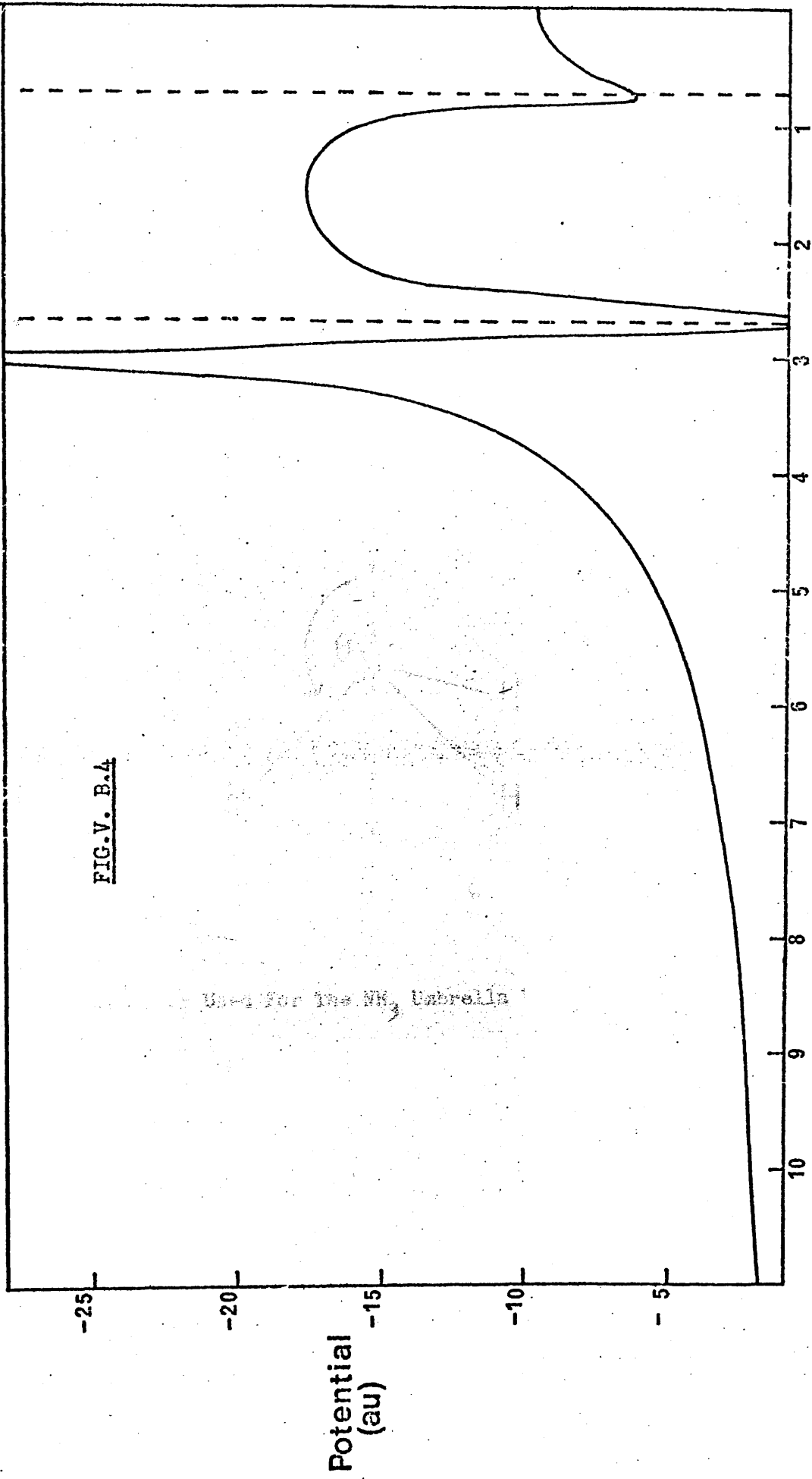
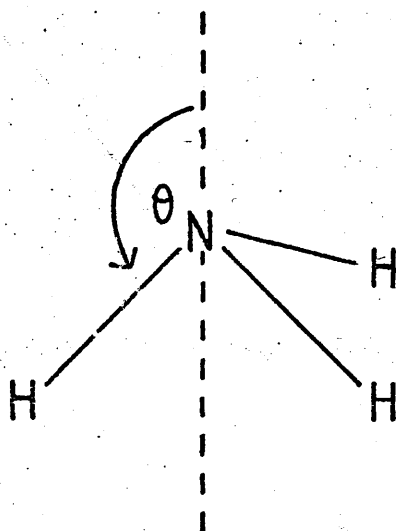


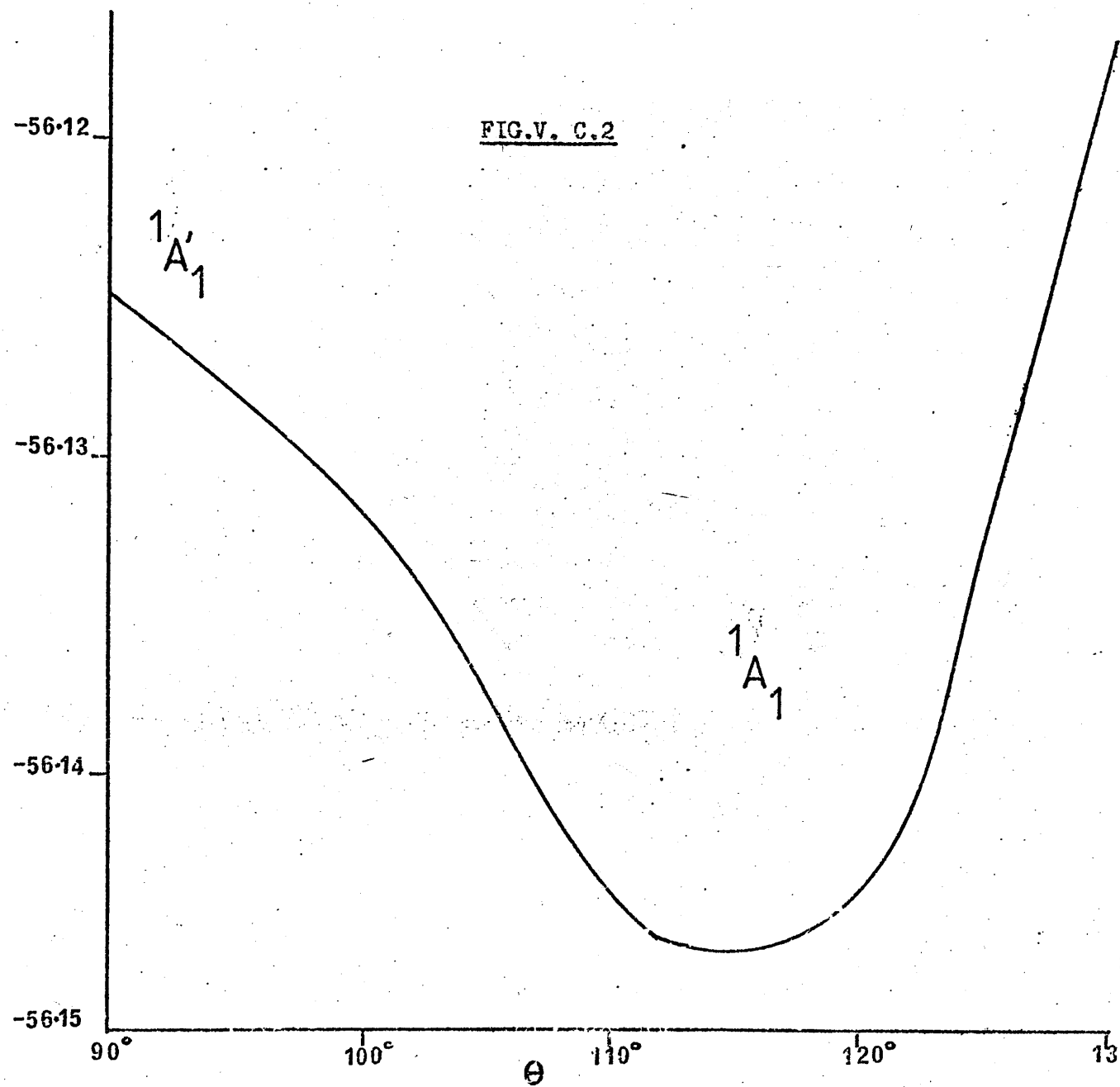
FIG.V. B.4

Use for the NH₃ Umbrella

Distance from Centre of Molecule Along N-H...H-N Axis (au). Ab Initio Calculations on (NH₃)²
Cluster. N...N = 5.6 au. Hyperdiffuse Basis (¹A_g State). Potential Versus Distance from
Centre of Cluster.

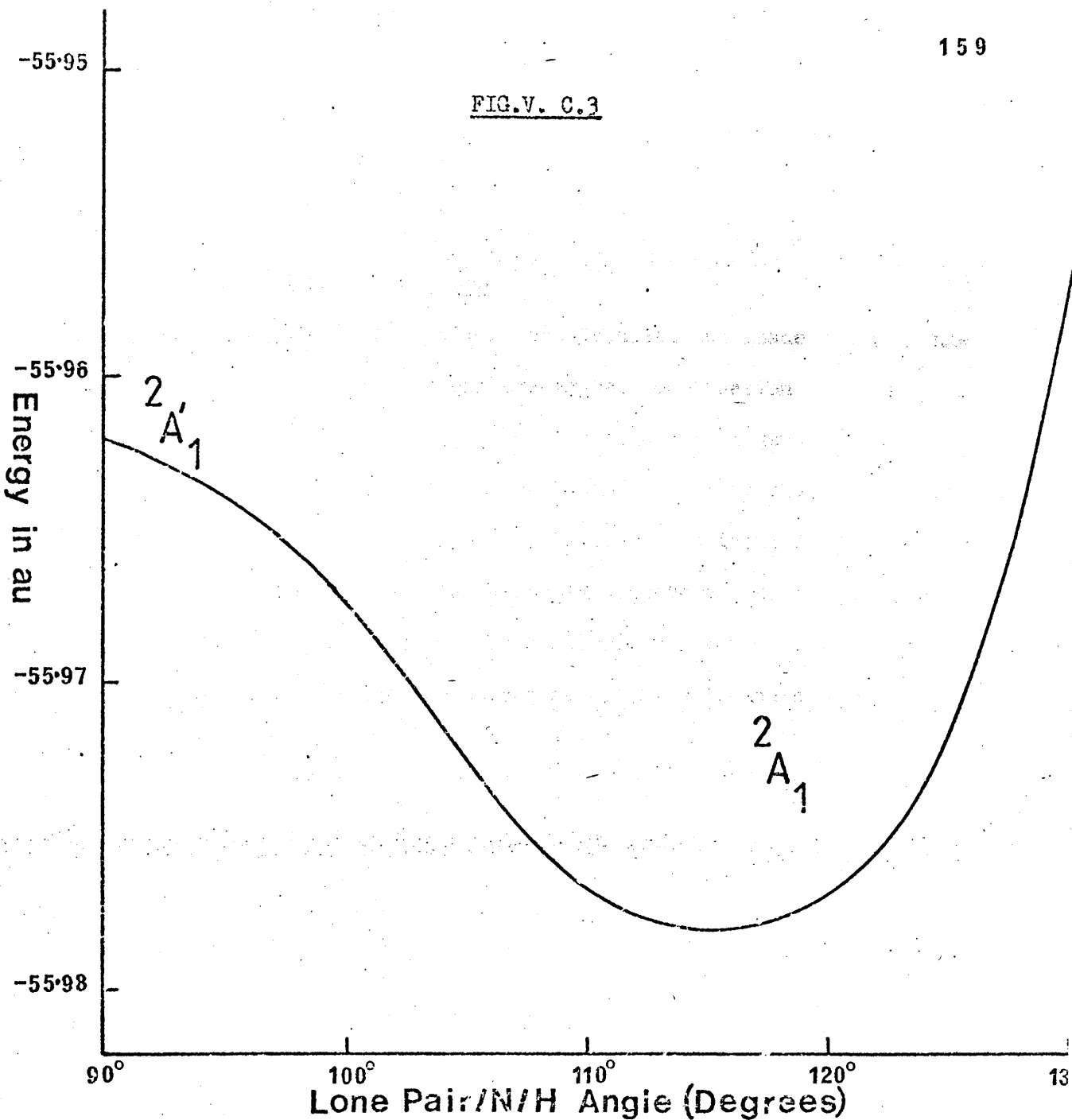
FIG.V. C.1

Parameter Used For The NH₃ Umbrella Vibration Calculations.



NH_3 Monomer: Umbrella Vibration. Neutral State ($1A_1'/1A_1$).
Energy (au) Versus Lone Pair/H/H Angle ($^\circ$). Diffuse Basis.

FIG.V. C.3



NH_3 Monomer: Umbrella Vibration. Excess Electron State ($2A_1/2A_1$).
Energy (au) Versus Lone Pair/N/H Angle ($^\circ$). Diffuse Basis.

VI

Short and Long-Range Effects - a ResolutionA. General Methods of Approach

Structural model calculations are detailed but inadequate; long-range potentials considered alone are vague. Combination of both approaches would seem to be the next step, since spin densities and excitation energies must be affected to some extent by the long-range polarisation field of the surrounding medium. The ideal method would be a detailed SCF calculation on an assembly of several hundred medium molecules in the presence of an excess electron; the practical approach is to include the polarisation potential of the surrounding medium in a cluster-type calculation.

Pioneering work by Newton ⁽¹⁾ has used a spherical cavity surrounding various clusters, assuming also a spherical free charge distribution for the purposes of calculating the potential. The fractional charge method of Noell and Morokuma ⁽¹⁴⁾ should also be noted.

It was therefore decided by the present author to present a theoretical analysis of the problem, highlighting the various approximation methods which might be necessary.

B. Derivation of a Suitable Potential(i) Energetic Considerations

Consider a charged molecule in the vicinity of a dielectric medium. One may replace the polarised medium by a set of bound surface and volume charges (see Section II. B), induced in the dielectric by the fields of the nuclei and electrons in the molecule. Thus the total energy of the system is

$$W = E + \Pi + \epsilon ,$$

where E is the energy of the molecule in vacuo, Π is the energy required to polarise the dielectric, and ϵ is the molecule/polarised dielectric interaction energy. (see Equation II. B.4).

Thus the additional energy in the presence of a dielectric is (from Equation II. B.5)

$$\epsilon = \Pi + \epsilon = \frac{1}{2} \int \rho(\underline{r}) V_p(\underline{r}) d\tau,$$

where $V_p(\underline{r})$ is the potential due to the induced surface and volume charges in the dielectric, and $\rho(\underline{r})$ includes the nuclear and electronic charge distributions. Inclusion of a dielectric in the calculation thus requires an expression for $V_p(\underline{r})$.

(ii) Calculation of the Polarisation Potential, $V_p(\underline{r})$

As illustrated in Section II. B, the dielectric may be replaced by a set of bound volume charges ρ' , so that

$$\rho' = -\nabla \cdot \underline{P},$$

and surface charges σ' , so that

$$\sigma' = -\underline{P} \cdot \underline{\tilde{n}}',$$

where $\underline{\tilde{n}}'$ is the unit vector pointing into the dielectric.

By Equation II. B.13, the polarisation potential in SI units is

$$V_p(\underline{r}) = \frac{1}{4\pi\epsilon_0} \oint_S \frac{\underline{P}(\underline{r}') \cdot d\underline{s}'(\underline{r}')}{|\underline{r} - \underline{r}'|} - \frac{1}{4\pi\epsilon_0} \int_V \frac{\nabla_{\underline{r}'} \cdot \underline{P}(\underline{r}') d\tau'}{|\underline{r} - \underline{r}'|},$$

where the first integral is over the closed surface of any cavity which is in the dielectric, and the second integral is over the volume of the dielectric,

or

$$V_p(\underline{r}) = -\frac{1}{4\pi\epsilon_0} \oint_S \frac{\sigma'(\underline{r}') d\underline{s}'(\underline{r}')}{|\underline{r} - \underline{r}'|} + \frac{1}{4\pi\epsilon_0} \int_V \frac{\rho(\underline{r}') d\tau'}{|\underline{r} - \underline{r}'|},$$

or in the form of Equation II. B.19,

$$V_p(\underline{r}) = -\left(1 - \frac{1}{d}\right)V_f(\underline{r}) - \frac{\left(1 - \frac{1}{d}\right)}{4\pi\epsilon_0} \int_{\substack{\text{inside} \\ \text{cavity}}} D(\underline{r}') \cdot \nabla_{\underline{r}'} \left(\frac{1}{|\underline{r} - \underline{r}'|} \right) d\tau' \quad \text{--- (VI. B.1.)}$$

where V_f is the potential due to the free charge distribution, and d is the dielectric constant of the medium.

Approximations can be effected as follows:

(a) No cavity in dielectric.

In this (unrealistic) case, the potential reduces to:

$$V_p(\underline{r}) = -\left(1 - \frac{1}{d}\right)V_f(\underline{r}) \quad \text{--- (VI. B.2a)}$$

or

$$V_p(\underline{r}) = -\left(1 - \frac{1}{d}\right) \left\{ \sum_A \frac{Z_A}{|\underline{r} - \underline{R}_A|} + \int \frac{\rho(\underline{r}')}{|\underline{r} - \underline{r}'|} d\tau' \right\} \quad \text{--- (VI. B.2b)}$$

Thus the only integration required is over all space, and the potential can be readily incorporated in SCF calculations (see Section VI. C).

This method is simple but unrealistic, and the continuous dielectric medium cannot be supposed to extend into the interior of the molecule.

A cutoff radius for the medium, or cavity, should thus be considered, but the second integral in Equation VI. B.1. requires some simplification.

(b) Assumption of a cavity and spherical symmetry.

We may approximate instead by assuming the charge distribution and cavity to have spherical symmetry, when (see Section II. B) the spherically symmetric potential given by Equation II. B.16 is obtained, namely

$$V_p(\underline{r}) = -\frac{\left(1 - \frac{1}{d}\right)}{\epsilon_0} \left\{ \int_0^{\infty} \frac{\rho(r')}{r_{>}} r'^2 dr' \right\},$$

where $r_{>} = \max(r, r')$ when $r > R_0$ and $V_p(r) = V_p(R_0)$ when $r \leq R_0$.

$$\left. \begin{aligned} \text{i.e., } V_p(r) &= -(1 - \frac{1}{d})V_f(r) && \text{when } r > R_o \\ V_p(r) &= -(1 - \frac{1}{d})V_f(R_o) && \text{when } r \leq R_o \end{aligned} \right\} \text{--- (VI. B.3.)}$$

This leads to a formalism similar to that of Newton ⁽¹⁾; however, this potential must also be considered to act on the nuclei as well as the electrons.

(c) Wavefunction in cavity.

Here the most drastic assumption is made that the wavefunction is spherically symmetrical and included totally in the cavity.

Thus the charged cluster is regarded as a spherically symmetric charge distribution of net value -1 lying in the cavity. Since there is no free charge in the medium, only surface polarisation charges appear at the cavity boundary, and the potential V_p is that of a spherical distribution of radius R_o , the cavity radius, and total charge $4\pi R_o^2 \sigma'$.

By Equation II. B.13a, this gives (in SI units)

$$V_p(r) = - \frac{(1 - \frac{1}{d})}{4\pi\epsilon_o} \frac{Q}{r}, \quad \text{when } r > R_o$$

$$\text{and } V_p(r) = - \frac{(1 - \frac{1}{d})}{4\pi\epsilon_o} \frac{Q}{R_o}, \quad \text{when } r \leq R_o$$

$$\text{or, } V_p(r) = - (1 - \frac{1}{d}) \frac{Q}{r}, \quad r > R_o$$

$$\left. \begin{aligned} \text{in au, } V_p(r) &= - (1 - \frac{1}{d}) \frac{Q}{R_o}, && r \leq R_o \end{aligned} \right\} \text{--- (VI. B.4.)}$$

C. Incorporation of the Potential in the Cluster Model - Approximate Methods

(i) The No-Cavity Approximation

Assuming every electron in the molecule to move in an average polarisation potential due to the induced charges in the medium, (this method neglects specific electron-medium correlation energies), then

the total energy due to the presence of the medium is

$$\mathcal{E} = \frac{1}{2} \int \rho(\underline{r}) V_p(\underline{r}) d\tau + \frac{1}{2} \sum_A Z_A V_p(\underline{r}_A)$$

and we may write the Hamiltonian for the system as

$$\mathcal{H} = - \sum_i \frac{\nabla_i^2}{2} - \sum_i \sum_A \frac{Z_A}{R_{iA}} + \sum_{i < j} \frac{1}{r_{ij}} + \sum_{A < B} \frac{Z_A Z_B}{R_{AB}} - \frac{1}{2} \sum_i V_i + \frac{1}{2} \sum_A Z_A V_A,$$

where $V_i = V_p(\underline{r}_i)$, etc.

Now in Section II. B, it was seen that $\mathcal{E} = \Pi$ (medium rearrangement energy) + \mathcal{E} (charge/medium interaction), where $\mathcal{E} = \frac{1}{2} \int \rho(\underline{r}) V_p(\underline{r}) d\tau$,

$\Pi = -\mathcal{E}$ and $\mathcal{E} = 2\mathcal{E}$. Thus for the electronic term,

$$\mathcal{E} = \frac{1}{2} \sum_i V_i - \sum_i V_i$$

Separating out (a) all terms involving the nuclei alone, i.e.,

terms four and six, and (b) the medium rearrangement energy, viz.

$\frac{1}{2} \sum_i V_i$ for the electronic part, we have

$$\mathcal{H}^{el} = - \sum_i \frac{\nabla_i^2}{2} - \sum_i \sum_A \frac{Z_A}{r_{iA}} + \sum_{i < j} \frac{1}{r_{ij}} - \sum_i V_i \quad \text{--- (VI. C.1.)}$$

Treatment of $V_p(\underline{r}_i)$ as a one-electron term analogous to $\mathcal{H}^{core}(i)$

gives the total electronic energy contribution as

$$\bar{E} = 2 \sum_i H_{ii} - 2 \sum_i V_{ii} + \sum_{i,j} (2J_{ij} - K_{ij}),$$

where $V_{ii} = \int \psi_i^* V_p(\underline{r}_i) \psi_i d\tau$.

Similarly, by analogy with III. C.2a, we obtain for the modified

Fock matrix in the RHF formalism

$$F'_{\mu\nu} = H_{\mu\nu} + \sum_{\lambda\sigma} P_{\lambda\sigma} [(\mu\nu|\lambda\sigma) - \frac{1}{2}(\mu\lambda|\nu\sigma)] - V_{\mu\nu}, \quad \text{--- (VI. C.2.)}$$

where $V_{\mu\nu} = \int Q_{\mu}(1) V_p(\underline{r}_1) Q_{\nu}(1) d\tau_1$,

But by Equation VI. B.2b,

$$V_p(\underline{r}) = 1(1 - \frac{1}{d}) \left\{ \sum_A \frac{Z_A}{|\underline{r} - \underline{r}_A|} + \int \frac{\rho(\underline{r}')}{|\underline{r} - \underline{r}'|} d\tau' \right\}$$

So

$$V_{\mu\nu} = -(1 - \frac{1}{d}) \left\{ \sum_A \frac{\phi_\mu(1) Z_A \phi_\nu(1)}{r_{1A}} d\tau_1 - \int \phi_\mu(1) \left(\frac{\sum_{\lambda\sigma} P_{\lambda\sigma} \phi_\lambda(2) \phi_\sigma(2) d\tau_2}{r_{12}} \phi_\nu(1) d\tau_1 \right) \right\}$$

$$\text{since } \rho(\underline{r}_2) = - \sum_{\lambda\sigma} P_{\lambda\sigma} \phi_\lambda(2) \phi_\sigma(2)$$

i.e.,

$$V_{\mu\nu} = -(1 - \frac{1}{d}) \left\{ \sum_A \int \frac{Z_A \phi_\mu(1) \phi_\nu(1) d\tau_1}{r_{1A}} - \sum_{\lambda\sigma} P_{\lambda\sigma} (\mu\nu|\lambda\sigma) \right\} \text{--- (VI. C.3.)}$$

$$\text{Since } H_{\mu\nu} = \langle \mu | \mathcal{H}^{\text{core}}(1) | \nu \rangle = \int \phi_\mu(1) \left\{ -\frac{\nabla_1^2}{2} - \sum_A \frac{Z_A}{r_{1A}} \right\} \phi_\nu(1) d\tau_1,$$

the first term of Equation VI. C.3 may be incorporated in this, to give

$$H'_{\mu\nu} = \int \phi_\mu(1) \left\{ -\frac{\nabla_1^2}{2} - \frac{1}{d} \sum_A \frac{Z_A}{r_{1A}} \right\} \phi_\nu(1) d\tau_1 \text{--- (VI. C.4.)}$$

Similarly, the second term may be incorporated in the two-electron part of $F_{\mu\nu}$, so that

$$F'_{\mu\nu} = H'_{\mu\nu} + \sum_{\lambda\sigma} P_{\lambda\sigma} \left[\frac{(\mu\nu|\lambda\sigma)}{d} - \frac{1}{2}(\mu\lambda|\nu\sigma) \right] \text{--- (VI. C.5.)}$$

As can be seen, this gives the normal Fock matrix when $d = 1$ (i.e., when the medium is absent).

Consideration of the SUHF equations of Section III.D. leads, by analogy with IV. D.2, to

$$F'_{\mu\nu}^\alpha = H_{\mu\nu} + \sum_{\lambda\sigma} \left[P_{\lambda\sigma} (\mu\nu|\lambda\sigma) - P_{\lambda\sigma}^\alpha (\mu\sigma|\lambda\nu) \right] - V_{\mu\nu}$$

i.e.,

$$\left. \begin{aligned} F'_{\mu\nu}{}^{\alpha} &= H'_{\mu\nu} + \sum_{\lambda\sigma} \left[\frac{P_{\lambda\sigma}}{d} (\mu\nu|\lambda\sigma) - P_{\lambda}^{\alpha} (\mu\sigma|\lambda\nu) \right] \\ F'_{\mu\nu}{}^{\beta} &= H'_{\mu\nu} + \sum_{\lambda\sigma} \left[\frac{P_{\lambda\sigma}}{d} (\mu\nu|\lambda\sigma) - P_{\lambda}^{\beta} (\mu\sigma|\lambda\nu) \right] \end{aligned} \right\} \text{--- (VI. C.6.)}$$

Again, when $d = 1$, these give the normal Fock matrices

where $H'_{\mu\nu}$ is given by Equation VI. C.4.

Thus only minor modification is required in an ab initio SCF programme. When self-consistency is achieved, the addition of the nuclear energies and medium rearrangement energy will give the total energy of the cluster in a continuous dielectric medium. Although application of this technique is relatively simple, the permeation of the cluster by a continuous dielectric is unrealistic, and overlarge stabilisation energies are thus expected.

(ii) The Spherical Symmetry Approximation (With Cavity)

With a cavity, or cutoff region for the dielectric, the assumption of spherical symmetry leads to simplification. This is the approach used by Newton (1).

The Fock operator becomes

$$F' = \mathcal{H}^{\text{core}} + \sum_j (2J_j - K_j) - V_j,$$

where $V_j = V_p(\underline{r}_j)$

From Equation VI. B.3,

$$V_p(r) = -(1 - \frac{1}{d})V_f(r), \quad r > R_0$$

$$\text{and } V_p(r) = -(1 - \frac{1}{d})V_f(R_0), \quad r \leq R_0$$

where R_0 is the "cavity radius," d the relevant dielectric constant, and V_f the potential due to all the free charges in the system.

Thus

$$V_p(r) = -(1 - \frac{1}{d}) \left\{ \sum_A \frac{Z_A}{r} - \sum_i \int \frac{\psi_i^2(r')}{r_{>}} d\tau' \right\},$$

where $r_{>}$ is the larger of r and r' , and for $r \leq R_0$,

$$V_p(r) = V_p(R_0)$$

The charges Z_A are restricted to the cavity for simplicity.

The problem of evaluating the integral $\int \frac{\psi_i^2(r')}{r_{>}} d\tau'$ may be tackled numerically, but the procedure can be time-consuming. Newton has solved this problem using a combination of analytical and numerical techniques.

However, one important difference emerges: although he correctly includes nuclear charges in the expression for V_p , he does not take the interaction between V_p and the Z_A into account in the total energy.

Thus the term

$$\frac{1}{2} \sum_A Z_A V_p(r_A), \text{ or since the } Z_A \text{ all lie within the cavity,}$$

$$\frac{1}{2} V_p(R_0) \sum_A Z_A, \text{ is missing from the total energy,}$$

obtainable from the expression

$$\mathcal{E} = \frac{1}{2} \int \rho(\underline{r}) V_p(\underline{r}) d\underline{r} + \frac{1}{2} \sum_A Z_A V_p(\underline{r}_A), \text{ by substitution of the expressions for } V_p(\underline{r}).$$

(iii) The Localisation in Cavity Approximation

Since, in this approximation, we assume a spherical charge distribution confined within a spherical cavity, the potential (see Equation VI. B.4) is

$$V_p(r) = -(1 - \frac{1}{d}) \frac{Q}{r_{>}}, \text{ where } r_{>} = \max(r, R_0)$$

and since the charge distribution Q is confined to the cavity,

$$\epsilon = -\frac{1}{2} \times Q \times \left(1 - \frac{1}{d}\right) \frac{Q}{R_0} ,$$

$$\text{i.e., } \epsilon = -\frac{1}{2} \frac{Q^2}{R_0} \left(1 - \frac{1}{d}\right) \quad \text{----- (VI. B.8.)}$$

Thus the energy due to the presence of the medium is independent of the size of the charge distribution Q , and is merely added to the result of a suitable SCF cluster calculation.

D. The Optimum Model ?

(i) Practical Drawbacks of Theoretical Models

None of the methods of Section C is ideal. The full treatment of a macroscopic cluster by ab initio methods is at present prohibitive. Even full inclusion of dielectric with a cutoff radius round a central cluster (see Equation VI. B.1) is intractable without assumption of spherical symmetry, and the total neglect of a cutoff radius (see Section VI. C.(i)) is feasible but unrealistic.

The method of Section VI. C.(ii) and Newton, which invokes spherical symmetry, and possible penetration of the trapped electron beyond the cutoff radius, requires considerable extra computation.

The final method of Section VI. C.(iii), although mathematically very simple, merely makes the one additional assumption that the trapped electron does not extend sufficiently outwards to penetrate the surrounding dielectric medium to any great extent. This may not be unreasonable: the cavity model of Section II. E for H_2O shows that 60 - 70% of the electron density is typically contained in the cavity, and the cluster calculations of Sections IV. B and IV. C indicate a very rapid fall-off of spin density from the centre of the cluster. Newton, too, on dipole-oriented $(H_2O)_4^-$ finds 84% containment for a radius of 2.65 \AA .

(ii) Application of the Localisation in Cavity Model

The procedure in this case is to perform an SCF calculation on the excess electron cluster in vacuo, using a reasonably flexible and diffuse basis set, the energy term of Equation VI. B.8 then being added. Thus the spin densities and excitation energies are evaluated by the SCF calculation, while the energy of solvation is determined by the "cavity size," that is, the radius at which the continuous dielectric medium is supposed to commence. Calculated values of stabilisation energies for liquid H_2O and liquid NH_3 are shown in Table VI. D.1.

Since the calculated energy difference between the excess electron and neutral structures is small (e.g., for the hyperdiffuse basis on planar NH_3 (see Table IV. C.1), $\Delta E = 0.03$ eV) for a sufficiently flexible and diffuse basis, we may take the calculated stabilisation energies in Table VI. D.1 as representing the whole of the solvation energy. Furthermore, the derivations of Sections VI.B and VI.C calculate ϵ , the difference between the energy of an unpolarised dielectric containing a cavity and the polarised dielectric with a spherically symmetric charged cluster wholly within the cavity; thus V_0 , the energy of injection of an electron into the medium ^(2,3,4) is included in ϵ . Terms involving energy of cavity formation, such as "surface tension" ^(1,5) will have no bearing on ϵ if the cavities are preformed by thermal motion and radiation effects ⁽⁶⁾.

From the table, water appears to form energetically deeper traps than ammonia at the same cavity radius, and Newton's calculations confirm this ^(1b), showing stabilisations of -1.62 eV for H_2O with $R_0 = 2.65$ Å, and -0.82 eV for NH_3 with $R_0 = 2.75$ Å. In the present author's model, to fit the observed heats of solvation for water and ammonia, namely -1.7 eV and -1.7 ± 0.7 eV, radii of 4.18 Å and 4.04 Å respectively are required. Thus, if a continuous dielectric medium is

considered to start at a radius $\gg 4 \text{ \AA}^0$ from the molecule(s) on which an electron is localised, the solvation energy can be fitted quite well to experiment. However, restriction of the diffuseness of the orbitals is necessary to prevent the excess electron "drifting off" in this model, whereas SCF calculations allowing for penetration into the medium will automatically prevent this occurrence.

The main problems of the structural/continuum models can be summarised thus:

(a) the present work, by extending the flexibility of ab initio calculations on structures containing e^- , has inferred that such a model does not stabilise an excess electron when the cluster size is limited: alone, such clusters would be centres for transient electron capture rather than long-term stabilisation. Previous structural models claiming stability (7, 8) have not had sufficiently flexible or optimised basis sets.

(b) the cluster model does not predict the optimum orientation for electron trapping: only by trial and error are some orientations found to be the lowest in energy,

(c) the long-range stabilisation energy is large compared to the energy differences between different possible cluster orientations.

(iii) A Suggested Qualitative Scheme

Taking into account the discussion in Section I.A and the theoretical data, a rough scheme for electron solvation in crystalline ice and liquid water can be suggested. This may also apply to liquid NH_3 , but the situation in alkaline glasses appears to be totally different.

Electron stabilisation occurs mainly at a defect in the crystal structure. In ice at 77K the defects are few, leading to low yields of e_t^- , but the trap population may be increased by heating,

incorporation of F^- ion or dosage with radiation.

One type of defect predominates, with a small percentage of deeper and shallower traps.

E. Addendum - Experiment Versus Theory

As discussed earlier, (Section IV. C) various investigators have found the most stable conformation of $(H_2O)_2^-$ to be that illustrated in Fig. IV. C.4., where two protons face each other, according to energetic (9) and spin density (10) considerations. Naleway and Schwartz point out the similarity of this trapping centre to the Bjerrum D defect in ice (11, 12), suggesting that these may be the trapping centres in the medium. This is also intuitively appealing, since an H...H centre should appear more positively charged to an excess electron than, say, O-H...O or O...O. However, Kawabata (13) has found that the trapping of e^- in crystalline ice is much enhanced by the presence of F^- ion in the crystalline lattice. If, as he suggests, F^- replaces an H_2O molecule, the expected effect would be the orientation of protons toward F^- , with consequent propagation of Bjerrum L defects (O...O type) throughout the lattice. Since the F^- has no other effect on the shape of the optical spectrum of e_t^- , or the photobleaching behaviour, it would appear that the electron is not trapped near F^- , but near one of the resultant L defects.

In view of this experimental result, it may be more pertinent to examine theoretically very large H_2O crystal fragments containing an L defect, rather than a D one, if and when this type of SCF calculation becomes feasible.

References VI

1. (a) M.D. Newton, J. Chem. Phys., 58 (1973) 5833.
(b) M.D. Newton, J. Phys. Chem., 79 (1975) 2795.
2. B.E. Springett, M.H. Cohen and J. Jortner, Phys. Rev., 159 (1967) 183.
3. B.E. Springett, J. Jortner and M.H. Cohen, J. Chem. Phys., 48 (1968) 2720.
4. R.A. Holroyd and M. Allen, J. Chem. Phys., 54 (1971) 5014.
5. K. Fueki, D-F. Fang, L. Kevan and R.E. Christoffersen, J. Phys. Chem., 75 (1971) 2297.
6. K. Kawabata, S. Okabe and H. Horii, Chem. Phys. Lett., 20 (1973) 586.
7. M. Weissmann and N.V. Cohan, Chem. Phys. Lett., 7 (1970) 445.
8. S. Ishimaru, H. Kato, T. Yamabe and K. Fukui, J. Phys. Chem., 77 (1973) 1450.
9. C.A. Naleway and M.E. Schwartz, J. Phys. Chem., 76 (1972) 3905.
10. C.M.L. Kerr and F. Williams, J. Phys. Chem., 76 (1972) 3838.
11. N. Bjerrum, K. Dan. Vidensk.Slesk. Mat. Fys. Skr., 27 (1951) 1.
12. R. Catterall and N.F. Mott, Adv. Physics, 18 (1969) 665.
13. K. Kawabata, J. Chem. Phys., 55 (1971) 3672.
14. J.O. Noell and K. Morokuma, J. Phys. Chem., 81 (1977) 2295.

TABLE VI. D.1.

Simple Cavity Model: Stabilisation Energies (eV) for water and liquid ammonia for Different Cavity Radii (\AA°)

Radius (\AA°)	Energy (eV)	
	NH ₃ (1)	H ₂ O (2)
1.0	-6.87	-7.11
1.5	-4.58	-4.74
2.0	-3.44	-3.56
2.5	-2.75	-2.84
3.0	-2.29	-2.37
4.0	-1.72	-1.78
5.0	-1.37	-1.42
6.0	-1.15	-1.18
7.0	-0.982	-1.02
8.0	-0.859	-0.839
9.0	-0.764	-0.790
10.0	-0.687	-0.711

(1) Static dielectric constant = 22

(2) Static dielectric constant = 80.37

